

# **Affinity-based methods for the isolation and detection of extracellular vesicles, bacteria and biomarkers in body fluids**

**Julia Neumair**

Vollständiger Abdruck der von der TUM School of Natural Sciences der Technischen Universität München zur Erlangung einer

**Doktorin der Naturwissenschaften (Dr. rer. nat.)**

genehmigten Dissertation.

Vorsitz: Prof. Dr. Matthias Feige

Prüfer der Dissertation:

1. Priv.-Doz. Dr. Michael Seidel
2. Prof. Dr. Ario de Marco

Die Dissertation wurde am 30.10.2024 bei der Technischen Universität München eingereicht und durch die TUM School of Natural Sciences am 26.11.2024 angenommen.





Nicht weil es schwer ist, wagen wir es nicht,  
sondern weil wir es nicht wagen, ist es schwer.

- Lucius Annaeus Seneca

## Danksagung

Ich möchte mich als erstes bei meinem Doktorvater **PD Dr. Michael Seidel** bedanken, der mir die Möglichkeit gegeben hat, diese Promotion bei ihm durchzuführen. Danke für deine Unterstützung und deinen hilfreichen Input, der mir sogar schon seit der Bachelorarbeit geholfen hat! Außerdem möchte ich mich bei meinem Mentor **Prof. Dr. Martin Elsner** bedanken, dass ich an seinem Lehrstuhl diese Arbeit schreiben konnte. Danke auch für deinen hilfreichen Input! Dankeschön an die **IGSSE**, die meine Forschung über das Projekt REP-MAF in den ersten drei Jahren finanziert hat.

Ich danke allen Institutsmitgliedern, die mich in meiner Zeit begleitet haben! Danke, ihr habt die Zeit dort zu etwas ganz Besonderem gemacht und ich konnte viel von euch lernen! Allen voran möchte ich meinen Kollegen aus der „**BiopritschlerInnen**“-Gruppe danken: Danke **Lisa**, dass du mich so herzlich in deinem Büro aufgenommen hast. Deine Position als „wandelndes Lexikon des Instituts“ habe ich ehrenvoll weitergeführt. Danke **Katy**, für die inspirierenden Gespräche. Danke **Julia**, dein Enthusiasmus für all das, was du tust, ist echt inspirierend. **Philipp**, danke für all die lustigen „Subway-Montage“. **Andi**, es war mir eine Ehre, AJ zu sein. Danke **Gerhard**, für die spannenden Rätsel in den Mittagspausen. Danke **Lena**, dass du mir geholfen hast, die manchmal etwas „wilden“ Jungs zu bändigen. **Yiao**, danke für das authentische chinesische Essen, das wir über dich bestellen konnten. Danke **Sandra**, für die netten Gespräche, wenn du es mal zu uns nach Garching geschafft hast. Die Zeit mit euch allen hat mir echt Spaß gemacht. Besonders unsere Mittagspausen haben mir durch die Zeiten geholfen, wenn es gerade mal nicht so gut lief.

Danke an alle anderen Doktoranden, die ich nicht namentlich genannt habe, aber die mich in der Zeit hier begleitet haben. Unsere Kaffee-/Tee- und Mittagspausen, in denen wir uns zwar auch oft über private Themen unterhalten haben, aber durch die trotzdem immer wieder Probleme aus dem Labor gelöst werden konnten, werde ich vermissen.

Danke an **Conny**, **Christine** und **Sonja**, ohne euch würde das Institut nie so gut laufen. Danke für die netten Gespräche zwischendurch. Danke **Christine**, **Susi**, **Roland** und **Sebastian** für eure Hilfe, ob im Labor oder durch technische Unterstützung.

Mein Dank geht an meine Studentinnen, die ich ihn während meiner Promotion begleiten durfte. Danke meinen Forschungspraktikantinnen **Steffi** und **Aoife**. Ganz besonders will ich meiner Masterstudentin **Marie** danken, deren Masterarbeit wir erfolgreich publizieren konnten. Es hat Spaß gemacht, mir dir zusammen zu arbeiten und gemeinsam die Ergebnisse zu diskutieren.

Danke **Prof. Dr. Ario de Marco**, dass ich drei Monate in deinem Labor im *Laboratory for Environmental and Life Sciences* (LELS) an der Universität Nova Gorica verbringen durfte. Danke für die freundliche Aufnahme und den hilfreichen Input. Ebenso möchte ich mich bei allen anderen LELS-Angehörigen, sowie den anderen internationalen Studenten bedanken, die mich im Labor unterstützt und die Zeit dort besonders gemacht haben. Danke **Claudia, Petra, Matteo, Bhavani, Sinead** und allen anderen.

Zum Schluss möchte ich mich bei meiner **Familie**, im Besonderen meinen Eltern **Roland** und **Nicky**, meiner Schwester **Sonja** und meinem Mann **Johannes**, für ihre Unterstützung danken. Ohne euch wäre ich nicht da, wo ich jetzt bin.

## Kurzzusammenfassung

Affinität beschreibt eine spezifische, nicht-kovalente und dadurch reversible Wechselwirkung zwischen zwei Partnern: einem Affinitätsbinder und seinem Zielmolekül. Ein bekanntes Beispiel sind Antikörper und ihre Antigene. Affinitätsbasierte Analyse- und Trennmethode werden in der Bioanalytik eingesetzt, um verschiedene Analyten wie kleine Moleküle, Proteine oder sogar Zellen und Bakterien selektiv zu isolieren und zu detektieren. Das Vorhandensein spezifischer Analyten wie Biomarker oder Bakterienzellen in Körperflüssigkeiten kann Hinweise auf eine Infektionskrankheit, eine entstehende Sepsis oder andere Krankheiten geben. In dieser Doktorarbeit wurden drei verschiedene Ansätze verfolgt, um die Anwendbarkeit von affinitätsbasierten Nachweis- und Isolierungsmethoden für drei unterschiedliche Analyten aus drei verschiedenen Körperflüssigkeiten zu zeigen.

Für die Isolierung von extrazellulären Vesikeln (EVs) aus Urin wurde ein neuartiger monolithischer Immunfiltrationsassay unter Verwendung von *Nanobodies* entwickelt. EVs sind kleine, membranumschlossene Vesikel, die von Zellen freigesetzt werden. Als Träger von zellulären Informationen wie Proteinen, DNA oder RNA können EVs und ihre Fracht als Biomarker für verschiedene Krankheiten, wie z.B. Krebs oder neurodegenerative Erkrankungen verwendet werden. Traditionelle Isolierungsmethoden, die auf einer größenabhängigen Trennung basieren, wie Ultrafiltration, Ultrazentrifugation, oder asymmetrische Fluss-Feld-Fluss-Fraktionierung können nicht zwischen den verschiedenen Zelltypen unterscheiden, aus denen die EVs stammen. Immunaффinitätsbasierte Methoden können dieses Problem überwinden. Einzel-Domänen-Antikörper mit einer hoher Antigenaffinität, sogenannte *Nanobodies*, wurden als Affinitätsbinder verwendet. *Nanobodies*, die auf das Oberflächenprotein CD63 abzielen, wurden indirekt über eine zweite *Nanobody*-Antigen-Interaktion auf einem makroporösen Epoxid-basierten Monolithen mit Porengrößen von  $22,4 \pm 8,8 \mu\text{m}$  immobilisiert. Nach Fangen der EVs wurde die Elution zuerst kompetitiv, dann pH-abhängig, durchgeführt. Mit dieser *Nanobody*-basierten monolithischen Immunfiltration war es erstmals möglich, etwa  $3 \times 10^{10}$  EVs unterteilt in zwei verschiedene Größenklassen von etwa 36 und 130 nm aus 7,5 mL Urin zu isolieren.

Infektionen in Körperflüssigkeiten sind kritische Zustände, die schnell und gerichtet behandelt werden müssen. In einigen Fällen ist dies nicht einfach, wie zum Beispiel bei infiziertem Aszites. Aszites ist eine lebensbedrohliche Komplikation von Krankheiten, wie der Leberzirrhose, die zu einer großen Flüssigkeitsansammlung in der Bauchhöhle führt. Eine Infektion mit Bakterien wie *Escherichia coli* oder *Enterococcus faecalis* ist nicht nur eine der Hauptursachen für Aszites-bedingte Sepsis und demzufolge Todesfälle, sondern wegen der sehr geringen Bakterienkonzentration durch Kultur auch schwer zu diagnostizieren.

Molekulare Methoden dagegen sind zwar schneller, aber teurer und aufwendiger. Hier kann eine affinitäts-basierte Aufkonzentrierung helfen, die Identifizierung und Behandlung zu beschleunigen. Für eine effektive Affinitätsfiltration, die eine Diagnose durch Kultur beschleunigen kann, ist eine Kombination aus selektiven Affinitätsbindern und desorbierend wirkenden Elutionspuffern notwendig. Deren Zusammenspiel ist jedoch nicht immer leicht vorhersehbar, weswegen für die Definition beider Komponenten eine hohe Zahl an Tests durchgeführt werden muss. Der Einsatz von bioanalytischen Screening-Plattformen kann hierbei den Testaufwand deutlich reduzieren. Aus diesem Grund wurde in dieser Doktorarbeit ein flussbasierter Microarray-Screening-Chemilumineszenz (CL)-Bioassay auf der automatisierten Analyseplattform *Microarray Chip Reader – Research* (MCR-R) etabliert. Für den Bindungsnachweis von Bakterien an immobilisierte Affinitätsbinder wurden lebende *E. coli*- und *E. faecalis*-Zellen mit Biotin markiert, an das Streptavidin-Meerrettichperoxidase-Konjugate für eine CL-Detektion auf dem MCR-R binden konnten. Die Wiederfindungen für lebende *E. coli* und *E. faecalis* lagen bei  $98 \pm 8,8 \%$  beziehungsweise  $75 \pm 28 \%$ . Verschiedene Kandidaten für Affinitätsbinder, wie Antikörper oder antibiotisch wirksame Moleküle, wurden in Reihen von jeweils fünf Spots auf der Oberfläche von Polykarbonat-basierten Microarray-Chips immobilisiert. Die Biotin-markierten Bakterien wurden durch den Microarray-Chip gepumpt, damit sie mit den gebundenen Affinitätsbindern interagieren können, und mit dem CL-Assay detektiert. Manuelles Spülen des Microarray-Chips mit Elutionspuffer und ein zweiter CL-Detektionsschritt ermöglichten nicht nur ein simultanes Screening nach Affinitätsbindern, sondern auch ein simultanes Screening nach geeigneten Elutionspuffern. Während die besten Affinitätsbinder die Antikörper gegen die jeweiligen Bakterien waren, wurde das Antibiotikum Polymyxin B als ein Affinitätsbinder für beide Bakterien identifiziert. Der Zucker Methyl-alpha-D-Mannopyranosid wurde aufgrund der gleichzeitigen Elutionsstudien überraschenderweise als geeigneter Elutionspuffer für Polymyxin B entdeckt.

Obwohl Erkrankungen der oberen Atemwege durch Allergie oder bakterielle bzw. virale Infektionen unterschiedlich behandelt werden müssen, können sie aufgrund ähnlicher Symptome schwer unterschieden werden. Biomarker in Nasensekreten, wie Zytokine, können dabei zur Differenzierung verwendet werden. Um eine schnelle und präzise Behandlung zu ermöglichen, ist der schnelle und gleichzeitige Nachweis von verschiedenen Biomarkern entscheidend. Flussbasierte Microarray-Assays übertreffen traditionelle statische Nachweismethoden in Bezug auf Geschwindigkeit und dem gleichzeitigen Nachweis mehrerer Analyten. Daher wurde auf dem MCR-R ein flussbasierter CL-SMIA (Sandwich-Mikroarray-Immunoassay) zur Quantifizierung von Interferon-beta etabliert. Für die Assayentwicklung wurden kommerziell verfügbare Antikörper verwendet, die für einen Sandwich-ELISA

(enzymgekoppelter Immunadsorptionstest) entworfen worden sind. Der Vergleich mit ELISA zeigte vergleichbare Nachweisgrenzen für ELISA und CL-SMIA mit  $1,60 \text{ pg mL}^{-1}$  bzw.  $4,53 \text{ pg mL}^{-1}$ . Während der ELISA 5 Stunden und 40 Minuten benötigte, wurden die Ergebnisse des CL-SMIA bereits nach 1 Stunde und 15 Minuten erhalten. Der Vergleich zeigte, dass ein CL-SMIA bei der gleichzeitigen Detektion mehrerer Analyten und kleineren Probenmengen zeit- und kosteneffizienter ist als ein ELISA. Obwohl in dieser *Proof-of-Principle*-Studie nur ein Biomarker eingesetzt wurde, ebnet sie den Weg für eine zukünftige gleichzeitige Analyse von mehreren Biomarkern im Nasensekret.

Zusammenfassend konnte in dieser Arbeit das große Potenzial affinitätsbasierter Bioassays für die Detektion und die Isolierung komplexer Analyten aus Körperflüssigkeiten auf drei einzigartige Weisen aufgezeigt werden. Die vorgestellte Arbeit kann als Grundlage für zukünftige Entwicklungen in der Diagnostik für besondere Körperflüssigkeiten verwendet werden.

## Abstract

Affinity describes a specific, non-covalent, and therefore reversible interaction between two partners; an affinity binder and its target. One well-known example are antibodies and their antigens. Affinity-based analysis and separation techniques are applied to isolate and detect various analytes like small molecules, proteins, or even cells or bacteria. The presence of specific analytes like biomarkers or bacterial cells in various body fluids can give hints for infections, sepsis, or other diseases. In this thesis, three different approaches were performed to show the application of affinity-based detection and isolation methods for three different analytes from three different body fluids.

For the isolation of extracellular vesicles (EVs) from urine a novel monolithic immunofiltration assay using nanobodies was developed. EVs are small membrane-enclosed vesicles released from cells. Being carriers of cellular information such as proteins, DNA or RNA, EVs and their cargo can be used as biomarkers for different diseases like cancer or neurodegenerative diseases. Traditional isolation methods focusing on size-dependent discrimination like filtration, ultracentrifugation or asymmetrical flow field-flow fractionation, unfortunately lack the ability to discriminate between the cell types the EV origin from. Immunoaffinity-based methods can overcome this problem. Single domain antibodies with high antigen affinity, so called nanobodies, were used as affinity binders. Nanobodies targeting the surface-associated protein CD63 were immobilized indirectly via another nanobody-antigen interaction on a macroporous epoxy-based monolith with pore sizes of  $22.4 \pm 8.8 \mu\text{m}$ . After EV capturing, elution was carried out first competitive followed by pH-dependent elution. With this nanobody-based monolithic immunofiltration it was possible for the first time to isolate roughly  $3 \times 10^{10}$  EVs in two different size categories of about 36 and 130 nm from 7.5 mL of urine.

Infections in body fluids are critical conditions, that have to be treated rapidly and appropriately. In some cases, this is not easily done, like for infected ascites. Ascites is a life-threatening complication of diseases like liver cirrhosis, leading to a large fluid accumulation in the abdominal cavity. Infection with pathogenic bacteria like *Escherichia coli* or *Enterococcus faecalis* is not only one of the biggest causes of ascites-related death but also difficult to diagnose by culture due to very low bacterial concentration. Molecular methods are faster, but more expensive and labor intensive. Here affinity-based enrichment can help to facilitate identification and treatment. Crucial for effective affinity filtration that can facilitate diagnosis through culture are a combination of selective affinity binders and desorbing acting elution buffer. But their interactions are unfortunately not always easily predictable, which leads to a high number of tests that have to be performed to determine both components. The use of bioanalytical screening platforms can hereby reduce the work effort. Therefore, in this thesis, a

flow-based chemiluminescence (CL) microarray screening assay was established on the automated analysis platform, the Microarray Chip Reader – Research (MCR-R). For binding verification of bacteria to immobilized affinity binders, living *E. coli* and *E. faecalis* cells were tagged with biotin. These labeled bacteria were able to bind to streptavidin horseradish conjugates for CL detection on MCR-R. Recoveries of living cells were found to be  $98 \pm 8.8\%$  and  $75 \pm 28\%$  for *E. coli* and *E. faecalis*, respectively. Multiple affinity binder candidates like antibodies or antibiotic acting molecules were immobilized in rows of 5 spots each onto a surface of polycarbonate foil-based microarray chips. Biotin-tagged bacteria were pumped through the microarray chip to interact with the bound affinity binders and detected with the CL assay. Manual flushing of the microarray chip with elution buffer and a second CL detection step allowed not only for simultaneous screening for affinity binders, but also for simultaneous screening of suitable elution buffers. While the best affinity binders were found to be antibodies against the respective bacteria, the antibiotic Polymyxin B was found as an affinity binder for both bacteria. The sugar methyl alpha-D-mannopyranoside was discovered surprisingly as a suitable elution buffer for Polymyxin B, found due to the simultaneous elution studies.

Although upper airways diseases caused by allergy or bacterial or viral infections must be treated differently, it can be hard to distinguish due to similar symptoms. Biomarkers present in nasal secretion like cytokines can be used for discrimination. To enable rapid and precise treatment, fast and simultaneous detection of various biomarkers is crucial. Flow-based microarray assays outdo traditional static detection methods in means of speed and simultaneous detection of multiple analytes. Therefore, a flow-based CL-SMIA (sandwich microarray immunoassay) for the quantification of interferon-beta was established on the MCR-R. Commercially available antibodies designed for a sandwich enzyme-linked immunosorbent assay (ELISA) were used for the assay development. Comparison to the ELISA showed comparable detection limits for ELISA and CL-SMIA with  $1.60 \text{ pg mL}^{-1}$  and  $4.53 \text{ pg mL}^{-1}$ , respectively. While the ELISA took 5 h 40 min to complete, the results from CL-SMIA were obtained after 1 h 15 min. The comparison study showed that CL-SMIA is more efficient in time and cost for simultaneous detection of multiple analytes and fewer sample sizes than ELISA. While in this proof-of-principle study only one biomarker was used, it paves the way for future simultaneous analysis of multiple biomarkers in nasal secretion

Summarizing, in this thesis it was possible to show the great potential of affinity-based bioassays for detection and isolation of complex analytes from body fluids in three unique ways. The work presented can be used as a foundation for future developments of diagnosis in special body fluids.

## List of Abbreviations

AF4	asymmetrical flow field-flow fractionation
BSA	bovine serum albumin
CF	centrifugal force
CL	chemiluminescence
C <sub>q</sub>	quantification cycle
DAB	detection antibody
DNA	deoxyribonucleic acid
ECL	electrochemiluminescence
EDC	1-ethyl-3-(3-(dimethylamino)propyl)carbodiimide
ELISA	enzyme-linked immunosorbent assay
EV	extracellular vesicle
GFP	green fluorescent protein
IFNAR	interferon-alpha/beta receptor
IFN- $\beta$	interferon-beta
Ig	immunoglobulin
ILV	intraluminal vesicle
ISG	interferon-stimulated genes
JAK	Janus-activated kinase
K <sub>d</sub>	dissociation constant
MCR-R	Microarray Chip Reader - Research
MVB	multivesicular bodies
PBS	phosphate buffered saline
PCR	polymerase chain reaction
PEG	polyethylene glycol
PMN	polymorphonuclear
REP-MAF	Rapid Enrichment for Early and High Sensitive Pathogens Detection in Human Body Fluids with Monolithic Affinity Filtration
RNA	ribonucleic acid
SAAG	serum-ascites albumin gradient
SBP	spontaneous bacterial peritonitis
SEC	size exclusion chromatography
SMIA	sandwich microarray immunoassay
SPR	surface plasmon resonance
STAT	signal transducer and activator of transcription

strep-HRP	horseradish-peroxidase-labeled streptavidin
sulfo-NHS	N-hydroxysulfosuccinimide sodium salt
T-RFLP	terminal restriction fraction length polymorphism
TYK	tyrosine kinase
uEV	urinary extracellular vesicle
vHH	single-domain antibodies, nanobodies

## List of Publications

- (1) **Neumair, J.**; Elsner, M.; Seidel, M. Flow-Based Chemiluminescence Microarrays as Screening Platform for Affinity Binders to Capture and Elute Bacteria. *Sensors* **2022**, *22*, 8606.
- (2) **Neumair, J.**; D'Ercole, C.; De March, M.; Elsner, M.; Seidel, M.; de Marco, A. Macroporous Epoxy-Based Monoliths Functionalized with Anti-CD63 Nanobodies for Effective Isolation of Extracellular Vesicles in Urine. *International Journal of Molecular Sciences* **2023**, *24*, 6131.
- (3) **Neumair, J.**<sup>1</sup>; Kröger, M.<sup>1</sup>; Stütz, E.; Jerin, C.; Chaker, A.M.; Schmidt-Weber, C.B.; Seidel, M. Flow-Based CL-SMIA for the Quantification of Protein Biomarkers from Nasal Secretions in Comparison with Sandwich ELISA. *Biosensors* **2023**, *13*, 670.

<sup>1</sup>Shared first authorship.

# Table of Contents

Danksagung .....	i
Kurzzusammenfassung .....	iii
Abstract .....	vi
List of Abbreviations .....	viii
List of Publications .....	x
Table of Contents .....	xi
1 Introduction .....	1
2 Theoretical Background.....	3
2.1 (Immuno-)Affinity.....	3
2.2 Affinity Binders.....	4
2.2.1 Antibodies .....	4
2.2.2 Nanobodies.....	5
2.2.3 Other Affinity Binders .....	6
2.3 Body Fluids .....	7
2.3.1 Urine .....	7
2.3.1.1 Definition and Composition.....	7
2.3.1.2 Formation .....	8
2.3.1.3 Sample Collection.....	8
2.3.2 Ascites .....	9
2.3.2.1 Definition and Sampling.....	9
2.3.2.2 Symptoms and Diagnosis.....	9
2.3.2.3 Etiology and Pathophysiology.....	9
2.3.2.4 Classification and Treatment .....	10
2.3.2.5 Complications.....	10
2.3.3 Nasal Secretion.....	11
2.3.3.1 Definition and Composition.....	11
2.3.3.2 Secretion .....	11
2.3.3.3 Functions.....	11
2.3.3.4 Sample Collection.....	12
2.4 Biomarkers in Body Fluids.....	13
2.4.1 Urinary Extracellular Vesicles as Biomarker .....	13
2.4.1.1 Extracellular Vesicles .....	13
2.4.1.2 Biogenesis of EVs .....	13
2.4.1.3 EV Cargo and Functions.....	14
2.4.1.4 Urinary EVs .....	14

2.4.1.5	Isolation of Urinary EVs .....	15
2.4.1.5.1	Ultracentrifugation.....	15
2.4.1.5.2	Density Gradient Centrifugation .....	15
2.4.1.5.3	Centrifugal Ultrafiltration .....	16
2.4.1.5.4	Size Exclusion Chromatography .....	16
2.4.1.5.5	Precipitation.....	16
2.4.1.5.6	(Immuno)Affinity-based methods .....	17
2.4.1.5.7	Asymmetrical Flow Field-Flow Fractionation .....	17
2.4.1.5.8	Microfluidics.....	18
2.4.1.5.9	Other Methods.....	18
2.4.2	Bacterial Infections in Ascites.....	18
2.4.2.1	Pathogenic Bacteria in Ascites .....	18
2.4.2.2	Detection of Pathogenic Bacteria in Ascites.....	19
2.4.2.2.1	Culture-based .....	19
2.4.2.2.2	Molecular .....	19
2.4.3	Interferon-beta in Nasal Secretions as Biomarker .....	22
2.4.3.1	Biomarkers in Nasal Secretions.....	22
2.4.3.2	Interferon-beta.....	22
2.4.3.2.1	Signaling Pathway of IFN- $\beta$ .....	22
2.4.3.3	Quantification of IFN- $\beta$ in Nasal Secretions .....	23
2.4.3.3.1	ELISA .....	23
2.4.3.3.2	Microarrays/Multiplex Methods .....	23
3	Objectives .....	26
4	Methods .....	28
4.1	Immunoaffinity-based Isolation of uEVs .....	28
4.1.1	Production and Modification of Monolithic Filter for uEV Isolation.....	28
4.1.2	Isolation of EVs from Urine.....	29
4.1.3	Evaluation of Protein Binding Capacity of Monolith .....	29
4.2	Microarray Experiments .....	30
4.2.1	Flow-based Microarray Platform MCR-R.....	30
4.2.2	Production of Polycarbonate Microarray Chips.....	31
4.2.3	Screening Assay for Affinity Binder .....	31
4.2.4	CL-SMIA for IFN- $\beta$ .....	33
4.3	Biotinylation of Bacteria.....	34
4.4	Sandwich ELISA for IFN- $\beta$ quantification .....	34
5	Results.....	36

5.1	Publication 1: Macroporous Epoxy-Based Monoliths Functionalized with Anti-CD63 Nanobodies for Effective Isolation of Extracellular Vesicles in Urine .....	36
5.1.1	Summary.....	36
5.1.2	Own Contribution .....	36
5.1.3	Reprint Permission.....	37
	Reprint of Publication .....	38
5.2	Publication 2: Flow-Based Chemiluminescence Microarrays as Screening Platform for Affinity Binders to Capture and Elute Bacteria .....	51
5.2.1	Summary.....	51
5.2.2	Own Contribution .....	51
5.2.3	Reprint Permission.....	52
	Reprint of Publication .....	53
5.3	Publication 3: Flow-Based CL-SMIA for the Quantification of Protein Biomarkers from Nasal Secretions in Comparison with Sandwich ELISA .....	68
5.3.1	Summary.....	68
5.3.2	Own Contribution .....	68
5.3.3	Reprint Permission.....	69
	Reprint of Publication .....	70
6	Conclusion and Outlook .....	84
7	References.....	90

# 1 Introduction

For most diseases or conditions, a precise and fast diagnosis is crucial for a tailored and successful treatment. Some diseases, such as the common cold or a stomach bug, are often only diagnosed according to the patient's symptoms and physical examination. In other cases, further examination by laboratory examination of body fluids or tissue and imaging techniques such as ultrasound or magnetic resonance tomography is necessary. The human body consists of about 60% water [1]; hence, body fluids make up a large amount of our body. Body fluid biomarkers, such as proteins, cells, biomolecules, and antibodies can be used as biomarkers for diagnosis. Good examples are the high blood sugar concentration for diabetes mellitus diseases [2], multiple cancer markers (proteins, oncogenes, etc.) [3], or antibodies for infections. [4]. In routine analysis, urine and blood, or, more precisely, its fractions serum and plasma, are the most commonly used body fluid. Other body fluids include saliva, cerebrospinal fluid, pleural effusion, lymph, tears, sputum, bronchoalveolar lavage fluid, nasal (lavage) fluid, ascites, pancreatic juice, bile, sweat, amniotic fluid, breast milk, and semen [5,6].

Sample availability hereby depends on the specific volume it is occurring, and the method of sampling, with non-invasive collection making them more accessible. Considering sample volumes, the complexity of the body fluid matrix, and biomarker type and concentration, different approaches for biomarker detection have to be made. Very low biomarker concentrations, as well as complex matrices, require a prior isolation step to increase the effectiveness of their detection. Applying affinity-based methods on medical issues can facilitate biomarker detection and therefore diagnosis and treatment. Affinity-based methods rely on the non-covalent and reversible binding interaction between an analyte and an affinity binder, which occurs between different partners, such as proteins, molecules, or antibodies. Its specific and reversible interactions are great for using it in isolation methods.

Finding an affinity-based method to enrich pathogenic bacteria from ascites and enhancing their detection was also part of the project REP-MAF (Rapid Enrichment for Early and High Sensitive Pathogens Detection in Human Body Fluids with Monolithic Affinity Filtration), a cooperation between the *Klinikum Rechts der Isar* and the Chair of Analytical Chemistry and Water Chemistry. As part of this project, suitable affinity binders had to be chosen. While the binding interaction should be rapid, strong, and, in some cases, quite specific, reversing it to release the analyte should be easy and need conditions that do not harm the analyte. Therefore, in the second part of this thesis, a flow-based chemiluminescence (CL) microarray screening assay was implemented. Targets were pathogenic bacteria in ascites, an abnormal accumulation of peritoneal fluid [7], which can cause life-threatening infections such as spontaneous bacterial peritonitis [8].

Another part of this thesis is the application of immunoaffinity filtration for extracellular vesicles (EVs) from urine. EVs, small membrane-enclosed vesicles released from cells and representing the cell they were released from, gain more and more interest as biomarker carriers. The protein and genetic cargo of urinary EVs (uEVs) hold a great opportunity as biomarkers for diseases such as cancer [9], kidney diseases [10], or even neurological diseases [11]. Additionally, proteins expressed on the EVs surface can be used to determine the cell type they were released from. While the standard isolation methods such as ultracentrifugation or size exclusion chromatography cannot isolate EVs regarding these surface-associated proteins, (immuno-)affinity-based procedures are able to discriminate between these surface associated proteins through their specific interactions. Antibodies, which are part of the immune system of vertebrates, can nowadays be produced and engineered for the desired need relatively easily. Nonetheless, the traditional antibody structure holds some limitations. Single-domain-antibodies, also called nanobodies, can overcome these problems.

Biomarkers in nasal secretion can give evidence of respiratory tract diseases like allergies or infections. To fight these diseases, the human body releases special signaling proteins, such as interferons, which are responsible for immune response in viral infections [12]. Although nasal secretions can be collected non-invasively, the small sample volume requires analytical methods capable of such small sample sizes. Methods testing for multiple analytes are here preferred, as they can analyze multiple analytes with only one measurement and therefore needing less sample for multiple analytes. On-site disease diagnosis requires such multi-analyte methods, that are rapid and easy to use as well. Here again flow-based microarray assays can help. In this thesis's third part, a flow-based CL sandwich microarray immunoassay (SMIA) was developed as a proof-of-concept for biomarker analysis in nasal secretions.

## 2 Theoretical Background

### 2.1 (Immuno-)Affinity

Affinity describes the non-covalent, reversible interaction between two partners: an affinity binder and its target molecule. The higher the affinity towards a molecule, the higher is its selectivity to this molecule. Typical biochemical examples are enzymes and their substrates, membrane receptors and their ligands, or antibodies and their antigens, whereas affinity between the latter is also called immunoaffinity. Affinity strength is specified through the equilibrium dissociation constant  $K_d$ . For an affinity reaction the following applies:



with  $[A]$  and  $[B]$  as the concentration of the affinity binder and the target, and  $[AB]$  as the concentration of the complex. In equilibrium the following is true:

$$K_d = \frac{[A][B]}{[AB]} \quad (2)$$

describing the concentration of target in solution that binds to half of the affinity binder in an equilibrium. The higher the affinity, the lower  $K_d$  [13].

The affinity interaction between (strept-)avidin and biotin is the strongest affinity known with a  $K_d$  of  $10^{-15}$  M. The (strept-) avidin-biotin system is used in various bioanalytical applications such as enzyme-linked immunosorbent assay (ELISA), biosensors, affinity chromatography, immunoprecipitation, cell sorting applications and microarray-based immunoassays [14–16].

$K_d$  can be determined through multiple approaches, whereas methods utilizing surface plasmon resonance (SPR) are mostly used. With SPR the changes of the refractive index close to a metal surface is measured, which is impacted by surface modification. To measure the strength of the affinity, one of the affinity partners is immobilized on the surface while the other one is introduced in solution. The system detects changes of the refractive index near the surface of the sensor, which is dependent on the surrounding fluid and immobilized mass. So, the affinity binding and thereof  $K_d$  can be determined through changes in the angle of the reflected light [17]. Isothermal titration calorimetry is also used for determination of  $K_d$ . It is label free and performed under isothermal and isobaric conditions, measuring the changes in temperature during binding of two molecules, which correlates to a change in enthalpy [18]. Other methods, that are not used that much include ELISA [19] and Förster resonance energy transfer assays [20].

## 2.2 Affinity Binders

### 2.2.1 Antibodies

Antibodies are often used as affinity binders. Antibodies, also called immunoglobulins (Igs), play an important role in the adaptive immune system of vertebrates [21]. If an organism is exposed to an antigen – the target molecule of an antibody –, antibodies are produced by antigen-reactive B-cells. After their maturation into plasma cells, each of them produces antibodies, whereby the binding sites and thus the target structures of the antibodies are very distinct. This leads to a cocktail of different antibodies targeting the same antigen. These antibodies are called polyclonal antibodies. Because the composition of polyclonal antibodies depends on B-cells, it varies over time and also between the immunized individuals. But for well-defined analytical assays, well-defined antibodies are important. Here, monoclonal antibodies can be used. For their production, B-cells from the spleen of immunized organisms are isolated and fused with immortal myeloma cells. Through multiple selection steps, myeloma cells fused to only one clone of B-cells can be selected as a stable hybridoma cell line, which is used for monoclonal antibody production [22]. Another method for antibody production is the generation of recombinant antibodies. Antibody coding genes are inserted into host cells such as bacteria, where they are expressed and can be harvested. The gene responsible for the desired antibody is selected by phage display. Therefore, antibody coding cells are first inserted into bacteriophages, small viruses, where the respective antibody is displayed on the surface. A library is created by a mixture of phages displaying diverse antibodies. The antigen against which the antibody is produced is immobilized and the phage library added. By washing away those phages that do not bind or only bind weakly, only phages carrying the gene for antibodies with good affinity will be obtained. This allows for a higher diversity of antibody structures [23]. Table 1 shows the advantages and disadvantages of the three antibody production strategies.

The main body of an antibody consists of four polypeptide chains: two larger ones, named heavy chains, and two shorter ones, named light chains. The two heavy chains, linked together through disulfide bonds, form the typical Y-form of the antibody. On the outside of the top of the Y, one light chain is connected through disulfide bonds to the heavy chain (Figure 1, left). The heavy and the light chains are the same on both sides, resulting in two identical binding sites. The antibody sequence on the top end of the four chains differs between every antibody type, forming variable regions, the binding sites for the antigens. On the other hand, the rest of the antibody is conserved, forming the constant region [24]. In accordance to differences in their heavy chains, antibodies are divided into five classes: IgA, IgD, IgE, IgG and IgM [25].

Table 1. Advantages and disadvantages of different antibody preparation techniques.

	<b>Polyclonal</b>	<b>Monoclonal</b>	<b>Recombinant</b>
<b>Procedure</b>	Isolation from serum	Fusion of B-cells with myeloma cells	Engineering of genes, expression in host cells
<b>Advantages</b>	Higher affinity, better detection of native protein, easy preparation	Batch-to-batch consistency, specific to one epitope	No need for animals, alteration of antibodies, fast, high quality, batch-to-batch consistency
<b>Disadvantages</b>	Animal use, batch-to-batch variation, no alteration, cross-reactivity	Slow production, animal use, no alteration	Misfolding of proteins, higher costs
<b>Sources</b>	[26]	[23,26]	[23,27]

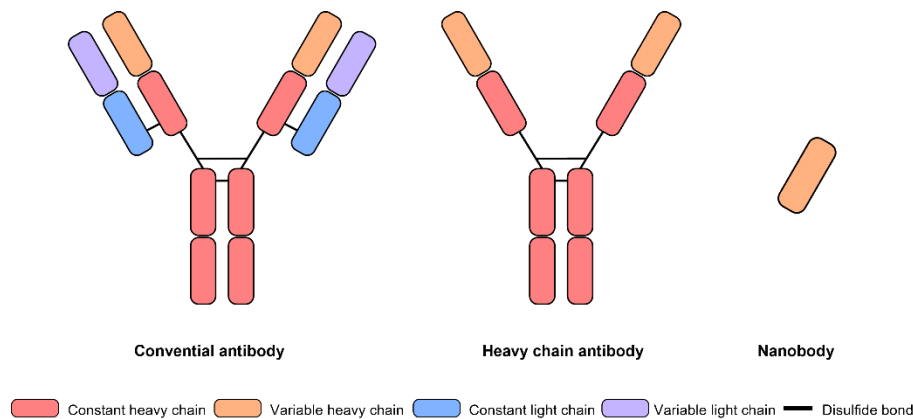


Figure 1. Schematic representation of a conventional antibody, a heavy chain antibody, and a nanobody.

## 2.2.2 Nanobodies

One type of antibody produced recombinantly are nanobodies (Figure 1, right). They resemble the variable domain of a heavy chain antibody and are therefore also called single-domain antibodies or vHH. Heavy chain antibodies, which lack the light chains completely (Figure 1, middle), are commonly found in camelids. Their vHH are just as specific and have the same binding affinity as a whole antibody, becoming a model for nanobodies. In the last 20 years, nanobodies started to gain more and more attention and are also used as constructs of dimers

or polymers. Their recombinant production allows the addition of tags or other modifications before expression. While bacterial expression is cheaper, mammalian cells allow for more complex nanobodies [28]. With their size of under 15 kDa, nanobodies are ten times smaller than traditional IgGs. Nanobodies hold many advantages, such as low-cost production, stability, small size, strong tissue penetration, high affinity and good solubility [29]. Thus, their application in medical research is of high interest. They are used in molecular imaging of tumors and cancers as fluorescent or radio-labeled markers and also for the use as therapeutic agents for example in oncology, neurodegenerative diseases, or infectious diseases [30].

Additionally, they are used in bioanalytical assays such as ELISA [31] or immunomagnetic assays [32]. Through immobilization on chromatographic phases, nanobodies can also be used for immunoaffinity chromatography [33]. Recently, nanobodies against EVs were isolated by immunoaffinity chromatography holding great opportunities for EV concentration from body fluids [34].

### **2.2.3 Other Affinity Binders**

Peptides are also often used in affinity-based applications. Compared to antibodies, they can be produced more easily and more cost-efficiently, are easier to modify and label, and for therapeutic applications, penetrate tissue easier and can even additionally function as therapeutic agents. While natural peptides can lack in affinity and specificity, biochemical engineered peptides can overcome this issue [35]. For optimal antimicrobial activity antimicrobial peptides need high affinity towards their target. Their interaction with cell wall-associated structures allows the binding of a sufficient amount of peptides to the target to be effective in cell destruction [36]. So, for example Polymyxin B, an antibiotic polypeptide, binds through its cationic properties to the phospholipids and lipopolysaccharides of gram-negative bacteria where it destabilizes the outer cell membrane [37]. This affinity was already utilized for a monolith-based affinity filtration of *Escherichia coli* [38].

Also, bigger proteins like the lectin Concanavalin A can be used as affinity binders. Concanavalin A interacts with sugar moiety on the surface of bacterial cells and is already used in biosensors [39]. As mentioned in 2.1, enzymes and their substrates also connect via affinity. The higher the affinity of a substrate, the more likely the enzyme will favor it [40]. In this way also the enzyme lysozyme interacts with the peptidoglycans of gram-negative cell walls to destroy and kill the bacterial cells [41].

## 2.3 Body Fluids

Since the human body consists of about 50 - 60% water, body fluids make up a majority of the human body [42]. Examples for body fluids are blood, urine, saliva, sperm, nasal secretions, ascitic fluids, lymph, tears, cerebrospinal fluid, or milk. They serve all different purposes and differ in their consistence, appearance and composition. Proteins and other molecules can serve as biomarkers for the overall health status or diseases of a patient and make them interesting for clinical diagnosis [43]. Depending on the accessibility of body fluids, they are sampled either invasively like blood or other internal fluids or non-invasively such as urine or sweat. Table 2 gives an overview of which body fluids are typically collected invasively or non-invasively. In the next subchapters, the three body fluids relevant to this thesis – urine, ascites and nasal secretions – are described in more detail.

Table 2. Different body fluids and their classification according to invasive or non-invasive sampling.

<b>Body fluid</b>	<b>Sampling</b>	<b>Source</b>
<b>Blood</b>	Invasive	[44]
<b>Saliva</b>	Non-invasive Invasive (from special glands)	[45]
<b>Urine</b>	Non- invasive Invasive (catheter)	[46,47]
<b>Nasal secretion</b>	Non-invasive	[48,49]
<b>Cerebrospinal fluid</b>	Invasive	[50]
<b>Ascites</b>	Invasive	[51]

### 2.3.1 Urine

#### 2.3.1.1 Definition and Composition

Urine is a sterile, slightly yellow body fluid stored in the urinary bladder until excreting through the urethra. Its primary function is removing metabolic waste products and bioactive substances like drugs or hormones from the blood. Additionally, urine excretion regulates the human body fluid content and electrolytes [52]. It is produced in the kidney and is composed of water (approximately 95%), urea, creatine, uric acid, ammonia, and water-soluble compounds like toxins and electrolytes [53,54]. Urochrome and the degradation product of hemoglobin, urobilin, are responsible for the yellow color [55]. The intensity of the color depends on the concentration of these pigments, which can make the color an indicator of hydration [55,56].

### **2.3.1.2 Formation**

The human body produces around 1.7 liters of urine every day. Urine is produced in the kidneys, where the blood is filtered. The process starts at the glomeruli, capillary systems surrounded by a capsule and parts of the nephrons, small parts of the kidneys. Inside these glomeruli, water and soluble components of the blood pass a membrane into the glomerular capsule, whereas large components like blood cells or large proteins are retained in the blood. However, not only waste is filtered from the blood, but also essential substances like amino acids, glucose, smaller proteins, or ions. As the filtrate, the so-called primary urine, enters deeper into the nephron, it passes the renal tubule. Here, the essential substances and some of the water are reabsorbed into adjacent capillaries and, consequently, the blood. Simultaneously, waste ions and hydrogen ions absorb into the renal tubule. The combination of these components and the remaining filtrate is what is called urine. The urine exits the nephrons and the kidney and enters the urinary bladder over the ureter, where it is stored until it is excreted through the urethra [57,58].

### **2.3.1.3 Sample Collection**

Urine is typically sampled non-invasively during urination. The urine is hereby collected in a container. Samples are collected either in spot collections, where the urine of only one urination is collected or in pooled collections of all urine over 24 h. As for a 24-hour collection the effort, expenses, and the discomfort of the patient are high, as well as contamination, degradation over time, and incomplete sampling play a role, a single collection is mostly preferred [47,59]. Spot collection can either be performed randomly over the day [60] or timed, where mostly the first [61] or second urine of the day is collected [62]. Other sampling techniques include first-void catches, where only the first 20–30 mL of urine are collected [63], and midstream urine sampling, where the first part of the urine stream is discarded, and only the middle part is collected [64], what is mainly used for diagnostics of infections [64,65]. Occasionally, urine is also collected through catheters [46].

## **2.3.2 Ascites**

### **2.3.2.1 Definition and Sampling**

Ascites is an abnormal accumulation of peritoneal fluid inside the peritoneal cavity, the space between the membranes (peritoneum) that line the organs, abdomen, and pelvis. In healthy individuals, the volume of peritoneal fluid is about 5–75 mL [66–68]. Ascitic fluid, however, can accumulate up to several liters [69], with as many as 40 L possible [70]. The composition of ascitic fluid is complex, consisting of water, proteins, enzymes, sugars, cellular elements, electrolytes, and other components like bilirubin (a colored component) and, occasionally, lipids [71,72]. Ascitic fluid is collected invasively by paracentesis, via inserting a needle or catheter into the peritoneal cavity. The fluid is collected into a syringe for small volumes or into vacuum bottles or drainage bags for larger volumes [51].

### **2.3.2.2 Symptoms and Diagnosis**

The symptoms of ascites are an increase in abdominal girth, weight gain, feelings of satiety, abdominal pain, and, in case of more extensive fluid accumulation, a shortness of breath [66,73]. Ascites is diagnosed through physical examination and patient history evaluation and confirmed through abdominal ultrasound. After successful diagnosis of ascites, diagnostic paracentesis and subsequent analysis of the ascitic fluid is performed to find the underlying cause [66,68,73,74].

### **2.3.2.3 Etiology and Pathophysiology**

The leading cause of ascites is liver cirrhosis, accounting for approximately 80% of all cases. Additionally, cancer (malignant ascites, 10%), cardiac failure (3%), tuberculosis (2%), and other (3%) are causes of ascites [7]. The serum-ascites albumin gradient (SAAG) is an indicator if ascites development is caused by portal hypertension ( $\text{SAAG} \geq 1.1 \text{ g dL}^{-1}$ ) or other causes like malignancy, tuberculosis, or nephrotic syndrome. Portal hypertension, described as an elevated pressure over 12 mmHg on the liver's portal veins, along with sodium and water retention, is the main causative factor of ascites [66]. In cases where the SAAG indicates portal hypertension, the total protein content of the ascitic fluid provides more information on the underlying cause. A value below  $2.5 \text{ g dL}^{-1}$  suggests cirrhosis or late Budd-Chiari syndrome – a liver illness. However, a value above  $2.5 \text{ g dL}^{-1}$  indicates early Budd-Chiari syndrome, heart problems, or sinusoidal obstruction syndrome – a liver vascular injury disease [75]. For patients with liver cirrhosis, approximately 50% of compensated cirrhosis – meaning in the asymptomatic stage – develop ascites within the next ten years [76]. The pathophysiology of

malignant ascites includes the blocking of the lymphatic drainage, which leads to insufficient removal of lymph and consequent accumulation of ascitic fluid, as well as an increased vascular permeability caused by growth factors and cytokines [77].

#### **2.3.2.4 Classification and Treatment**

The International Club of Ascites categorized ascites into three stages based on their severeness. *Stage 1* is a mild form that is not yet visible and can only be detected by ultrasound examination. *Stage 2*, also called moderate ascites, is already visible through moderate abdominal distension. In *Stage 3*, also called large ascites, the distensions already grow larger [78]. For *Stage 1* ascites, the primary focus lies in treating the underlying cause of ascites. Nevertheless, a low-sodium diet is recommended to counteract the development of *Stage 2* ascites. Patients with *Stage 2* ascites are treated with a low-sodium diet and the administration of diuretics. For *Stage 3*, a large-volume paracentesis is recommended, accompanied by an albumin infusion [77–80]. According to the International Club of Ascites, if standard treatment of ascites with a low sodium diet or diuretics cannot decrease the amount of ascites (at least to *Stage 1*) or prevent further ascites formation after therapeutical paracentesis, it is called refractory ascites [81]. For cirrhotic ascites, 5–10% of cases develop into refractory ascites each year [82], where the survival one year after diagnosis is only 50% [7]. Treatment of refractory ascites typically involves therapeutical paracentesis or the use of a transjugular intrahepatic portosystemic shunt [79].

#### **2.3.2.5 Complications**

The emergence of cirrhotic ascites often comes with other complications like hepatic hydrothorax, hepatorenal syndrome, and various infections. Hepatic hydrothorax is a pleural effusion without cardiac or pulmonary cause [83]. Hepatorenal syndrome describes the decrease in kidney function due to liver cirrhosis. An insufficient blood volume in the arteries leads to narrowing of the blood vessels inside the kidney (renal vasoconstriction), which causes a decrease in their function [84,85]. Bacterial [8] and fungal infections [86–88] of the ascitic fluid are other complications.

### **2.3.3 Nasal Secretion**

#### **2.3.3.1 Definition and Composition**

Nasal secretion is a viscoelastic bilayer fluid covering the epithelium inside the nose with a thin film. The bottom part of the bilayer fluid, called periciliary fluid or sol-layer, has a lower viscosity and covers the epithelium and its cilia [89]. These are hair-like extensions on the epithelium cell walls that can move in a rhythmic motion, also called beating [90]. The top layer is formed by high-viscous mucus [89]. Nasal secretions consist of 95% water, 2% glycoproteins (mucin), 1% electrolytes, 1% lipids, and 1% other proteins, where albumin makes up the most prominent part with 15% [91,92]. Mucins, large, liquid-binding glycoproteins, are responsible for the density of the nasal secretions. Through their complex structures, they form gel-like structures through crosslinking [93]. They also facilitate the trapping of bacterial cells inside the mucus layer through interactions of the bacterial cell wall and the present mucins [94].

#### **2.3.3.2 Secretion**

Nasal secretion is produced in the surface epithelial goblet cells, submucosal glands, and surface epithelial serous cells [95]. Elevated production of nasal fluid can lead to a running nose, also called rhinorrhea, and a postnasal drip, where the fluid runs down the throat. Causes for this elevated nasal secretion production are sinusitis (inflammation of the nasal sinuses) [96], nasal polyps [97], cold weather [98], or rhinitis. Rhinitis describes an inflammation of the nasal mucosa and has, besides rhinorrhea, other symptoms like sneezing, nose itching, or nasal obstruction. Rhinitis can be classified into four groups: allergic rhinitis, infectious rhinitis, non-allergic, non-infectious rhinitis, and mixed rhinitis [99]. Non-allergic, non-infectious rhinitis is described as rhinitis without detectable infection or measurable IgE levels, suggesting an allergy [99]. It can be caused by drugs [100], hormones (e.g. in pregnancies) [101], and hot or spicy food (gustatory rhinitis) [102]. Also, age-related rhinitis [103] and idiomatic rhinitis [104], with no identifiable cause, exist. Additionally, rhinitis can be classified as occupational rhinitis, where permanent exposure to workplace-related triggers like flour dust or animal hairs leads to allergic or non-allergic rhinitis [105].

#### **2.3.3.3 Functions**

One function of the nasal secretion is the protection of the epithelium and the respiratory tract from environmental impacts entering the nose along with the breathing air. These particles, such as dust, bacteria, viruses, or allergens, are captured in the mucus layer, which is then transported out of the nose by cilia beating, also called nasal mucociliary clearance [106,107].

Additionally, nasal secretion holds antimicrobial properties due to present immunoglobins [108] and antimicrobial peptides like lysozyme, lactoferrin, and defensins [109]. Other functions of nasal secretions involve lubrication of the nose and humidification of the inhaled air [110], as well as being a transport medium of odors in olfaction (smelling) [111].

#### **2.3.3.4 Sample Collection**

Nasal fluid collection can be performed in multiple ways: through spontaneous secretion, washing of the nasal cavities, or absorption-based methods. The former includes nose blowing [112] and aspiration via suction [48]. This can be problematic for healthy individuals, as they do not produce a sufficient amount of nasal secretions. Large differences in sample volumes may occur, as it depends on the volume of nasal secretion present during sampling. Those collection methods class together with nasal washing, or also lavage, as bulk collection methods. For nasal washing, the washing liquid is introduced into the nose and collected afterwards, leading to a large sample volume but also to unknown and high sample dilutions. The sampling fluid, commonly buffered saline, can either be run through the nose (nasal irrigation) or incubated there for 20–30 minutes before collection (nasal pool). Using a NaCl spray as a washing fluid allows for smaller sample volumes. The most preferred is a sample collection via absorption-based methods, which collect nasal secretions focally. Various materials are used, like cotton, polyurethane sponges, filter paper, synthetic absorptive matrices [49], and sinus packs [113]. The absorptive materials are placed in the nose and incubated for 1–10 minutes before removing them. The nasal fluid is removed from the absorptive material via optional buffer addition and centrifugation. Concluding has to be remarked that every sampling method has its benefits but also drawbacks. This makes it necessary to consider before use which one might be suitable [114]. Also, it has to be considered that a - probably unknown - dilution during sampling might influence the analyte concentration [115].

## **2.4 Biomarkers in Body Fluids**

Biomarkers are “*characteristic[s] that [...] [are] objectively measured and evaluated as [...] indicator[s] of normal biological processes, pathogenic processes, or pharmacologic responses to a therapeutic intervention*” [2]. For body fluids these can be blood sugar [2], proteins [43], antibodies [4] or cancer markers [3]. As biomarkers are of great value for diagnosis, their isolation and detection have to be perfected. In the following, an overview of the three different biomarkers relevant to this thesis will be given.

### **2.4.1 Urinary Extracellular Vesicles as Biomarker**

#### **2.4.1.1 Extracellular Vesicles**

EVs are heterogeneous, membrane-enclosed bilayer vesicles released by various cells into the surrounding extracellular space and responsible for cell-to-cell communication [116]. EVs are broadly divided into subgroups, depending on their size as well as place and mechanism of origin. Exosomes, with a size of 40–150 nm, are produced from the endosomal system, whereas the bigger microvesicles (size range 150–1000 nm) - also called shedding vesicles or ectosomes - originate in the plasma membrane. As a third big group, apoptotic bodies are released during programmed cell death from apoptotic cells and range between 1–5000 nm [117]. Other groups of EVs, like matrix vesicles, stressed EVs, or autophagic EVs, have been discovered but are not as prominent as the other three “classical” groups mentioned beforehand [117]. As research on EVs only started in the 1980s and is still ongoing and evolving [118], the classification of these groups is still changing and adapting [117,119].

#### **2.4.1.2 Biogenesis of EVs**

As mentioned before, the subgroups of extracellular vesicles differ in their place and mechanism of formation. Exosomes are formed in the cells, starting from endosomes. Through inward budding of the endosomal membrane, also called invagination, the exosome cargo is introduced into the endosomes as intraluminal vesicles (ILVs), converting the endosomes into late endosomes/multivesicular bodies (MVBs) [120]. Transport of the MVBs along microtubules to the plasma membrane and their fusion releases the ILVs as exosomes into the extracellular space (Figure 2, right). Fusion of the MVBs with lysosomes or autophagosomes, on the other hand, leads to intracellular degradation [121,122]. Microvesicles are formed by an outward budding of the plasma membrane (Figure 2, top left). A change in the proteins and lipids on the cell wall is responsible for the cell membrane change [123]. Apoptotic bodies are formed during the apoptosis of cells and the decay of their

membrane. The cell membrane forms circular blebs that are released into the extracellular space. Depending on the cell type, either single vesicles or a “beads-on-a-string” systematic are formed (Figure 2, bottom left) [124,125]. After secretion, EVs can be found in various body fluids such as blood [126], urine, saliva [127], breast milk [128], ascitic fluid [129], or cerebrospinal fluid [130].

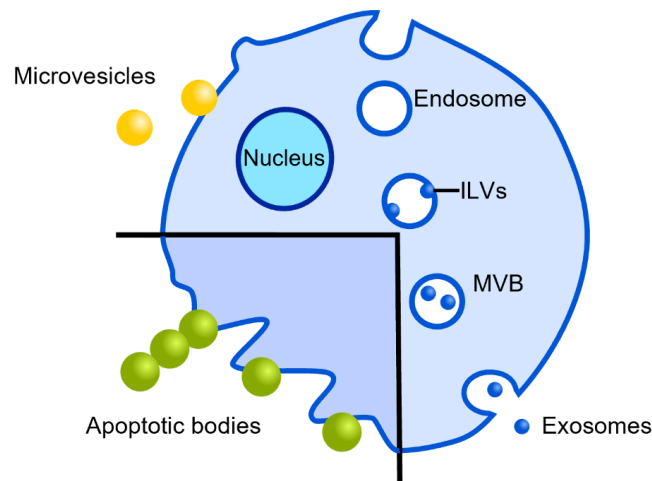


Figure 2. Biogenesis of extracellular vesicles (EVs).

#### 2.4.1.3 EV Cargo and Functions

Extracellular vesicles carry various bioactive molecules such as proteins, deoxyribonucleic acid (DNA), ribonucleic acid (RNA), and lipids [131]. When first discovered, it was believed that cells removed unwanted material via EVs [132]. However, further research showed their function in physiologically and pathologically cell-to-cell communication. Through interchanging their bioactive cargo, EVs are responsible for intercellular signaling [116], hemostasis [133], immune response [134], and disease progression such as tumorigenesis [9], spreading of viruses [135] or other neurodegenerative diseases like Alzheimer’s disease [136]. Membrane-associated proteins on the EVs are not only markers for their origin cell but also affect the cell type of the acceptor cell and can even help with their uptake [136].

#### 2.4.1.4 Urinary EVs

As urine can be collected easily, non-invasive, and in large volumes, it makes a suitable matrix for EVs. UEVs are secreted from cells inside the urinary tract, including the kidney, urinary bladder, as well as the ureter and urethrae. This allows us to use them as biomarkers for renal [10,137,138] and urogenital diseases [139,140], but also for neurological diseases [11].

### **2.4.1.5 Isolation of Urinary EVs**

For the isolation of uEVs, multiple methods have been developed. Most of the separation methods rely on physical parameters like density, weight, or size. This allows on the one hand for size-dependent isolation, but on the other hand neglect the differentiation of their cells of origin. Affinity-based methods can overcome this, but then lose the size-dependent isolation.

#### **2.4.1.5.1 Ultracentrifugation**

Ultracentrifugation is currently the most applied method for the isolation of uEVs. Here, the urine sample is centrifuged with a high velocity over a long period. A speed of 100,000–200,000 × g over at least one hour is commonly used [141,142]. For better isolation, often differential ultracentrifugation is performed, where before the ultracentrifugation a slower centrifugation step at 1000–20,000 × g is introduced to remove other larger vesicles, dead cells, and debris (Figure 3, a) [143].

Although ultracentrifugation is commonly used, it yields a low recovery rate for uEVs. Responsible are the damaging of cells due to high centrifugal forces and incomplete sedimentation of the vesicles [144,145]. For differential ultracentrifugation, some uEVs are discarded through the pellet during the slower centrifugation steps [146].

During ultracentrifugation, the polymeric network forming Tamm-Horsfall protein – also called uromodulin - is enriched as well. In this network, EVs can be trapped, influencing their yield. The addition of dithiothreitol can disturb the network and increase the yield of EVs [141,147]. Another method to eliminate the Tamm-Horsfall protein is the addition of salt [148]. In proteinuria – abnormal urine with a high amount of proteins - ultracentrifugation not only enriches EVs but also the highly abundant proteins, which can interfere with a proteomic analysis of the vesicles. Here, a combination of ultracentrifugation with subsequent size exclusion chromatography eliminates these proteins [149].

#### **2.4.1.5.2 Density Gradient Centrifugation**

Another centrifugation-based isolation method for uEVs is density gradient centrifugation. A density gradient is generated over the centrifugation tube using sucrose [148] or iodaxonal [150], with the sample added to the top [148] or bottom [150] of the gradient. During centrifugation with approximately 100,000 × g, the components of the sample travel through the density gradient and pool at that point, where their buoyant density and the density of the gradient correspond (Figure 3, b) [151]. In this way, fractions containing different sizes of uEVs

can be obtained. Again, the Tamm-Horsfall protein must be removed for density gradient centrifugation [150].

#### **2.4.1.5.3 Centrifugal Ultrafiltration**

An easy to perform approach for uEV isolation is centrifugal ultrafiltration using nanomembrane filters. Urinary samples are added into these filters with cut-offs at 10 to 100 kDa and centrifuged until the desired volume remains in the filter reservoir (Figure 3, c). This method is fast and easy to implement but also enriches other proteins [152]. Centrifugal filtration is primarily performed in combination with other methods for enriching the uEVs (and other components of the urine) before the actual isolation method. This is especially done before techniques that separate the uEVs into size-dependent fractions [144].

#### **2.4.1.5.4 Size Exclusion Chromatography**

Size exclusion chromatography (SEC) separates particles according to their size inside a stationary phase. This stationary phase, also called gel, consists of beads of porous materials like silica [144] or polymerized agarose [153], dextran, polyacrylamide, or allyldextran [154]. While smaller particles are trapped inside the pores during the passing of the column and, therefore, need a longer time to be eluted, larger particles pass the pores and are eluted first (Figure 3, d) [155]. This allows a size-dependent fractionation of the obtained uEVs [156]. Before SEC, the urine sample is often processed and enriched through filtration [153,157]. The sample is loaded on top of the SEC column, flushed with a running buffer, and collected in fractions.

#### **2.4.1.5.5 Precipitation**

Another method for isolating uEVs is precipitation. Adding a hydrophobic precipitation agent decreases the solubility and sedimentation rate of the uEVs, allowing for pelleting the uEVs using a slow centrifugation speed (Figure 3, e) [158]. Commonly used as a precipitation agent is polyethylene glycol (PEG) [139,159]. Combining another aggregation agent with PEG can enhance the uEV isolation [160]. Commercially precipitation-based kits like ExoQuick-TC from System Biosciences [161] or the Total Exosome Isolation Reagent from Invitrogen™ [162] are available.

#### 2.4.1.5.6 (Immuno)Affinity-based methods

For more specific and pure isolation of uEVs, (immuno)affinity-based methods are available. These methods aim for membrane-associated molecules of the uEVs. Lectins are also used due to their ability to bind to saccharide residues. They cause an aggregation of the uEVs, which can be pelleted through centrifugation [163]. Peptides binding to heat shock proteins use the same mechanism [164]. For immunoaffinity approaches, antibodies mainly against the tetraspanins CD63, CD9, and CD82 are used [143]. The antibodies are bound onto carriers like magnetic beads (Figure 3, f) [165] or microtiter plates [143], allowing for a versatile application.

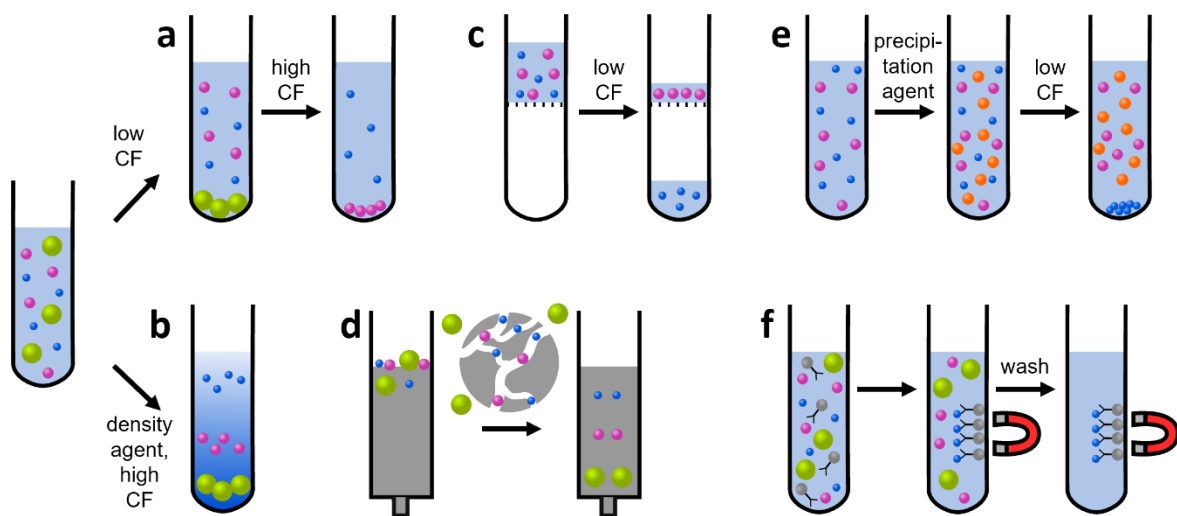


Figure 3. Schematic presentation of isolation methods for urinary extracellular vesicles (uEVs). a) Differential ultracentrifugation using low centrifugal force (CF) followed by a high CF. b) Density gradient centrifugation. c) Centrifugal ultrafiltration. d) Size exclusion chromatography (SEC). e) Precipitation of uEVs followed by low CF. f) Immunomagnetic isolation.

#### 2.4.1.5.7 Asymmetrical Flow Field-Flow Fractionation

Recently, asymmetrical flow field-flow fractionation (AF4) has started being used to isolate uEVs. Here, two streams separate particles based on their size and molecular weight. By applying a cross-flow over the main stream, particles and, therefore, EVs are distracted from their initially straight path, separating different particle species. After a prior isolation of the particles, AF4 can be used to separate uEVs into fractions with different sizes [166].

#### **2.4.1.5.8 Microfluidics**

Multiple microfluidic approaches were made to enhance the speed and effectiveness of the isolation of uEVs. They rely on the concepts previously described, like filtration [167] or flow field-flow fractionation [168], but also on others, like acoustic trapping [169] or deterministic lateral displacement using pillar arrays [170]. Microfluidic devices can be operated by centrifugation [167] or by pumping the fluid through the device [171]. Microfluidic approaches allow for the easy integration of subsequent analysis [167,171].

#### **2.4.1.5.9 Other Methods**

There are different other methods for the isolation of uEVs. In hydrostatic filtration dialysis, the dialysis tube is connected to a sample reservoir, which passes the dialysis tube through hydrostatic pressure. The particles are trapped inside the dialysis tube according to its weight cutoff and are concentrated into a smaller volume [172].

Another method is the isolation using a two-phase system. A mixture of PEG and dextran is added to the urine sample, separating the PEG and dextran phase. Through centrifugation the uEVs are then trapped in the latter [173].

### **2.4.2 Bacterial Infections in Ascites**

#### **2.4.2.1 Pathogenic Bacteria in Ascites**

Bacterial infections of ascites are serious complications which can lead to sepsis, a systemic inflammatory response syndrome due to infection. Starting with fever, elevated pulse and respiration, the symptoms can worsen to organ failure (severe sepsis) or circulatory failure and even death (septic shock) [174].

Ascitic infections can be divided into five groups: monomicrobial non-neutrocytic bacterascites, polymicrobial bacterascites, secondary bacterial peritonitis, spontaneous bacterial peritonitis (SBP), and culture-negative neutrocytic ascites. Bacterascites is diagnosed with an amount of polymorphonuclear (PMN) cells in the ascitic fluid of less than 250 cells per microliter. In contrast, an amount of more than 250 cells per microliter of PMN cells are found if peritonitis or culture-negative neutrocytic ascites is diagnosed [8]. While for secondary bacterial peritonitis, the source of bacteria can be treated surgically, SBP has no such source and is caused by bacterial translocation. SBP is a severe complication, leading to a mortality rate of 30–90% within the first year after its first occurrence. Although SBP is most common in cirrhotic

ascites, cases with other types of ascites have also been reported, like cardiac ascites [175], nephrotic ascites [176], or malignant ascites [177]. Responsible for SBP are both gram-negative and gram-positive bacteria [178,179]. Bacterial species include *E. coli*, *Klebsiella*, *Enterococcus*, *Staphylococcus*, and *Streptococcus* [180,181]. SBP is treated by the administration of antibiotics and injections of albumin [8].

## **2.4.2.2 Detection of Pathogenic Bacteria in Ascites**

### **2.4.2.2.1 Culture-based**

Bacterial detection in ascitic fluids is a crucial step for treatment of ascites-related infections. The current gold standard for clinical detection are culture methods. Ascitic samples are inoculated either into blood-culture bottles or applied on culture plates. After a positive culture result, bacterial species are identified mainly using mass spectrometry [182]. Not only does incubation take up to several days, but false negative results are also common, especially if antibiotic treatment has already started [183]. Molecular approaches were developed to overcome this issue.

### **2.4.2.2.2 Molecular**

Culture-independent molecular approaches like polymerase chain reaction (PCR) [184–186], terminal restriction fragment length polymorphism (T-RFLP) analysis [184,187], sequencing [188] and hybridization were developed to detect bacteria in ascites rapidly. Drawbacks of this methods are the higher costs and the need of special trained personal. In the following, the mentioned molecular methods will be described in more detail.

#### *PCR*

PCR (Figure 4) is a common molecular method to multiply DNA and to identify the source of this DNA. First, the double-stranded DNA is denatured into single strands to which, in the second step, the annealing, primers bind to the single-stranded DNA. Primers are short single-stranded sequences (10–30 nucleotides) that correspond complementary to specific regions in the target DNA, allowing for their hybridization. Primers are used as pairs, one for the one strand of double-stranded DNA (5' to 3') and one for the other (3' to 5'), marking the beginning and end of the sequence to be amplified. The last step is the elongation step where the polymerase binds to the single-stranded DNA at the end of the primer and starts incorporating nucleotides complementary to the single-stranded DNA, leading to elongation of the primer, hybridization to the single-stranded DNA to double-stranded DNA and consequently to a copy of the double-stranded DNA. Typically, these three steps are repeated for 20–40 cycles [189].

For quantitative determinations, also called real-time PCR, fluorescence is introduced into the amplified sequences, which multiplies with every cycle [190].

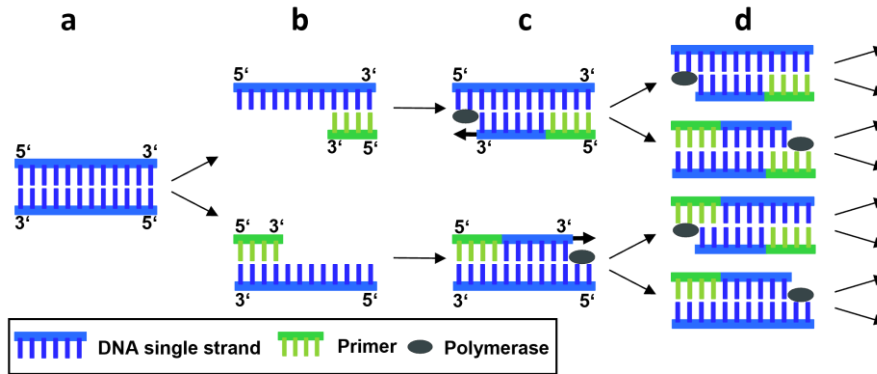


Figure 4. Schematic illustration of the polymerase chain reaction (PCR). A) Double-stranded deoxyribonucleic acid (DNA) is spliced into b) single-stranded DNA through denaturation. In the annealing step, primers bind to the single-stranded DNA, complementary to their sequence. c) During the elongation step, polymerase elongates the primer sequence according to the complementary single-stranded DNA. D) Multiple PCR cycles are performed to obtain a sufficient amount of DNA.

### *T-RFLP*

T-RFLP profiling is a fingerprinting assay based on PCR and electrophoresis. Depending on the length between the restriction site and the labeled ends of the amplified gene, a T-RF band is generated, that can be associated with a bacterial species. First, the DNA is amplified using fluorescence-labeled primers. Then, restriction enzymes cut the amplicons at specific restriction sites into fragments. During gel electrophoreses, these fragments are separated according to their length. Only the fluorescence-labeled fragments are detected by a sequencer, leading to identification and quantification of bacterial species according to the length of the labeled and restricted fragment (Figure 5) [191]. In ascites, T-RFLP is performed after a centrifugation step before DNA extraction. Because in the T-RFLP all fragments are detected according to their length, even more than one species can be detected in one sample [184,187]. In the presented studies, up to 79 different T-RF bands were able to detect [184].

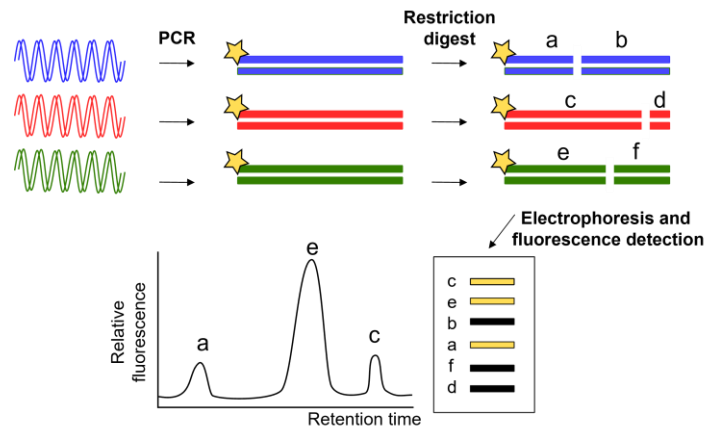


Figure 5. Graphical representation of terminal restriction fragment length polymorphism (T-RFLP) analysis. Sample DNA is amplified with fluorescence-labeled primer and digested with restriction enzymes, leading to various labeled and unlabeled fragments. The fragments are separated through gel electrophoresis, and fluorescence is detected.

### Sequencing

The sequence of bases in DNA or RNA can be determined, through sequencing. In principle, sequencing works by amplifying the sample DNA after an initial PCR step, adding color-coded fluorescent bases and reading the sequence of the fluorescence. The first sequencing method developed was the Sanger-sequencing, where the normal bases and fluorescence-labeled bases are added to the sample DNA. Additionally, the fluorescent bases were coupled to a chain terminator. These different sized fragments, which are coded regarding their last base, are separated by electrophoresis and analyzed. As this method is slow and expensive, next-generation sequencing was developed. Here, the DNA is fragmented, immobilized on a support surface and amplified with fluorescent bases. After every amplification step, fluorescence is measured, creating the sequence of DNA. Without the use of prior amplification, third generation sequencing evolved. One of the most used methods is nanopore sequencing, which can determine the sequence in real time by measuring the changes in ion flow while the DNA passes a narrow channel [192].

In ascites, sequencing is performed without sample preparation, but after a prior PCR. Next-generation sequencing [188,193], but also sanger sequencing [186,194] or nanopore sequencing [188,194] were applied for bacterial identification in ascites.

## **2.4.3 Interferon-beta in Nasal Secretions as Biomarker**

### **2.4.3.1 Biomarkers in Nasal Secretions**

To correctly diagnose and treat diseases of the upper airway, especially to distinguish between different types of rhinitis, biomarkers in nasal secretions can be analyzed [195]. Typical biomarkers are for example IgE for allergic rhinitis [196], or cytokines. Cytokines are a family of proteins that help regulating the immune system by participating in cell-to-cell signaling. The cytokine super-family holds hundreds of members, mostly from sub-families, including tumor necrosis factors, the transforming growth factor- $\beta$  family, interleukins, chemokines, and interferons [197]. Analyzing the change of cytokine levels during diseases, conclusions on the underlying cause can be drawn [198], for example elevated Interferon type I levels for viral infections [199]. Interferons are growth-inhibiting and potent antiviral. Their name even was derived from their ability to interfere with viral replication [200]. Interferons are grouped into three classes according to their genetic sequence: types I, II, and III. One member of the type I class is Interferon-beta (IFN- $\beta$ ).

### **2.4.3.2 Interferon-beta**

IFN- $\beta$  is produced in a variety of cells like macrophages, endothelial cells, and fibroblasts. Upon viral infection, the cell's pattern recognition receptors recognize the virus through their pathogen-associated molecular patterns and activate the IFN production. Therefore, the interferon response factor 3 is phosphorylated, dimerized, and transported into the cell's nucleus. Here, together with the nuclear factor kappa B and the activator protein 1, it triggers transcription of the IFN- $\beta$  gene, and IFN- $\beta$  is produced and secreted from the cell [12].

#### **2.4.3.2.1 Signaling Pathway of IFN- $\beta$**

On cell surfaces there are binding receptors for type I IFN. These receptors consist of two subunits, Interferon-alpha/beta receptor (IFNAR) 1 and IFNAR2, which interact with two members of the Janus-activated kinase (JAK) family - tyrosine kinase 2 (TYK2) and JAK1, respectively. When a type I IFN connects with the binding receptor, it causes IFNAR1 and IFNAR2 to rearrange and dimerize, and signal transducing begins. TYK2 and JAK1 then become autophosphorylated and activated, after which they regulate the phosphorylation and activation of STATs (signal transducer and activator of transcription). These STATs form homo- or heterodimers together with the Interferon-regulatory factor 9, which then enter into the cell nucleus, where they bind onto IFN-stimulated genes (ISGs) and start their transcription [201]. The proteins coded by these ISGs are, among other things, involved in antiviral defense

[202], immune modulation [203], and tumorigenesis regulation [204]. This entire pathway is known as the JAK-STAT pathway.

### **2.4.3.3 Quantification of IFN- $\beta$ in Nasal Secretions**

For quantification of IFN- $\beta$  in nasal secretions, multiple immunoaffinity-based methods are applied. In the following, these methods will be described in more detail.

#### **2.4.3.3.1 ELISA**

ELISA is a common method for quantifying cytokines/interferons [199,205]. This singleplex, antibody-based assay is performed in microtiter plates, and while there are multiple variants of ELISA, the sandwich ELISA is commonly used. Here, a capture antibody is immobilized in the well, to which the analyte in the sample binds. A second antibody is added, the detection antibody that binds to a different epitope of the analyte. Depending on whether the ELISA is direct or indirect, this second antibody is either labeled or unlabeled for detection, respectively. In the latter case, another secondary detection antibody is added, which will be labeled for detection. The label on the detection antibody is commonly a horseradish peroxidase or biotin, which allows coupling to a horseradish-peroxidase-labeled streptavidin (strep-HRP) [206]. Detection of the ELISA is done colorimetric, with fluorescence or CL [207]. For IFN- $\beta$  or general cytokine quantification in nasal secretion, the assay is performed in untreated samples. There are already various commercial antibody pairs available, therefore those are mostly used [199,205]. Typically, an ELISA takes multiple hours, if preparation of the well plate, which usually takes overnight, is already provided.

#### **2.4.3.3.2 Microarrays/Multiplex Methods**

As for biomarker profiling, various biomarkers must be analyzed and quantified; singleplex approaches like ELISA need too much time, money, and effort. An alternative are multiplexed methods that allow the analysis of multiple analytes in one measurement. These multiplex methods are performed either bead-based or in microtiter plates.

##### *Bead-based/Luminex*

Luminex™ assays are multi-analyte profiling methods using labeled beads in a flow cytometric application. Plastic microspheres are internally dyed using red and infrared dyes, leading to a matrix of many fluorescence profiles. These fluorescent beads are then functionalized with a capture ligand, for cytokine detection typically antibodies, so each fluorescence profile corresponds to a specific antibody. After sample incubation, binding of the analyte, and

washing, fluorescence-labeled detection antibodies are added, which bind to the bound analyte. Detection takes place on a special flow cytometer. Here, the sample is led through a capillary, leading to only one bead at a time in the measuring point. A red laser is used to induce fluorescence of the beads, and a green laser is used to induce fluorescence of the detection antibodies (Figure 6). The obtained fluorescence profile of the beads gives the identity of the analyte, and the intensity of the corresponding detection antibody gives the concentration of the analyte [208]. Luminex Corporation developed these xMAP® beads, but also other beads such as from Thermo Fisher Scientific, are used for IFN- $\beta$  quantification in nasal secretion after a prior centrifugation step [209].

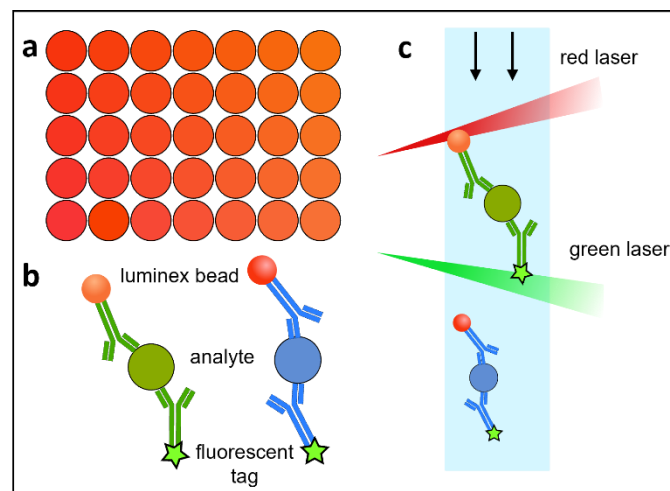


Figure 6. Luminex assay. a) Fluorescence profile matrix. The beads of each profile are coated with one type of antibody. b) The bead-bound antibodies and fluorescence-labeled antibodies bind the analyte. c) Detection inside the flow cytometric device. Fluorescent beads are detected with a red laser, the fluorescence tag with a green laser.

### *Mesoscale*

The mesoscale discovery system is a microtiter-plate-based assay, allowing for the simultaneous detection of up to ten analytes. Ten spots of different capture antibodies are immobilized on the ground of the microtiter plate wells. The sample is incubated in the well, whereby the analytes bind to their corresponding antibody. After washing any unbound analyte away, a SULFO-TAG labeled detection antibody is added [210]. After another washing step, electrochemiluminescent detection via the SULFO-TAG and the working electrode is performed (Figure 7) [211]. The mesoscale discovery system was also applied to quantify interferons in nasal fluids, using the nasal fluid directly and without sample pre-treatment [212,213]. The disadvantage of the mesoscale is the high cost.

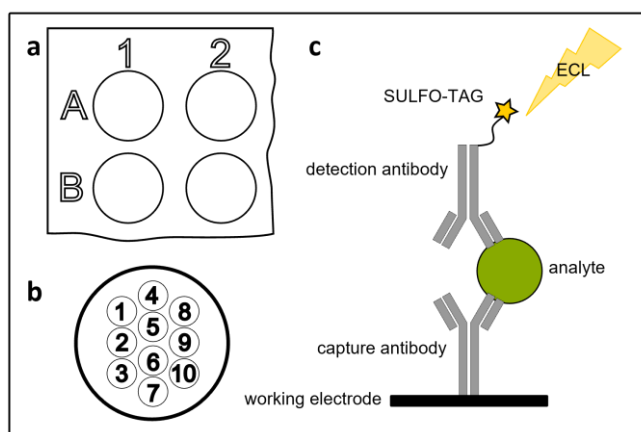


Figure 7. Mesoscale discovery assay. a) microtiter plate with b) multi-spot wells. c) Assay principle: immobilized capture antibody captures analyte, then binds the SULFO-TAG-labeled detection body. Over the working electrodes, electrochemiluminescence (ECL) is induced.

### *Proximity extension assay/Olink®*

Another multiplexed immunoassay used for cytokine/interferon quantification is the Olink® proximity extension assay [214]. This immunoassay works with a pair of antibodies per analyte. The antibodies from each pair are labeled with an oligonucleotide, which is able to hybridize only with the oligonucleotide on its partner antibody. This hybridization takes place only if the antibodies are in near proximity after both binding to the antibody, which reduces false positive readout due to unspecific binding (Figure 8). The amplicon generated by the hybridization can then be analyzed and quantified either with real-time quantitative PCR or next-generation sequencing [215]. For IFN- $\beta$  analysis in nasal secretion, no prior sample preparation is needed [214].

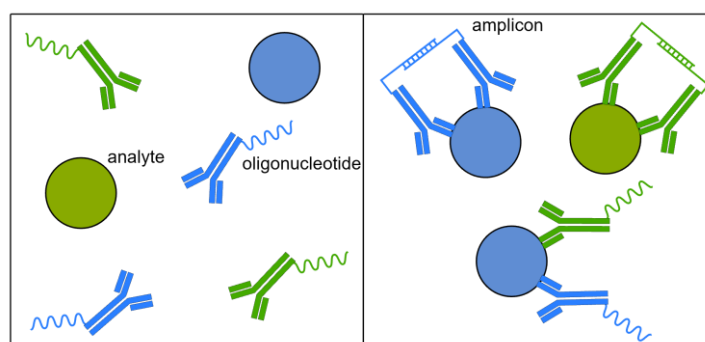


Figure 8. Proximity extension assay. An amplicon is formed when the two antibodies of the same pair bind to the correct analyte. No amplicon is formed if they bind due to unspecific binding to the wrong analyte.

### 3 Objectives

The isolation and detection of biomarkers in body fluids are important steps for the diagnosis and treatment of various diseases. The variety of biomarkers and body fluids regarding amount and composition make different methodological approaches necessary. Affinity-based methods are very versatile and can be tailored for varying analytes and matrices. In this thesis, the capability of affinity-based methods will be shown by developing different isolation and detection strategies for three analyte and body fluid combinations.

Urinary EVs are carriers of cellular information which can be used as biomarkers for diseases like urologic cancers or neurodegenerative diseases. Traditional methods lack simultaneous discrimination between EV size and its cell origin. Affinity-based isolation via binding to surface-associated proteins is utilized for cell origin discrimination. Nanobodies as an alternative to traditional antibodies are relatively new studied but show already great potential for EV purification due to their low-cost production, stability, small size and high affinity. In this thesis, nanobodies against CD63 are used together with epoxy-based monoliths for immunoaffinity filtration. Their macroporous characteristic of the monolith allows larger sample matrix particles to pass, while analytes can bind to immobilized nanobodies. The monolith itself is easily produced and modified. To realize the combination of monoliths and nanobodies, first an immobilization strategy for the nanobodies has to be developed followed by binding and elution studies. Key requirements are the retention of their affinity after immobilization and a reversible immobilization allowing for EV elution.

Bacterial infection followed by sepsis is one common and life-threatening complication of ascites. While a rapid and precise detection of causing pathogens facilitates the diagnosis and treatment, culture-based methods are slow and not sensitive enough due to the low concentration. Elaborated methods like PCR and sequencing are often expensive and complex. Sample preconcentration can close this gap, for example using affinity-based methods. To find appropriate affinity binders and corresponding desorption buffers for affinity-based isolation, as part of the REP-MAF project, a screening platform can accelerate this process. The flow-based microarray platform Microarray Chip Reader – Research (MCR-R) is used to enable rapid, automated, and multiplexed screening by immobilizing affinity binder candidates on the microarray chip surface. Multiple affinity binders such as a peptide, a lectin, an enzyme and antibodies are tested. For detection of captured living bacteria via CL through strep-HRP, living *E. coli* and *E. faecalis* have to be labeled with biotin. Elution has to be tested with different elution buffers and methods.

The detection and quantification of biomarkers in nasal secretions hold a great chance for diagnosis of upper airway diseases like viral or bacterial infections and allergies. Point-of-care analysis needs to be fast, easy to perform, detect multiple analytes, and be as cost-efficient as possible. Current detection methods cannot fulfill all these requirements. Therefore, in the third project a flow-based immunoassay for the detection of IFN- $\beta$  has to be developed as a foundation for prospective multiplexing. A commercially available antibody set designed for

ELISA is used to show that these antibodies can be transformed to other assays such as the CL-SMIA as well. After assay development, the assay is also tested with real samples. To show the potential of the CL-SMIA, an ELISA is performed and compared to it regarding assay performance and economical aspects both for single- and multi-analyte measurements.

## 4 Methods

### 4.1 Immunoaffinity-based Isolation of uEVs

#### 4.1.1 Production and Modification of Monolithic Filter for uEV Isolation

Epoxy-based monolithic discs used for affinity-based isolation were produced and modified in-house by following already published protocols [38,216] with modifications. First, toluene and tert-butyl methyl ether (60:40, v/v) were mixed to form the porogenic mixture and heated to 29 °C. Then, the initiator mixture (trifluoride diethyl etherate (BF<sub>3</sub>-Et<sub>2</sub>O) in 1,4-dioxane (1:10, v/v)) was added to reach a concentration of 1.25% and everything was mixed well. After adding the monomer polyglycerol-3-glycidyl ether (CL9) (ratio 20:80, v/v) and thoroughly mixing, the solution was filled into polytetrafluorethylene molds (16.3 × 60.0 mm internal diameter) and incubated for 45 min at 29 °C. After the reaction (Figure 9, left) finished, the monolithic columns were removed from their molds and stored in methanol overnight. After air-drying they resulted in columns with a diameter of 16 mm which were cut into filter discs with a height of 3 mm before use. Quality control of the monolith was performed through scanning electron microscopy on a ZEISS SIGMA VP Field Emission Scanning Electron Microscope (Carl Zeiss Microscopy GmbH, Jena, Germany) by analyzing pore sizes and polymer globule diameters as described elsewhere [217].

For modification procedures and EV filtration, monolithic filters were inserted into filtration units (Figure 9, Right) consisting of the shell of a 10 mL syringe, an O-ring (nitrile butadiene rubber, 16 × 2.5 mm outer diameter) placed below the filter, and an adapter that is connected with tubing and a peristaltic pump.

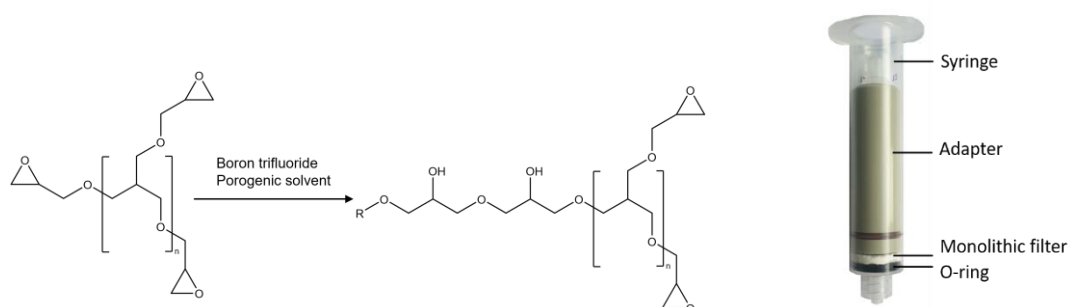


Figure 9. Left: Reaction scheme of polymerization of polyglycerol-3-polyglycidylether-based monolith. Right: Setup of filtration unit.

To modify the filter, it was washed and equilibrated with 20 mL 0.1 M borate buffer pH 9.0 (2 mL min<sup>-1</sup>). Then, 2 mL of SpyTag-anti-GFP (green fluorescent protein) fusion nanobody solution (0.36 mg mL<sup>-1</sup>) in 0.1 M borate buffer were circulated overnight with a flow rate of

0.5 mL min<sup>-1</sup> and washed again. For surface blocking, 5 mL of 1% bovine serum albumin (BSA) in 0.1 M borate buffer was circulated for 1 hour. After washing with 20 mL phosphate buffered saline (PBS), 800 µL of a solution of GFP-anti-CD63 fusion nanobody (0.23 mg mL<sup>-1</sup>) were loaded on the filter and incubated statically for 1 h. In the end, the filter was washed again with 20 mL PBS. Before and after immobilization of the GFP-anti-CD63, fluorescence was measured either with a Tecan Infinite F200 (Männedorf, Switzerland) and a Perkin Elmer, Viktor X2, 2030 Multilabel Reader (Waltham, MA, USA) at 485 nm (Excitation) and 535 nm (Emission).

#### **4.1.2 Isolation of EVs from Urine**

First morning urine was collected, centrifuged at 1800 × g for 10 min and stored at 4°C. 7.5 mL of pretreated urine were diluted to 30 mL (1:4 ratio) with 20 mM Tris-HCl (pH 9.0) and directly used for EV isolation. The solution was circulated overnight with a flow rate of 0.5 mL min<sup>-1</sup> over the GFP-anti-CD63 monolith. Elution was performed after washing with 200 mL PBS. For competitive elution, 800 µL of a 0.24 mg mL<sup>-1</sup> solution of an ascorbate peroxidase-fused anti-CD63 nanobody were loaded on the monolithic filter and incubated for 1 h. Before another wash, the elution fraction was removed from the filter and collected for further analysis. Then, for pH-dependent elution, 1.2 mL of 0.1 M glycine buffer (pH 2.5) were loaded on the filter and collected in fractions. The tubes for fraction collection were prior filled with 10% of 1 M borate buffer pH 9 to neutralize the pH.

#### **4.1.3 Evaluation of Protein Binding Capacity of Monolith**

Pristine monolithic filter discs were added into a filtration unit and washed and equilibrated with 20 mL 0.1 M borate buffer pH 9.0 (2 mL min<sup>-1</sup>). Afterwards, an eGFP solution in the same buffer was circulated over the monolithic filter with a flow rate of 0.5 mL min<sup>-1</sup>. Fluorescence was measured at 485 nm (excitation) and 535 nm (emission) every hour until the saturation point was reached. In the end, the modified filter was washed with 20 mL PBS and removed from the filtration unit to inspect a color change to green.

## 4.2 Microarray Experiments

### 4.2.1 Flow-based Microarray Platform MCR-R

The microarray assays in this thesis were performed on the flow-based platform MCR-R, which was developed at the Chair of Analytical Chemistry and Water Chemistry together with the manufacturer GWK Präzisionstechnik. It is the fourth generation of the MCR and is designed for flow-based CL bioassays. The flow is generated by a syringe pump and is distributed automatically by valves over polytetrafluorethylene tubes. Every step can be controlled regarding volume and flow rate using a defined program in its software. While the essential equipment includes the microarray chip holder, connections for the CL reagents luminol and hydrogen peroxide, a syringe pump for liquid control, additional syringe pumps for assay reagents, connections for the running buffer, and a charge-coupled device camera, additional features like an incubation loop for sample pre-incubation or an automated sample injector can be added if needed. Figure 10 shows the setup of the MCR-R (LegioAir version) used for this thesis.

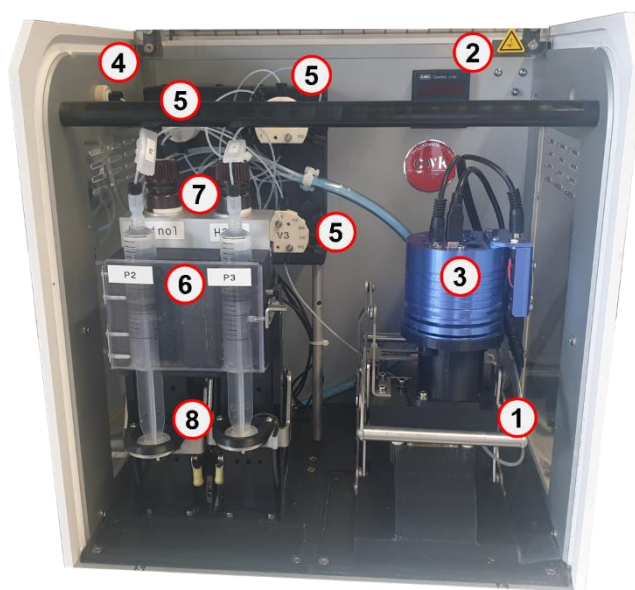


Figure 10. Microarray Chip Reader – Research (MCR-R, version LegioAir). 1) Temperature-controlled microarray chip holder. 2) Display for microarray chip temperature. 3) Charge-coupled device camera. 4) Sample inlet. 5) Valves. 6) Syringe pump for liquid control (not visible). 7) Vials for the chemiluminescence reagents luminol and hydrogen peroxide. 8) Syringe pumps for assay-dependent reagents.

Before measurements, the device was prepared by filling all tubes with running buffer (0.1% Tween<sup>®</sup> 20 solution in PBS), the CL reagents luminol and hydrogen peroxide as well as the individual reagents needed for each assay. Additionally, the microarray chip holder was heated

to the desired temperature. Before each measurement a microarray chip was inserted into the chip holder and flushed with running buffer. To obtain an initial darkframe picture, an image was recorded for 60 s. The signals of the darkframe are later subtracted automatically from the measurement results.

#### **4.2.2 Production of Polycarbonate Microarray Chips**

Microarray chips for measurements on the MCR-R were produced from polycarbonate foils (0.25 mm) according to a protocol published elsewhere [218]. A CE 6000–40 cutting plotter from Graphtec Corporation (Yokohama, Japan) was used to cut the plastic foils into sheets of 3 × 3 chips with sizes of 26 × 76 mm. Succinylated Jeffamine® ED-2003 was applied to the sheets with a screen printer. After incubation at 95 °C for 2 h the chips were washed, dried, and stored under reduced humidity. The contact spotter BioOdyssey Calligrapher® MiniArrayer from Bio-Rad (Hercules, USA) was used to immobilize the affinity binders in rows of five spots each. The spots of one row were 1100 µm apart; the rows 1300 µm (spot diameter 150 µm). Spotting and subsequent incubation were done at 20 °C and 55% relative humidity. Further information on spotting buffers, concentrations, controls, and incubation time are given in the chapters for each assay. The incubated sheets were divided into the individual chips and microarray chips were assembled. The chip is adhered to a black polyoxymethylene carrier plate with in- and outlets using a double-sided adhesive (thickness 140 µm) with a cut-out flow channel (56 µL). Until further use, microarray chips were stored at 4 °C.

#### **4.2.3 Screening Assay for Affinity Binder**

For the screening assay, multiple affinity binders were immobilized on the microarray chips according to the protocol in chapter 4.2.2. Lysozyme, Concanavalin A, Polymyxin B, an *E. coli* serotype O/K polyclonal antibody and an *Enterococcus* polyclonal antibody were diluted to a 1 mg mL<sup>-1</sup> concentration in spotting buffer containing 0.4 mg mL<sup>-1</sup> 1-ethyl-3-(3-(dimethylamino)propyl)carbodiimide (EDC), 1.1 mg mL<sup>-1</sup> N-hydroxysulfo-succinimide sodium salt (sulfo-NHS) in PBS. As positive controls served a polyclonal anti-peroxidase antibody from rabbit (1:40 dilution) and streptavidin (1 mg mL<sup>-1</sup>), both in spotting buffer, as negative control the pure spotting buffer. After spotting, microarray chips were incubated overnight.

To perform a screening measurement, the sample with biotinylated bacteria was injected into the sample port after which it was transported to the microarray chip (heated to 35 °C) and incubated in a stopped-flow manner. After flushing the microarray chip, a 1% casein solution in PBS for blocking was followed. Bound bacteria were detected with a strep-HRP solution flushed over the microarray chip, followed by the CL reagents and image recording for 60 s.

The chip was washed again and removed from the device for desorption experiments. 100  $\mu\text{L}$  of desorption buffer were injected into the microarray chip with a pipette and removed again. Back in the MCR-R, a second measurement starting from strep-HRP addition was performed. The detailed assay including flow rates and volumes is shown in Table 3.

Table 3. Measuring program of the screening assay on the MCR-R [219].

Step	Process	Volume / $\mu\text{L}$	Flow rate / $\mu\text{L s}^{-1}$	Comments
1	Transport sample to chip	118	50	
2	Sample incubation	600	1	10 increments, pause 30 s
3	Wash chip	2000	150	
4	Block chip	90 600	50 5	Casein in PBS
5	Wash chip	2000	150	
6	Incubate HRP-streptavidin	118 600	50 2	
7	Wash chip	2000	150	
8	Add CL reagents	400 (200 each)	100	Luminol and hydrogen peroxide
9	Take image			60 s exposure
10	Flush chip	1000	200	
11	Remove chip			Manual desorption
12	Flush device	2500 2500 2500	500 500 500	Sample loop Sample way Chip (extra washing chip)
13	Insert chip			
14	Incubate HRP-streptavidin	118 600	50 2	
15	Wash chip	2000	150	
16	Add CL reagents	400 (200 each)	100	Luminol and hydrogen peroxide
17	Take image			60 s exposure
18	Flush device	2500 2500 2500	500 500 500	Sample loop Sample way Chip

#### 4.2.4 CL-SMIA for IFN- $\beta$

For the CL-SMIA on the MCR-R, antibodies from R&D Systems Human IFN- $\beta$  DuoSet ELISA (Bio-Techne, Germany) were used. Different concentrations of the capture antibody (0.125, 0.25, 0.5 and 1 mg mL<sup>-1</sup> in spotting buffer) were immobilized on the microarray chips according to the protocol in chapter 4.2.2. Spotting buffer consisted of 50 mg mL<sup>-1</sup> trehalose dihydrate, 1 mg mL<sup>-1</sup> EDC, 1 mg mL<sup>-1</sup> sulfo-NHS and 0.01 mg mL<sup>-1</sup> Pluronic® F-127 in PBS. Positive control was a polyclonal anti-peroxidase antibody from rabbit (1:40 dilution) and negative control pure spotting buffer. Chips were incubated for 1 min.

The CL-SMIA consists of a preincubation step outside the microarray chip and the automated detection on the MCR-R. Sample mixed with detection antibody (DAB) was preincubated at 37 °C and 100 rpm before injected directly into the microarray chip and incubated again. Detection on the MCR-R was performed by flushing the strep-HRP solution and CL reagents over the chip and recording an image for 60 s. During the optimization process, dilution of strep-HRP, preincubation duration, on-chip incubation duration, DAB concentration and sample removing from the microarray chip were optimized. The detailed optimized assay including flow rates and volumes is shown in Table 4.

Table 4. Measuring program for the flow-based CL-SMIA on the MCR-R (Microarray Chip Reader-Research) [220].

Process	Volume / $\mu\text{L}$	Time / min	Comments
	Sample 50		
Pre-incubation	DAB 1.25	45	
	BSA 6.9		
Injection into chip	60	20	With pipette
Insert chip into device			
	Volume / $\mu\text{L}$	Flow rate / $\mu\text{L s}^{-1}$	
Direct sample over chip	50	0.5	
Wash chip	1500	325	2 increments, pause 1 s
Incubate strep-HRP	160	50	

	600	2	
Wash chip	1500	325	2 increments, pause 1 s
Add CL reagents	400	100	Mixture 1:1
Take image			60 s exposure
	2500	500	Sample loop
Flush device	2500	500	Sample way
	2500	500	Chip (extra washing chip)

### 4.3 Biotinylation of Bacteria

Bacterial cultures of *E. coli* (DSM 1003) and *E. faecalis* (DSM 2570) were performed on tryptic soy agar plates overnight at 37 °C. Cells were harvested, washed two times by centrifuging (10 min, 4500 rpm, 4 °C), and resuspended in PBS (pH 8). Cell concentrations were determined photometric on a NanoPhotometer from Implen (Munich, Germany). A suspension with  $10^9$  cells mL<sup>-1</sup> together with 2 mg mL<sup>-1</sup> biotin 3-sulfo-N-hydroxysuccinimide ester sodium salt was incubated on ice for 30 min at 100 rpm. After two washes with 0.1 M glycine in PBS and one wash with PBS (10 min, 4500 rpm, 4 °C), the biotinylated bacterial cells were resuspended in PBS. Cell concentrations were determined photometric and via culture. Until further use, biotinylated bacteria were stored at 4 °C.

### 4.4 Sandwich ELISA for IFN- $\beta$ quantification

The sandwich ELISA for IFN- $\beta$  was performed according the protocol from the manufacturer with minor changes. In MICROLON<sup>®</sup> 600, high binding, polystyrene 96-well plates (Greiner Bio-One, Germany), 100  $\mu$ L of the capture antibody (2.0  $\mu$ g mL<sup>-1</sup>) were incubated overnight at room temperature. After washing with a 0.05% Tween<sup>®</sup> 20 solution in PBS using the ELx405 Select plate washer (BioTek, VT, USA), active sides were blocked for 1 h with 300  $\mu$ L of 1% casein in PBS. Sample (100  $\mu$ L) together with 15  $\mu$ L of a BSA solution (7.7% in PBS) was added after washing and incubated for 2 h at room temperature and 100 rpm. After another washing step, 100  $\mu$ L of a 62.5 ng mL<sup>-1</sup> solution of the DAB in 1% BSA were incubated for another 2 h at 100 rpm and washed again. 100  $\mu$ L of a 40-fold dilution of strep-HRP were

incubated 20 min at 100 rpm and washed, too. Lastly, 100  $\mu$ L substrate solution were incubated in the dark until a baby blue color developed or maximum 20 min. To stop the color reaction, 50  $\mu$ L of a 1 M sulfuric acid were added to the substrate solution. The intensity of the occurring yellow color was detected at 450 and 540 nm using a Synergy HT plate reader.

## 5 Results

### 5.1 Publication 1: Macroporous Epoxy-Based Monoliths Functionalized with Anti-CD63 Nanobodies for Effective Isolation of Extracellular Vesicles in Urine

#### 5.1.1 Summary

In this publication, a new affinity chromatography method for the effective isolation of uEVs was developed. Monolithic epoxy-based filters modified with nanobodies against the surface-associated tetraspanin CD63 were used as chromatographic matrix. The monolithic filters were synthesized in-house and characterized through scanning electron microscopy and the evaluation of its protein binding capacity. Proof-of-principle experiments using covalently bound anti-CD63 nanobodies combined with EV detection directly on the monoliths, showed the feasibility of this approach, but were not sufficient for elution. Therefore, different approaches for indirect immobilization of the anti-CD63 nanobody were tested. Eventually, a GFP-labeled anti-CD63 nanobody was coupled to an anti-GFP nanobody, previously immobilized to the monolith. This functionalization procedure could be achieved with high reproducibility and efficiency. This functionalized monolith then was used to capture uEVs from 7.5 mL urine, which subsequently were eluted in two steps. First, competitive elution was performed with another anti-CD63 nanobody labeled with ascorbate peroxidase; the remaining EVs were eluted with a glycine buffer at pH 2.5. Herby, a size fractionation was found; smaller vesicles were eluted with the competitive elution and bigger vesicles with the pH-dependent elution. In summary, it could be shown that macroporous epoxy-based monoliths functionalized with nanobodies are suitable for isolating EVs from urine, and through the stagger of different elution methods, even a size fragmentation was possible.

#### 5.1.2 Own Contribution

- Planning of own experiments (together with PD Michael Seidel and Prof. Ario de Marco)
- Preparation of monolithic filters (together with Julia Klüpfel)
- Analysis of scanning electron microscopy pictures of the monoliths
- Testing of the two-step approaches for nanobody binding on the monolith
- Protein binding experiments
- EV isolation from urine with the optimized protocol
- Data analysis of own generated data

- Writing of the manuscript (together with Prof. Dr. Ario de Marco)

My laboratory work for this publication was done as part of a research stay at the Laboratory of Environmental and Life Sciences at the University of Nova Gorica under the supervision of Prof. Ario de Marco.

### 5.1.3 Reprint Permission

Neumair, J.; D'Ercole, C.; De March, M.; Elsner, M.; Seidel, M.; de Marco, A. Macroporous Epoxy-Based Monoliths Functionalized with Anti-CD63 Nanobodies for Effective Isolation of Extracellular Vesicles in Urine. *Int. J. Mol. Sci.* **2023**, *24*, 6131. <https://doi.org/10.3390/ijms24076131>

### Open Access

© 2023 by the authors. Licensee MDPI, Basel, Switzerland. This article is an open access article distributed under the terms and conditions of the Creative Commons Attribution (CC BY) license (<https://creativecommons.org/licenses/by/4.0/>).

### Permissions

No special permission is required to reuse all or part of article published by MDPI, including figures and tables. For articles published under an open access Creative Common CC BY license, any part of the article may be reused without permission provided that the original article is clearly cited. Reuse of an article does not imply endorsement by the authors or MDPI.



Article

# Macroporous Epoxy-Based Monoliths Functionalized with Anti-CD63 Nanobodies for Effective Isolation of Extracellular Vesicles in Urine

Julia Neumair<sup>1</sup>, Claudia D'Ercole<sup>2</sup>, Matteo De March<sup>2</sup> , Martin Elsner<sup>1</sup>, Michael Seidel<sup>1</sup>   
and Ario de Marco<sup>2,\*</sup>

<sup>1</sup> Chair of Analytical Chemistry and Water Chemistry, Technical University of Munich, Lichtenbergstr. 4, 85748 Garching, Germany

<sup>2</sup> Laboratory of Environmental and Life Sciences, University of Nova Gorica, Vipavska Cesta 13, P.O. Box 301, SI-5000 Nova Gorica, Slovenia

\* Correspondence: ario.demarco@ung.si; Tel.: +386-(0)5-3315295

**Abstract:** Extracellular vesicles (EVs) have enormous potential for the implementation of liquid biopsy and as effective drug delivery means, but the fulfilment of these expectations requires overcoming at least two bottlenecks relative to their purification, namely the finalization of reliable and affordable protocols for: (i) EV sub-population selective isolation and (ii) the scalability of their production/isolation from complex biological fluids. In this work, we demonstrated that these objectives can be achieved by a conceptually new affinity chromatography platform composed of a macroporous epoxy monolith matrix functionalized with anti-CD63 nanobodies with afflux of samples and buffers regulated through a pump. Such a system successfully captured and released integral EVs from urine samples and showed negligible unspecific binding for circulating proteins. Additionally, size discrimination of eluted EVs was achieved by different elution approaches (competitive versus pH-dependent). The physical characteristics of monolith material and the inexpensive production of recombinant nanobodies make scaling-up the capture unit feasible and affordable. Additionally, the availability of nanobodies for further specific EV biomarkers will allow for the preparation of monolithic affinity filters selective for different EV subclasses.

**Keywords:** monolith chromatography; nanobodies; extracellular vesicles; affinity purification; CD63



**Citation:** Neumair, J.; D'Ercole, C.; De March, M.; Elsner, M.; Seidel, M.; de Marco, A. Macroporous Epoxy-Based Monoliths Functionalized with Anti-CD63 Nanobodies for Effective Isolation of Extracellular Vesicles in Urine. *Int. J. Mol. Sci.* **2023**, *24*, 6131. <https://doi.org/10.3390/ijms24076131>

Academic Editor: Sergej V. Tillib

Received: 21 February 2023

Revised: 17 March 2023

Accepted: 21 March 2023

Published: 24 March 2023



**Copyright:** © 2023 by the authors. Licensee MDPI, Basel, Switzerland. This article is an open access article distributed under the terms and conditions of the Creative Commons Attribution (CC BY) license (<https://creativecommons.org/licenses/by/4.0/>).

## 1. Introduction

Extracellular vesicles (EVs) are a class of heterogeneous particles with diameters in the nm range, secreted by any cell type, having a pivotal role in intercellular communication in both physiologic and pathologic processes and detectable in any body fluid [1,2]. Since the analysis of their molecular content possesses a high potential for the diagnosis of diseases [3,4] and EVs of different cellular origin co-exist in biological fluids, an effective protocol for the isolation of sufficient amounts of single EV sub-populations, particularly when rare or highly diluted, would be extremely beneficial for the reliability of diagnostic assessments. The conventional purification methods based on (gel) filtration, gradient ultracentrifugation and asymmetrical flow field-flow fractionation [5,6] are effective and reproducible for the separation of dimension classes but cannot discriminate among EVs of the same diameter that originated from different cell types. However, the biologically and clinically relevant information present inside EVs (proteins, nucleic acids, metabolites) depends on the source cells rather than EV dimension. Consequently, there has been an increasing effort to develop affinity purification methods exploiting ligands selective for EV-sub-type specific antigens and suitable for the immunocapture and separation of EVs of different origin [7–12]. Such methods mostly foresee the use of ligand-functionalized affinity substrates, commonly magnetic beads, and result in useful-to-isolate small amounts

of vesicles for downstream analyses. In contrast, the implementation of preparative purifications aimed at the selective concentration of EVs from large amounts of complex biological samples to use as biotherapeutic agents or for diagnostics [13] has not been achieved using conventional chromatographic material such as sepharose beads because large components tend to clog columns. This kind of drawback is prevented in chromatographic systems exploiting rigid structures such as monolith columns that can be derivatized with antibodies or binders of different origins to obtain affinity units, usually discs of variable height [14]. Monoliths can be manufactured using alternative components that confer different structural characteristics and provide a variety of active groups suitable for functionalization [14]. Silica and methacrylate monoliths have already been exploited for EV fractionation according to alternative chromatographic principles [15–17] and the sequential stacking of single methacrylate monolith elements activated with antibodies specific for different EV biomarkers that have succeeded in fractionating two EV sub-populations [18]. Monolith working capacity is independent of the element dimensions, but the cost of the affinity reagents necessary for its functionalization can rapidly become limiting during volume scaling-up. Therefore, it is meaningful to substitute expensive IgGs with recombinant antibody fragments expressed cost-efficiently in bacteria. Recently, we demonstrated that methacrylate monoliths functionalized with nanobodies effectively purified EVs from different biological samples, but the polymer pores were too small to enable the EVs access to the monolith inner space, and this condition compressed the yields [19]. Therefore, monoliths with larger pores ( $\mu\text{m}$  range) are highly appreciated because they can accommodate both capture macromolecules and EVs without impairing the flux of complex samples such as biological fluids. This condition should consequently enhance the yields of purified EVs and enable the processing of large sample volumes without affecting the system pressure because clogging risks are minimized. The epoxy-based monolith used in this work is generated by self-polymerization of polyglycerol-3-glycidyl ether with the Lewis acid boron trifluoride ( $\text{BF}_3$ ) as a catalyst, which allows for use in mild temperature conditions. Responsible for the macroporous structure (pore sizes of  $22 \pm 9 \mu\text{m}$  and total porosity of 79%) are the characteristics of the soluble porogenic mixture from which the solid polymer will be generated [20]. The polyepoxide groups at the monolith surface are active for further modifications and can be treated with solvents and acids similarly to glass chemistry established for protein microarrays [21]. Both the glass chemistry and the direct conjugation of primary amines to the free epoxides are used for protein/antibody immobilization and to transform the original monolithic filters into affinity purification elements [22].

Most of the work for the optimization of EV purification protocols has been performed using serum and cultured cells [13,23], but also, urine EVs have been the object of specific studies [24–27] because they represent a valuable and easily accessible resource for non-invasive recovery of diagnostic markers for renal altered functionality [28]. Specifically, EVs participate in kidney development and physiology as well as in both renal regenerative and pathological processes. Recently, a specialist network has provided guidelines to standardize some methodological aspects of urine EV separation [29] to improve the consistency of the recovered data and to minimize the bias introduced by the adopted purification methods [30].

In this work, we describe the successful concentration and recovery of urine EVs by exploiting a conceptually new monolith-based filtration disc functionalized with anti-CD63 nanobodies. Such proof-of-principle application of the new immunoaffinity format indicates the feasibility of the approach, but we expect that the matrix could be functionalized with binders selective for biomarkers specific for EV sub-types to isolate rare, although clinically relevant, EVs from large volumes of different biological fluids.

## 2. Results and Discussion

### 2.1. Monolith Filter Preparation and Characterization

Monolith filter manufacturing is described in detail in the Materials and Methods section [20]. Pore structure of synthesized monolithic filters was examined using scanning electron microscopy (Figures 1a and S3). The average pore size ( $22.4 \pm 8.8 \mu\text{m}$ ) was estimated analyzing 50 pores from one filter, and this value was in good agreement with the data available in the literature [20,22,31]. The filter globules had an average diameter of  $5.7 \pm 1.7 \mu\text{m}$ , as inferred by the analysis of 100 globules (Supplementary Figure S3) and resulted as slightly larger than the value of  $4.61 \mu\text{m}$  described previously [31]. The affinity unit was assembled as depicted in Figure 2a.

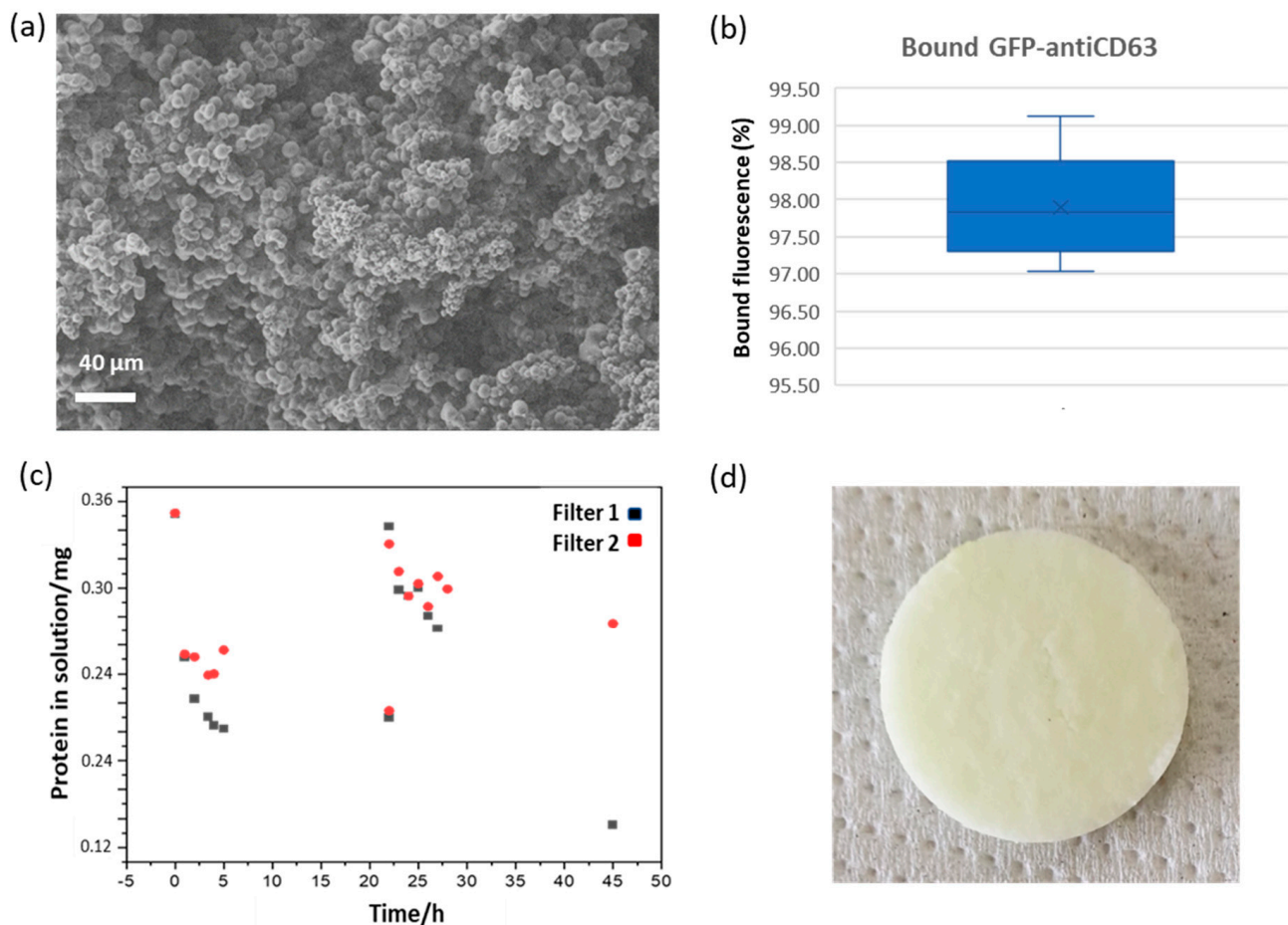


**Figure 1.** Monolith filter characteristics and its binding features. (a) Scanning electron microscope (SEM) imaging of an epoxy monolith disc. (b) Binding efficiency of the sandwich between anti-green fluorescent protein (GFP) nanobody and GFP-anti-CD63 nanobody. The data correspond to five independent experiments. (c) Evaluation of the binding capacity of the monolith filter. Fluorescent protein was circulated into the column until no apparent further binding was measured. Then, another aliquot of the concentrated solution was added and the protocol repeated. Two independent experiments are reported. (d) Macroscopic picture of the filter functionalized with eGFP (note the pale greenish color).

### 2.2. Filter Functionalization and Elution Issues

The first attempt to immunocapture EVs from urine samples was performed applying the protocol depicted in Supplementary Figure S4. The monolith filter was functionalized with an anti-CD63 nanobody fused to GFP, and the remaining active residues were blocked with BSA before circulating the urine sample. A sandwich system was prepared to detect the presence of EVs trapped in the column. First, mCherry-fused anti-CD63 nanobodies

were biotinylated, flushed over the filter, and then streptavidin–peroxidase was captured by interaction with the available biotin residues. EV actual presence in the column was indirectly confirmed by detecting the conversion of the peroxidase substrate 3,3',5,5'-tetramethylbenzidine (TMB) over time. However, it was not possible to elute the EVs in glycine buffer, even at pH 2.2, and the addition of detergent (Tween20, 10%) resulted in the recovery of samples negative for the EV membrane biomarker CD63 but enriched in the EV soluble biomarker Alix (Supplementary Figure S4). These results suggest that the harsh elution conditions induced EV lysis rather than promoting their release as integral particles from the functionalized monolith. Difficult EV release from affinity beads and monoliths was often reported [11,15,32], and we reasoned that the strong observed binding between the matrix and EVs could be the consequence of the avidity effect generated by multiple interactions between the nanobody-functionalized monolith pores and the EVs (Figure 2b,c). We also anticipated that these holding force could increase with EV diameter (Figure 2d,e). Such an avidity effect is significantly stronger when nanobodies are used because their small dimension allows for higher density and therefore more binding domains per surface unit that, in the case of soluble antigens, results in higher immunocapture yields with respect to the use of IgGs [33]. Consequently, three alternative capture modules compatible with mild elution protocols were designed (Supplementary Figure S5), and reagents fused to fluorescent proteins were used to simplify the evaluation of the binding efficiency.

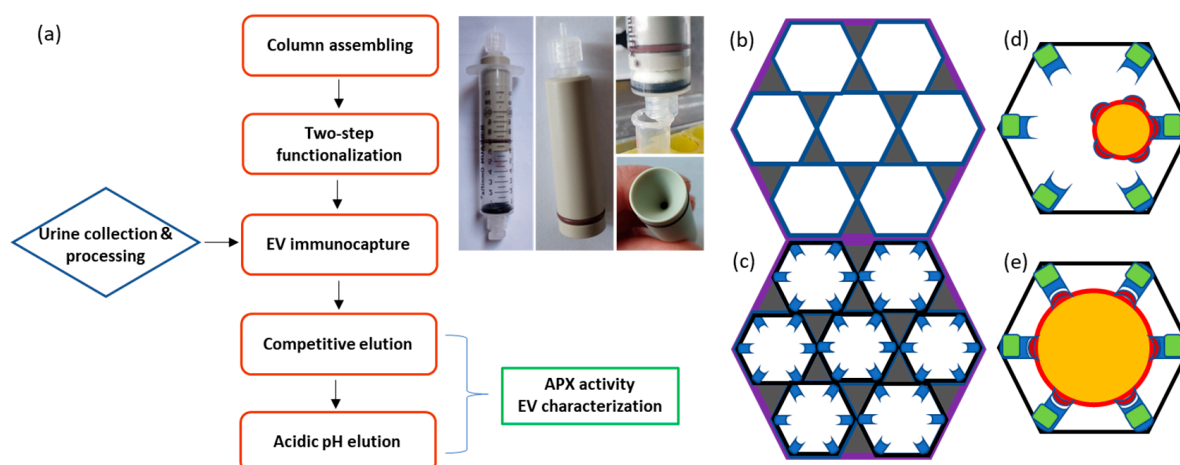


**Figure 2.** Flowchart of urine EV purification using a monolith filter and its use as chromatographic immunoaffinity matrix. (a) The chromatographic column was obtained by inserting the monolith disc into a syringe with hollow piston. Both syringe entrances have an adaptor for plastic tubing that is connected to a peristaltic pump. This helps to control the solution flux through the system. Once the column was assembled, the monolith surfaces were first functionalized with the first protein component, and then, the EV-specific nanobody was bound to it (Supplementary Figure S5). The EVs present in the pre-treated urine sample were selectively immunocaptured and then eluted in two steps, the first competitive and the second obtained by partial nanobody denaturation at low pH. The recovered EVs underwent characterization. (b) Schematic representation of a monolith filter structure. The dark areas represent the solid matter composed of globules, the white the internal cavities/pores. (c) Disuccinimidyl or epoxide active residues available on the inner matrix surfaces (pores) are used for promoting covalent binding with the primary amines of protein lysines. Filters functionalized with nanobodies specific for EV biomarkers are suitable to capture the EVs present in the mobile fraction (d,e). Smaller vesicles (d) have less surface and probably fewer displayed antigens suitable for binder interactions. The multiple antigens available on larger vesicles (e) may induce a stronger avidity effect by enabling the interaction with several binders at the same time.

In the first option (Supplementary Figure S5, top), a SpyCatcher fused to eGFP was bound to the filter and used to reconstitute a covalent bond with the SpyTag fused to a protease recognition site and the anti-CD63 nanobody. In this case, the nanobody can be cleaved from the anchoring complex by exploiting the 3C protease. In the second case, the anti-CD63 nanobody is fused to an ALFATag and is linked to the matrix through a reversible binding between its tag and a mutant anti-ALFATag nanobody (Supplementary Figure S5, middle). In the third combination, the GFP-antiCD63 nanobody can be released by the filter by inducing at low pH the reversible binding between GFP and the matrix-bound anti-GFP nanobody (Supplementary Figure S5, bottom). Preliminary tests indicated that the third option worked out more efficiently than the others and was selected for the successive protocol optimization steps. The binding and elution conditions were thoroughly analyzed in a set of optimization experiments.

Next, we tried to characterize the modality of protein immobilization on monolithic filter surfaces by direct coupling of the primary amino groups to the epoxy groups using 0.1 M borate, pH 9, as the coupling buffer. eGFP was used as a model protein because the measurement of its fluorescence before and after circulation into the monolithic filter was a convenient method to quantify the signal reduction. When eGFP was directly immobilized on active filter, 42.8% of the loaded protein (0.35 mg) was bound (Supplementary Table S1, left). Successively, the possibility to exploit the immunoaffinity between eGFP and an anti-GFP nanobody to build a pH-dependent bond to monolithic filters was assessed. After eGFP binding to the filter, this was coated with 1% BSA to quench the filter residual active sites before introducing the anti-GFP nanobody. After extensive washing, a visible fraction of the anti-GFP nanobody was recovered in the elution fraction obtained by addition of 0.1 M glycine, pH 2.5 (Supplementary Figure S6, left), confirming that the nanobodies effectively bound to their antigen.

In a second experimental design, the previous set-up was inverted by immobilizing 0.3 mg of the nanobody to the filter, quenching the active sites as above and then circulating the fluorescent protein (0.28 mg). Over time, the fluorescence signal decreased by 55.5% (Supplementary Table S1, middle). In parallel, it was possible to observe that the protein band intensity decreased as well in a sodium dodecyl sulfate–polyacrylamide gel electrophoresis (SDS-PAGE) loaded with samples collected at successive times (Supplementary Figure S6, middle). The addition of acidic buffer determined the eGFP release. Altogether, such results confirmed the effective and reversible binding between nanobody and eGFP.

Finally, a filter was functionalized first with anti-GFP nanobodies (0.72 mg), its active sites were quenched, and the resulting immunoaffinity matrix was used to capture GFP-labeled anti-CD63 nanobodies (0.18 mg). The fluorescence signal was reduced by 97.9% (Supplementary Table S1, right) after incubation, suggesting a very efficient binding of the circulating nanobodies to the captured nanobodies when the latter was in large stoichiometric excess. This result was confirmed by SDS-PAGE analysis in which the band corresponding to the GFP-anti-CD63 nanobody nearly disappeared over the incubation time but was recovered in the pH-dependent elution fraction (Supplementary Figure S6, right). This experiment was repeated a further four times using a new monolithic filter and the same amount of proteins every time. The average signal reduction was  $97.9 \pm 0.8\%$  ( $n = 5$ , Figure 1b). These results confirmed the high reproducibility of the procedure. Additionally, before starting the purification tests using urine, we wished to determine the maximal amount of protein that can be bound to the monolithic filters and to obtain some information about its binding kinetics. The eGFP solution was circulated over the filter, and its fluorescence was measured every single hour (Figure 1c). The amount of protein in solution decreased, until it reached a plateau after 22 h, and its progressive decrement indirectly suggested its effective capture into the monolithic filter. In two independent experiments, the amounts of immobilized protein per mL of monolithic filter were 0.24 and 0.23 mg. The same filters underwent a second immobilization round that resulted in total amounts of 0.58 and 0.32 mg of bound protein per mL of monolithic filter (Table 1). In parallel, the monolith filter turned its color from white to pale green, indicating that the fluorescent

protein removed from the circulating sample was bound to the monolithic filter (Figure 1d). Furthermore, in a control experiment, we did not notice any detectable binding of BSA to the functionalized filter when it was circulated in the system, and this result suggests that unspecific capture of proteins present in the original sample should be negligible.

**Table 1.** Characteristics of protein binding to monolith filter.

		Filter 1	Filter 2
First round	µg/mg	0.84	0.85
	mg/mL	0.24	0.23
Second round	µg/mg	1.23	0.34
	mg/mL	0.34	0.09
Total	µg/mg	2.07	1.20
	mg/mL	0.58	0.32

Two rounds of protein binding were performed using two filters. Amount of bound protein is given as µg protein per mg monolithic filter (µg/mg) and as mg protein per mL of monolithic filter (mg/mL).

### 2.3. EV Purification under Optimized Conditions

The adopted protocol (Supplementary Table S2 and Supplementary Figure S7) foresaw a step in which the actual presence of EVs trapped in the filter was indirectly monitored by first loading ascorbate peroxidase (APX) fused to anti-CD63 to the system and then measuring its enzymatic activity (Supplementary Figure S5, bottom). This step can be omitted after protocol optimization but helped to make an interesting observation. It resulted in that the APX-nanobody construct could effectively compete with the matrix-bound anti-CD63 construct and induce the release of some EVs from the filter. These exclusively belonged to the smallest EV fraction (Supplementary Figure S8), and the result confirmed the initial hypothesis that the avidity effect might affect the EV binding proportionally to their size (Figure 2d,e).

The remaining EVs were eluted adding glycine buffer, pH 2.5, into two fractions, whose nanosight profiles are reported in Figure 3a. Particle average diameter for the competitively eluted fraction 1 and the pH-dependent eluted fractions 2 and 3 were  $36 \pm 4$ ,  $126 \pm 16$ , and  $139 \pm 14$  nm, respectively (Table 2). It seems therefore that fraction 1 corresponds to the EV class of exomeres, whereas the others have exosome-like dimensions. It was already reported that immunoaffinity purification preferentially yielded small EVs [25]. The EV integrity, shape and dimension were verified qualitatively by TEM (Figure 3b), APX activity was measured as expected on fraction 1 where the enzyme was probably partly soluble and partly bound to the small EVs. However, a small amount of the APX-anti-CD63 nanobodies resisted to the extensive washing step and co-eluted with fractions 2 and 3 (Figure 4a).

**Table 2.** Characteristics of the EVs eluted from the monolith filter.

	Particle Number	Particle Average Diameter
Fraction 1 (competitive)	$1.13 \times 10^{10}$	$36 \pm 4$
Fraction 2 (pH-dependent)	$8.95 \times 10^9$	$126 \pm 16$
Fraction 3 (pH-dependent)	$9.31 \times 10^9$	$139 \pm 14$

Urine EVs immunocaptured from a 7.5 mL sample by anti-CD63 nanobodies bound to the monolith matrix were eluted first by the addition of competitive anti-CD63 nanobodies and successively by decreasing the buffer pH to 2.5. The values are means of three independent measurements performed using samples obtained from different experiments.

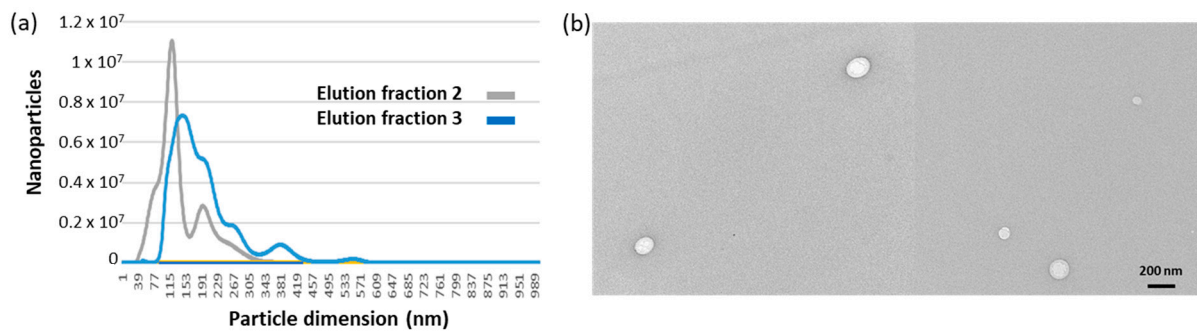


**Figure 3.** EV size distribution in samples corresponding to different elution fractions. (a) Nanosight profiles of immunopurified EVs. EVs bound to the monolith disc functionalized with anti-CD63 nanobodies were eluted by lowering the buffer to pH 2.5. The fraction corresponding to the void volume was removed, and two fractions, each roughly corresponding to the column volume, were collected, and the pH of their buffer was neutralized. (b) TEM images of immunopurified EVs.

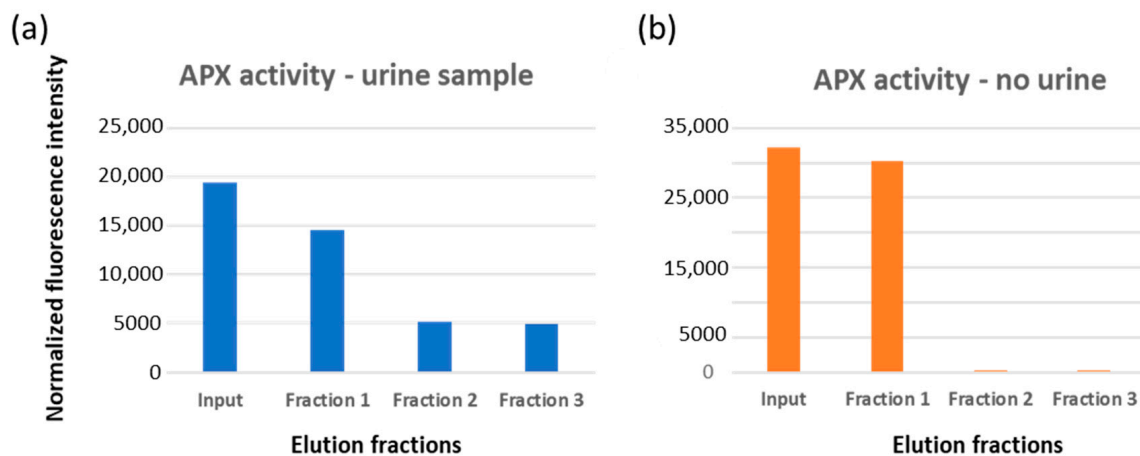


**Figure 4.** APX peroxidase activity in EV elution fraction. (a) The solution containing APX-anti-CD63 (input) was loaded onto a functionalized filter coated with EVs and recovered downstream (fraction 1). After extensive washing, EVs were eluted in 2–3 fractions by addition of acidic buffer. The enzymatic activity of each fraction was estimated by measuring the enzyme substrate conversion into a fluorescent component. (b) As a negative control to assess any direct binding of APX-anti-CD63 to the filter, the same experiment was performed in the absence of a urine sample.

APX did not show unspecific binding for the immunocapture system since it was not held in the filter in a control set. This was performed to functionalize the monolith with the same nanobody sandwich, but only PBS, and no urine, was loaded into the system (Figure 4b). Nanosight analysis also provided an estimation of the amount of purified EVs (Table 2). Altogether, the nanobody-functionalized filter enabled recovery of roughly  $3 \times 10^{10}$  EVs from a urine sample of 7.5 mL. The yields are comparable with the best results reported in the literature [24,34,35].

Since the urine volume used for the experiments was chosen arbitrarily, we wished to evaluate whether the filter EV binding capacity was already saturated at these concentrations or might capture more EVs from a larger volume (25 mL); the preliminary results indicated no significant difference in binding capacity. Once the feasibility of the approach is demonstrated in this work, future surveys will more precisely address this issue and further protocol improvements that might require tuning parameters such as the optimal reagent concentrations, the best ratio between the amounts of primary and secondary binders, the incubation times of the different steps, the effect of dynamic versus static incubations and the velocity of flows through the system. Furthermore, the structural characteristics of monolith will allow for simple scaling-up and -down of the platform.

Scaling-down would make sense for manufacturing small immunocapture cones to use inside pipette tips (“clinical format”) suitable for concentrating EVs from small biological samples, whereas scaling-up could be applied to recover extremely rare EVs from large volumes, for instance, as could be the case for disease-related EVs in urine or biotherapeutic EVs [13,28]. In this perspective, columns could be manufactured into formats suitable for automated HPLC/FPLC systems, as recently reported for other monolith systems [15,18]. The precise pump control and the on-line quantification of the circulating protein by means of a UV detector will improve the process reproducibility as well as the accurate monitoring of the binding, washing and elution kinetics.

The EV purification experiments reported in this work were performed using an anti-CD63 nanobody [36], namely a binder specific for a generic EV biomarker. In contrast to conventional antibodies, it is easy to produce inexpensively in bacteria, alone or fused to different tags suitable for simplifying directional functionalization procedures and downstream experiments. This approach was very convenient since it allowed for the comparison of several alternative methods during the optimization of the EV purification protocol that required an elevated number of repeats. Furthermore, scaling-up would remain affordable because large amounts of the binders can be purified quickly and cost-effectively. The same principle could be applied in the future for the selection of nanobodies specific for EV sub-populations characterized by the presence of exclusive biomarkers. In this perspective, we already demonstrated the possibility to isolate nanobodies from a phage display pre-immune library panning directly on EVs or on specific epitopes of soluble antigens [8,37].

### 3. Materials and Methods

#### 3.1. Chemicals and Proteins

Toluene, tert-butyl methyl ether, trifluoride diethyl etherate, 1,4-dioxane and methanol for the polymerization of the monolithic filters were all purchased from Sigma-Aldrich, subsidiary of Merck (Darmstadt, Germany). Polyglycerol-3-glycidyl ether (CL9) was purchased from IpoX Chemicals (Laupheim, Germany). Nanobodies were subcloned to be produced fused with appropriate tags, purified and analyzed as previously described [8]. The specific anti-CD63 nanobody used for EV capture has a  $K_D$  of 65 nM for its antigen [36]. Streptavidin conjugated to horseradish peroxidase (POX) was purchased from Sigma (18-152, St. Louis, MO, USA). SDS-PAGE gels were stained in Coomassie blue solution for 1 h and destained in 40% methanol and 10% acetic acid. PageRuler™ Prestained protein ladder (Thermo Scientific, Waltham, MA, USA) was used.

#### 3.2. Production of Monolithic Filter Discs

The polymerization of epoxy-based monoliths was already published elsewhere [20], and the monolithic filter discs used in this work were produced with adjustments after published protocols [38,39]. In short, polytetrafluoroethylene molds with  $16.3 \times 60.0$  mm of internal diameter were used (Supplementary Figure S1a) to obtain monolithic filter columns that were cut into discs with height of either 3 or 10 mm (Supplementary Figure S1c,d). The porogenic reaction mixture consisting of toluene and tert-butyl methyl ether (60:40, *v/v*) was heated to 29 °C. Subsequently, the initiator boron trifluoride diethyl etherate (BF<sub>3</sub>·Et<sub>2</sub>O) in 1,4-dioxane (1:10, *v/v*) was added to a concentration of 1.25%, and the components were mixed thoroughly. Then, the monomer polyglycerol-3-glycidyl ether (monomer/porogenic mixture ratio 20:80, *v/v*) was added, and after vigorous mixing, the solution was filled into the molds and incubated for 45 min at 29 °C (Supplementary Figure S1b). Afterward, the resulting monolithic columns were removed from their molds, stored in methanol overnight and air-dried. Scanning electron microscopy of monolithic filters was performed on a ZEISS SIGMA VP Field Emission Scanning Electron Microscope (Carl Zeiss Microscopy GmbH, Jena, Germany) as described elsewhere in detail [31].

### 3.3. Strategies for Immobilizing Proteins on Monolithic Filter Discs

Two different approaches for protein immobilization on the monolithic filter discs were tested: (i) Jeffamine<sup>®</sup> ED-2003 (a polyether diamine with dominantly PEG in the backbone) was used as a spacer and *N*-*N'*-Disuccinimidyl carbonate (DSC) for coupling protein primary amines; (ii) direct coupling of proteins via primary amines to the epoxide groups of the monolithic filter discs. For the first approach, monolithic filter discs with a height of 10 mm were submerged in a 2:1 mixture of Jeffamine<sup>®</sup> ED-2003 and carbonate buffer (15 mM Na<sub>2</sub>CO<sub>3</sub>, 35 mM NaHCO<sub>3</sub>, pH 9.8) and incubated for 48 h at 60 °C. After washing with 60 °C water, discs were activated for four hours at room temperature with a mixture of 93% dimethylformamide, 7% trimethylamine, 49 mM 4-dimethylaminopyridine and 214 mM DSC. After washing with methanol and water, disks were dried and stored at 4 °C until use. The resulting activated monolithic filter discs were first washed with PBS (2 mL/min), and then, the protein diluted in PBS was circulated over night at a flow rate of 0.5 mL/min (Supplementary Figure S2a). For the second approach, monolithic filter discs (height 3 mm) were washed with 0.1 M borate buffer pH 9.0 (2 mL/min), and protein diluted in borate buffer was circulated over night at room temperature at 0.5 mL/min (Supplementary Figure S2b).

### 3.4. Preparation of Monolith Columns and Assessment of Monolith Binding Capacity

The affinity unit was prepared by accommodating a monolith disc into the shell of a 10 mL syringe; an O-Ring (16 × 2.5 mm outer diameter) was placed below the filter and a hollow piston above it. Adapters were inserted on both the piston and the syringe for connecting the filtration unit to tubings (Figure 2a). Discs of different height can be used, and the mobile piston was shifted accordingly. By using a peristaltic pump, the flux of liquids (samples, buffers) through the filter unit can be operated either as a closed system, by connecting the syringe output and input through a tubing, or as an open system, with the input tubing that drives the sample from a tank and the output tubing dropping the content in a waste jar.

Then, the mounted monolith filter was used to evaluate its maximal protein binding capacity by means of circulating fluorescent proteins and monitoring their fluorescence. Filters were equilibrated by circulating 20 mL of 0.1 M borate buffer, pH 9.0, at a speed of 2 mL/min, and then, eGFP diluted in the same buffer was circulated over at 0.5 mL/min. Every hour, circulation was stopped, a sample was taken from the circulation solution, and fluorescence was measured at 485 nm (excitation) and 535 nm (emission) until no further variation was measured (saturation point). After washing in 20 mL PBS, the filter was removed for visive color evaluation.

### 3.5. Preparation of Immunocapture Monolithic Filters

Next, the same mounted monolith filters described above were used to prepare immunocapture systems. A filter (3 mm height) was washed in 20 mL of 0.1 M borate buffer pH 9.0 (2 mL/min) and functionalized by adding 0.72 mg of SpyTag-anti-GFP fusion nanobody resuspended in 2 mL of the same buffer. The protein solution was circulated at 0.5 mL/min over the filter overnight at room temperature. After washing the filter in borate buffer, 5 mL of 1% BSA in 0.1 M borate buffer was circulated for 1 h to block any active sites on the filter surface. The filter was washed with 20 mL of PBS, and then, 800 µL of a 0.23 mg/mL solution of GFP-anti-CD63 fusion nanobody was loaded on the filter and incubated statically for 1 h. Afterward, the filter was washed with 20 mL of PBS. The binding of eGFP-anti-CD63 was assessed by measuring the fluorescence of the sample at 485 nm (excitation) and 535 nm (emission) before and after immobilization. Fluorescence measurements were performed on a Tecan Infinite F200 (Männedorf, Switzerland) and a Perkin Elmer, Viktor X2, 2030 Multilabel Reader (Waltham, MA, USA). As a control, BSA was circulated over the filter functionalized with the anti-CD63 nanobody, and its concentration was monitored reading the absorbance at 280 nm to determine potential unspecific binding to the matrix.

### 3.6. Affinity EV Immunopurification from Urine

First, morning urine was collected and centrifuged at  $1800\times g$  for 10 min. Until use, samples were stored at 4 °C. For EV isolation, 7.5 (or 25) mL of urine was diluted 1:4 with 20 mM Tris·HCl pH 9.0, and the resulting 30 (or 100) mL of diluted urine was circulated at 0.5 mL/min over the functionalized monolith filters overnight at room temperature. After washing with 20 mL PBS, 800  $\mu$ L of a 0.24 mg/mL solution of APX fusion nanobody APX-anti-CD63 was incubated statically on the filter for 1 h. Filters were washed again, and EVs were eluted by adding 1.2 mL of 0.1 M glycine buffer, pH 2.5, to the filter. Elution fractions were collected in tubes and immediately neutralized by 1 M borate buffer, pH 9.

### 3.7. Western Blot

For Western blot, proteins separated by SDS-PAGE starting from EV lysates were transferred onto a PVDF membrane using semi-dry transfer at 8 mA for 1.5 h. Transfer buffer consisted of 48 mM Tris base, 39 mM glycine, 1 mM SDS and 20% (*v/v*) methanol. Membranes were either directly tested or stored at  $-20$  °C in 5% milk in PBS. Alix was detected with the commercial monoclonal antibody 3A9 (diluted 1:500, Thermo Fisher Scientific, Waltham, MA, USA) and CD63 with rabbit polyclonal antibodies (diluted 1:1000, PA5-92370, Thermo Fisher Scientific) both in combination with HRP-conjugated secondary antibodies.

### 3.8. EV Characterization

The presence of EVs bound to the functionalized monolith filter was assessed indirectly in situ by measuring the horseradish peroxidase-dependent 3,3',5,5'-tetramethylbenzidine (TMB) color conversion at 450 nm. Specifically, the enzyme was captured by anti-CD63 nanobodies bound to the EV surface that were either biotinylated or fused to a Fc domain. As an alternative, APX activity was measured using the Amplex™ UltraRed Reagent kit (Thermo Fisher Scientific) on the eluted fractions by mixing 100  $\mu$ L of the sample with 100  $\mu$ L of the substrate solution [40]. After 15 min of incubation in the dark, fluorescence was detected at  $\lambda_{\text{Exc}} = 560$  nm and at  $\lambda_{\text{Em}} = 595$  nm. EV size was evaluated by Nanosight measurement (NTA version 3.2 Dev Build 3.2.16, Malvern Panalytical Ltd., Malvern, UK) with automatic repeated data acquisition and overall analysis for calculation of particle concentration and dimension. EV morphology was evaluated by TEM: 5  $\mu$ L of EV suspension was adsorbed on carbon/formvar nickel grids (Electron Microscopy Sciences, Hatfield, PA, USA) and incubated 10 min before removing the sample excess using filter paper. The grids were then coated with 4  $\mu$ L of staining agent (uranyl acetate diluted 1:3 in distilled water) for further 10 min and washed 5 times in distilled water before being observed in a Philips CM 10 TEM (FEI, Eindhoven, The Netherlands) operated at 80 kV.

## 4. Conclusions

Monolithic affinity chromatography appears as a very effective method for the direct and selective capture and simultaneous concentration of EVs from biological fluids such as urine, because the large pores prevent clogging even after substrate accumulation, and the stable physical structure of the polymeric column can stand an elevated loading rate. These matrix characteristics also assure the scalability of the EV purification system. We demonstrated the approach feasibility using an anti-CD63 nanobody as the immunocapture reagent. However, monolith elements functionalized with binders specific for different biomarkers can be assembled in succession and in combination with further chromatographic elements, exploiting different separation principles such as ion-exchange or size-exclusion and allowing for the simultaneous and selective enrichment of different EV subclasses. The implementation of such a system will require the isolation of suitable binders and, specifically, of small recombinant reagents such as nanobodies that are inexpensive to produce, simple to engineer and are suitable for high-density functionalization of a monolith matrix.

**Supplementary Materials:** The following supporting information can be downloaded at: <https://www.mdpi.com/article/10.3390/ijms24076131/s1>.

**Author Contributions:** Conceptualization, A.d.M. and M.S.; methodology, J.N., C.D. and M.D.M.; validation, J.N., C.D., M.D.M. and A.d.M.; formal analysis, J.N., M.S. and A.d.M.; investigation, J.N.; resources, M.E., M.S. and A.d.M.; writing—first draft, J.N. and A.d.M.; writing—review and editing, J.N., M.S., A.d.M. and M.E.; supervision, M.S. and A.d.M.; funding acquisition, M.E., M.S. and A.d.M. All authors have read and agreed to the published version of the manuscript.

**Funding:** This research was financially supported by Deutsche Forschungsgemeinschaft (DFG) through the TUM International Graduate School of Science and Engineering (IGSSE), GSC 81 and by the grants ARRS/P3-0428 and N4-0282 provided by Javna Agencija za Raziskovalno Dejavnost Republike Slovenije.

**Institutional Review Board Statement:** Not applicable.

**Informed Consent Statement:** Not applicable.

**Data Availability Statement:** Data will be provided by request.

**Acknowledgments:** The authors wish to thank Jorge Adrián Guajardo Hernández, Julia Klüpfel, Federica Caponnetto, Lidija Filipović and Robert Bernedo for their technical support.

**Conflicts of Interest:** The authors declare no conflict of interest.

## References

1. Becker, A.; Thakur, B.K.; Weiss, J.M.; Kim, H.S.; Peinado, H.; Lyden, D. Extracellular Vesicles in Cancer: Cell-to-Cell Mediators of Metastasis. *Cancer Cell* **2016**, *30*, 836–848. [[CrossRef](#)] [[PubMed](#)]
2. Kalluri, R.; LeBleu, V.S. The biology, function, and biomedical applications of exosomes. *Science* **2020**, *367*, eaau6977. [[CrossRef](#)] [[PubMed](#)]
3. Roy, S.; Hochberg, F.H.; Jones, P.S. Extracellular vesicles: The growth as diagnostics and therapeutics; a survey. *J. Extracell. Vesicles* **2018**, *7*, 1438720. [[CrossRef](#)] [[PubMed](#)]
4. Mallocci, M.; Perdomo, L.; Veerasamy, M.; Andriantsitohaina, R.; Simard, G.; Martínez, M.C. Extracellular Vesicles: Mechanisms in Human Health and Disease. *Antioxid. Redox Signal.* **2019**, *30*, 813–856. [[CrossRef](#)]
5. Gardiner, C.; Di Vizio, D.; Sahoo, S.; Théry, C.; Witwer, K.W.; Wauben, M.; Hill, A.F. Techniques used for the isolation and characterization of extracellular vesicles: Results of a worldwide survey. *J. Extracell. Vesicles* **2016**, *5*, 32945. [[CrossRef](#)]
6. Chen, J.; Li, P.; Zhang, T.; Xu, Z.; Huang, X.; Wang, R.; Du, L. Review on Strategies and Technologies for Exosome Isolation and Purification. *Front. Bioeng. Biotechnol.* **2022**, *9*, 811971. [[CrossRef](#)]
7. Brett, S.I.; Lucien, F.; Guo, C.; Williams, K.C.; Kim, Y.; Durfee, P.N.; Brinker, C.J.; Chin, J.I.; Yang, J.; Leong, H.S. Immunoaffinity based methods are superior to kits for purification of prostate derived extracellular vesicles from plasma samples. *Prostate* **2017**, *77*, 1335–1343. [[CrossRef](#)]
8. Popovic, M.; Mazzega, E.; Toffoletto, B.; de Marco, A. Isolation of extra-cellular vesicle single-domain antibodies by direct panning on vesicle-enriched fractions. *Microb. Cell Fact.* **2018**, *17*, 6. [[CrossRef](#)]
9. Song, Z.; Mao, J.; Barrero, R.A.; Wang, P.; Zhang, F.; Wang, T. Development of a CD63 Aptamer for Efficient Cancer Immunochimistry and Immunoaffinity-Based Exosome Isolation. *Molecules* **2020**, *25*, 5585. [[CrossRef](#)]
10. Yu, Q.; Zhao, Q.; Wang, S.; Zhao, S.; Zhang, S.; Yin, Y.; Dong, Y. Development of a lateral flow aptamer assay strip for facile identification of theranostic exosomes isolated from human lung carcinoma cells. *Anal. Biochem.* **2020**, *594*, 113591. [[CrossRef](#)]
11. Liangsupree, T.; Multia, E.; Riekkola, M.L. Modern isolation and separation techniques for extracellular vesicles. *J. Chromatogr. A* **2021**, *636*, 461773. [[CrossRef](#)]
12. Liangsupree, T.; Multia, E.; Saarinen, J.; Ruiz-Jimenez, J.; Kemell, M.; Riekkola, M.L. Raman spectroscopy combined with comprehensive gas chromatography for label-free characterization of plasma-derived extracellular vesicle subpopulations. *Anal. Biochem.* **2022**, *647*, 114672. [[CrossRef](#)] [[PubMed](#)]
13. Staubach, S.; Bauer, F.N.; Tertel, T.; Börger, V.; Stambouli, O.; Salzig, D.; Giebel, B. Scaled preparation of extracellular vesicles from conditioned media. *Adv. Drug Deliv. Rev.* **2021**, *177*, 113940. [[CrossRef](#)] [[PubMed](#)]
14. Poddar, S.; Sharmeen, S.; Hage, D.S. Affinity monolith chromatography: A review of general principles and recent developments. *Electrophoresis* **2021**, *42*, 2577–2598. [[CrossRef](#)] [[PubMed](#)]
15. Multia, E.; Tear, C.J.Y.; Palviainen, M.; Siljander, P.; Riekkola, M.L. Fast isolation of highly specific population of platelet-derived extracellular vesicles from blood plasma by affinity monolithic column, immobilized with  $\alpha$ human CD61 antibody. *Anal. Chim. Acta* **2019**, *1091*, 160–168. [[CrossRef](#)]

16. Chen, H.; Zhang, L.; Zhang, W.; Wang, S. Construction of discontinuous capillary isoelectric focusing system and its application in pre-fractionation of exosomal proteins. *Talanta* **2020**, *208*, 119876. [[CrossRef](#)]
17. Zhang, H.; Deng, Y.; Liu, X.; Sun, J.; Ma, L.; Ding, Y.; Zhan, Z.; Zhang, H.; Yang, Y.; Gu, Y.; et al. Glass fiber-supported hybrid monolithic spin tip for enrichment of phosphopeptides from urinary extracellular vesicles. *Anal. Chem.* **2020**, *92*, 14790–14797. [[CrossRef](#)]
18. Multia, E.; Liangsupree, T.; Jussila, M.; Ruiz-Jimenez, J.; Kemell, M.; Riekkola, M.L. Automated on-line isolation and fractionation system for nanosized biomacromolecules from human plasma. *Anal. Chem.* **2020**, *92*, 13058–13065. [[CrossRef](#)]
19. Filipović, L.; Spasojević, M.; Prodanović, R.; Korać, A.; Matijašević, S.; Brajušković, G.; de Marco, A.; Popović, M. Affinity-based isolation of extracellular vesicles by means of single-domain antibodies bound to macroporous methacrylate-based copolymer. *New Biotechnol.* **2022**, *69*, 36–48. [[CrossRef](#)]
20. Peskoller, P.; Niessner, R.; Seidel, M. Development of epoxy-based monolith used for the affinity capturing of Escherichia coli bacteria. *J. Chromatogr. A* **2009**, *1216*, 3794–3801. [[CrossRef](#)]
21. Wolter, A.; Niessner, R.; Seidel, M. Preparation and characterization of functional poly(ethylene glycol) surfaces for the use of antibody microarrays. *Anal. Chem.* **2007**, *79*, 4529–4537. [[CrossRef](#)]
22. Ott, S.; Niessner, R.; Seidel, M. Preparation of epoxy-based microporous monolithic columns for the fast and efficient immunofiltration of Staphylococcus aureus. *J. Sep. Sci.* **2011**, *34*, 2181–2192. [[CrossRef](#)] [[PubMed](#)]
23. Buschmann, D.; Kirchner, B.; Hermann, S.; Märte, M.; Wurmser, C.; Brandes, F.; Kotschote, S.; Bonin, M.; Steinlein, O.K.; Pfaffl, M.W.; et al. Evaluation of serum extracellular vesicle isolation methods for profiling miRNAs by next-generation sequencing. *J. Extracell. Vesicles* **2018**, *7*, 1481321. [[CrossRef](#)] [[PubMed](#)]
24. Dhondt, B.; Van Deun, J.; Vermaerke, S.; de Marco, A.; Lumen, N.; De Wever, O.; Hendrix, A. Urinary extracellular vesicle biomarkers in urological cancers: From discovery towards clinical implementation. *Int. J. Biochem. Cell Biol.* **2018**, *99*, 236–256. [[CrossRef](#)] [[PubMed](#)]
25. Mussack, V.; Wittmann, G.; Pfaffl, M.W. Comparing small urinary extracellular vesicle purification methods with a view to RNA sequencing—Enabling robust and non-invasive biomarker research. *Biomol. Detect. Quantif.* **2019**, *17*, 100089. [[CrossRef](#)]
26. Guan, S.; Yu, H.; Yan, G.; Gao, M.; Sun, W.; Zhang, X. Characterization of urinary exosomes purified with size exclusion chromatography and ultracentrifugation. *J. Prot. Res.* **2020**, *19*, 2217–2225. [[CrossRef](#)]
27. Dhondt, B.; Geeurickx, E.; Tulkens, J.; Van Deun, J.; Vergauwenz, G.; Lippens, L.; Miinalainen, I.; Rappu, P.; Heino, J.; Ost, P.; et al. Unravelling the proteomic landscape of extracellular vesicles in prostate cancer by density-based fractionation of urine. *J. Extracell. Vesicles* **2020**, *9*, 1736935. [[CrossRef](#)] [[PubMed](#)]
28. Pomatto, M.A.C.; Gai, C.; Bussolati, B.; Camussi, G. Extracellular vesicles in renal pathophysiology. *Front. Mol. Biosci.* **2017**, *4*, 37. [[CrossRef](#)]
29. Erdbrügger, U.; Blijdorp, C.J.; Bijnsdorp, I.V.; Borràs, F.E.; Burger, D.; Bussolati, B.; Byrd, J.B.; Clayton, A.; Dear, J.W.; Falcón-Pérez, J.M.; et al. Urinary extracellular vesicles: A position paper by the Urine Task Force of the International Society for Extracellular Vesicles. *J. Extracell. Vesicles* **2021**, *10*, e12093. [[CrossRef](#)]
30. Svenningsen, P.; Sabaratnam, R.; Jensen, B.L. Urinary extracellular vesicles: Origin, role as intercellular messengers and biomarkers; efficient sorting and potential treatment options. *Acta Physiol.* **2020**, *228*, e13346. [[CrossRef](#)]
31. Göpfert, L.; Klüpfel, J.; Heinritz, C.; Elsner, M.; Seidel, M. Macroporous epoxy-based monoliths for rapid quantification of Pseudomonas aeruginosa by adsorption elution method optimized for qPCR. *Anal. Bioanal. Chem.* **2020**, *412*, 8185–8195. [[CrossRef](#)] [[PubMed](#)]
32. Konoshenko, M.Y.; Lekhnov, E.A.; Vlassov, A.V.; Laktionov, P.P. Isolation of extracellular vesicles: General methodologies and latest trends. *Biomed. Res. Int.* **2018**, *2018*, 8545347. [[CrossRef](#)]
33. Aliprandi, M.; Sparacio, E.; Pivetta, F.; Ossolengo, G.; Maestro, R.; de Marco, A. The availability of a recombinant anti-SNAP antibody in VHH format amplifies the application flexibility of SNAP-tagged proteins. *J. Biomed. Biotechnol.* **2010**, *2010*, 658954. [[CrossRef](#)] [[PubMed](#)]
34. Liang, L.G.; Kong, M.Q.; Zhou, S.; Sheng, Y.F.; Wang, P.; Yu, T.; Inci, F.; Kuo, W.P.; Li, L.J.; Demirci, U.; et al. An integrated double-filtration microfluidic device for isolation, enrichment and quantification of urinary extracellular vesicles for detection of bladder cancer. *Sci. Rep.* **2017**, *7*, 46224. [[CrossRef](#)]
35. Oeyen, E.; Van Mol, K.; Baggerman, G.; Willems, H.; Boonen, K.; Rolfo, C.; Pauwels, P.; Jacobs, A.; Schildermans, K.; Cho, W.C.; et al. Ultrafiltration and size exclusion chromatography combined with asymmetrical-flow field-flow fractionation for the isolation and characterisation of extracellular vesicles from urine. *J. Extracell. Vesicles* **2018**, *7*, 1490143. [[CrossRef](#)] [[PubMed](#)]
36. Ambrosetti, E.; Bernardinelli, G.; Hoffecker, I.; Hartmanis, L.; Kiriako, G.; de Marco, A.; Sandberg, R.; Högberg, B.; Teixeira, A.I. A DNA-nanoassembly-based approach to map membrane protein nanoenvironments. *Nat. Nanotechnol.* **2021**, *16*, 85–95. [[CrossRef](#)] [[PubMed](#)]
37. D’Agostino, S.; Mazzega, E.; Praček, K.; Piccinin, S.; Pivetta, F.; Armellin, M.; Fortuna, S.; Maestro, R.; de Marco, A. Interference of p53:Twist1 interaction through competing nanobodies. *Int. J. Biol. Macromol.* **2022**, *194*, 24–31. [[CrossRef](#)]
38. Kunze, A.; Pei, L.; Elsässer, D.; Niessner, R.; Seidel, M. High performance concentration method for viruses in drinking water. *J. Virol. Methods* **2015**, *222*, 132–137. [[CrossRef](#)]

39. Wunderlich, A.; Torggler, C.; Elsässer, D.; Lück, C.; Niessner, R.; Seidel, M. Rapid quantification method for *Legionella pneumophila* in surface water. *Anal. Bioanal. Chem.* **2016**, *408*, 2203–2213. [[CrossRef](#)]
40. Sherwood, L.J.; Hayhurst, A. Periplasmic Nanobody-APEX2 fusions enable facile visualization of Ebola, Marburg, and Mënglà virus nucleoproteins, alluding to similar antigenic landscapes among Marburgvirus and Dianlovirus. *Viruses* **2019**, *11*, 364. [[CrossRef](#)]

**Disclaimer/Publisher’s Note:** The statements, opinions and data contained in all publications are solely those of the individual author(s) and contributor(s) and not of MDPI and/or the editor(s). MDPI and/or the editor(s) disclaim responsibility for any injury to people or property resulting from any ideas, methods, instructions or products referred to in the content.

## 5.2 Publication 2: Flow-Based Chemiluminescence Microarrays as Screening Platform for Affinity Binders to Capture and Elute Bacteria

### 5.2.1 Summary

This publication presents a CL microarray screening assay on the flow-based platform MCR-R for affinity binders against bacteria. This proof-of-concept work demonstrates that the assay can be used to screen for new suitable affinity binders and their corresponding elution buffers. In the future, these affinity binders can be used for affinity-based methods for isolating and detecting pathogens in body fluids, such as ascites. First, *E. coli* and *E. faecalis* were labeled with *N*-hydroxysulfosuccinimidobiotin to allow a CL detection using strep-HRP. For the assay, multiple affinity binders (an anti-*E. coli* antibody and an anti-*Enterococcus* antibody, Concanavalin A, lysozyme, Polymyxin B) were immobilized on carboxy-functionalized polycarbonate foils via their primary amines using EDC and sulfo-NHS. In the MCR-R, the sample containing biotin-labeled bacteria was flushed over the microarray chip so that the bacteria could bind to the affinity binders. Through the biotin label, they can be detected with strep-HRP by CL. After manual desorption - with or without an incubation period - a second detection is performed. Assay performance was checked first regarding the unspecific binding of streptavidin-HRP to the bound affinity binders and consequential high blank signals. No unspecific binding was found for any tested affinity binder, except Concanavalin A, which was excluded from further testing. Unspecific binding of *N*-hydroxysulfosuccinimidobiotin remaining from the biotinylation process was also excluded. The optimal bacterial concentration was evaluated and found to be  $10^8$  cells mL<sup>-1</sup>. The respective antibodies were found to be the best affinity binders for each tested bacterium. For *E. coli*, a 0.01 M glycine buffer was found to be the best elution buffer. For *E. faecalis*, none of the tested buffers were suitable. An affinity binder suitable for both bacteria is Polymyxin B, with methyl alpha-D-mannopyranoside as elution buffer. The screening assay allows for a fast multiplex screening within 35 minutes, with the microarray chip having space for up to 18 different affinity binders.

### 5.2.2 Own Contribution

- Planning and performing of all experiments
- Establishing of polycarbonate foils as microarray surface
- Adaption of measurement program on the MCR-R
- Data analysis
- Writing of manuscript

### 5.2.3 Reprint Permission

Neumair, J.; Elsner, M.; Seidel, M. Flow-Based Chemiluminescence Microarrays as Screening Platform for Affinity Binders to Capture and Elute Bacteria. *Sensors* **2022**, *22*, 8606. <https://doi.org/10.3390/s22228606>

#### Open Access

© 2022 by the authors. Licensee MDPI, Basel, Switzerland. This article is an open access article distributed under the terms and conditions of the Creative Commons Attribution (CC BY) license (<https://creativecommons.org/licenses/by/4.0/>).

#### Permissions

No special permission is required to reuse all or part of article published by MDPI, including figures and tables. For articles published under an open access Creative Common CC BY license, any part of the article may be reused without permission provided that the original article is clearly cited. Reuse of an article does not imply endorsement by the authors or MDPI.

## Article

# Flow-Based Chemiluminescence Microarrays as Screening Platform for Affinity Binders to Capture and Elute Bacteria

Julia Neumair, Martin Elsner and Michael Seidel \* 

TUM School of Natural Sciences, Department of Chemistry, Technical University of Munich, 85748 Garching, Germany

\* Correspondence: michael.seidel@mytum.de; Tel.: +49-89-289-54506

**Abstract:** Affinity describes the non-covalent but selective interaction between an affinity binder (e.g., proteins, antibiotics, or antibodies) and its counterpart (e.g., bacteria). These affinity binders can serve to detect bacteria and respond to the need for selective concentration via affinity chromatography for trace analysis. By changing the pH value or salt and protein contents, affinity bindings can be reversed, and bacteria can be recovered for characterisation. Analytical microarrays use multiple affinity binders immobilised on the surface in a distinct pattern, which immensely reduces screening time for the discovery of superior binding motifs. Here, flow-based microarray systems can inform not only about binding, but also about desorption. In this work, we pioneer a screening assay for affinity binders against both gram-positive and negative bacteria based on an automated flow-based chemiluminescence (CL) microarray. Biotinylation of model organisms *E. coli* and *E. faecalis* enabled labelling with horseradish-peroxidase-coupled streptavidin, and detection with CL. Polymyxin B, an antibiotic against gram-negative bacteria, was found to bind both *E. coli* and *E. faecalis*. Simultaneous screening for desorption methods unexpectedly revealed methyl alpha-D-mannopyranoside as a promising buffer for desorption from Polymyxin B. This proof-of-principle study shows that our new platform greatly facilitates the screening of new affinity binders against bacteria, with promise for future automation.



**Citation:** Neumair, J.; Elsner, M.; Seidel, M. Flow-Based Chemiluminescence Microarrays as Screening Platform for Affinity Binders to Capture and Elute Bacteria. *Sensors* **2022**, *22*, 8606. <https://doi.org/10.3390/s22228606>

Academic Editor: Hugo Aguas

Received: 1 October 2022

Accepted: 4 November 2022

Published: 8 November 2022

**Publisher's Note:** MDPI stays neutral with regard to jurisdictional claims in published maps and institutional affiliations.



**Copyright:** © 2022 by the authors. Licensee MDPI, Basel, Switzerland. This article is an open access article distributed under the terms and conditions of the Creative Commons Attribution (CC BY) license (<https://creativecommons.org/licenses/by/4.0/>).

**Keywords:** pathogens; microarray; chemiluminescence; affinity

## 1. Introduction

The rapid and sensitive detection of bacteria is crucial in many areas like diagnostics, water and food analytics. Whilst pathogenic bacteria can already cause health problems in low concentrations, their detection at these low concentrations may be difficult. To overcome this problem, an enrichment of bacteria is necessary. Hereby, various methods for enrichment, such as centrifugation [1] or filtration [2], have been brought forward. If more specific enrichment methods are required, affinity-based methods [3–5] hold great promise. Here, an affinity between the used affinity binders and the bacterial cell walls is utilised to capture the bacteria and, in this way, to remove them from the sample matrix. Subsequently, a direct detection [6] or a desorption from the separation matrix before detection [7] can be performed. Various groups, such as antibodies [8], lectins [9,10], or antibiotics [3,5] can serve as affinity binders.

Affinity binding is also used in the concept of microarrays. Microarrays are multi-analyte platforms in which different types of probes are immobilised on the microarray chip surface. Utilizing the affinity between bacterial cells and immobilised probes, bacteria can be identified and quantified [11–16]. Although some microarrays follow a microtiter plate format [17,18], most are chip-based. To simplify the assay workload, many microarray assays rely on a lateral flow [19,20] or are flow-based [12,21,22]. For the latter, the liquid reagents are transported over the microarray chip surface by using a pump, which also allows for automation. The multiplexing manner of microarrays is one of its major advantages, as it allows for the simultaneous detection of multiple analytes with only one

measurement. However, the interaction of one analyte with multiple immobilised probes can also be investigated. The detection of bacterial cells on a microarray can either be performed label-free—for example, with electrochemical sensors [23–25]—or via labelling of the bacterial cells. Labelling—either direct labelling of the bacterial cells [26] or via a labelled second probe—is often performed using fluorescence [18] or chemiluminescence (CL) markers [14,27].

In this work, an existing automated-flow-based CL microarray platform [28] was used to establish the first assay to study the adsorption and desorption properties of affinity binders towards bacteria. Our aim was to pioneer a novel tool to greatly facilitate the screening for new affinity binders and their corresponding desorption buffers. To enable detection of bacteria using a CL microarray, the cells were biotinylated using biotin 3-sulfo-N-hydroxysuccinimide ester sodium salt (sNHS-biotin) which forms covalent bonds with free amino groups at the bacterial cell surface.

Different types of affinity binders were chosen to interact with the model organisms *Escherichia coli* and *Enterococcus faecalis*. The antibiotic polypeptide Polymyxin B (PmB) is a cyclic lipopeptide possessing a fatty acid tail [29,30] and is mainly used against gram-negative bacteria. Its cationic properties allow interaction with phospholipids and lipopolysaccharide structures of the cell wall of gram-negative bacteria [30]. It was already used in the affinity filtration of *Escherichia coli* [3] as well as in the removal of endotoxins [31]. Lysozyme is an enzyme that is known for its bacteriolytic properties, mostly for gram-positive bacteria. Hereby, it disrupts the peptidoglycans that the cell wall is built of [32]. As a third affinity binder, the lectin Concanavalin A (ConA) was used, which has a high affinity towards sugar moieties, which are present on the bacterial cell walls. It was already used in biosensors and for the enrichment of bacteria [33–35]. Additionally, antibodies were used as immuno-affinity binders, and one antibody against all O and K antigenic serotypes of *E. coli* and one against *Enterococcus species* were chosen.

In this proof-of-principle study, we could identify PmB as a highly promising affinity binder to the gram-negative bacterium *E. coli* and gram-positive bacterium *E. faecalis*. This was unexpected, as PmB is only used as an antibiotic against gram-negative bacteria. The multiplex manner of the screening platform allowed fast testing of various desorption reagents for all affinity binders at once. This facilitated the discovery of methyl alpha-D-mannopyranoside (MADM) as a new promising desorption reagent for PmB, although it was originally applied to the lectin ConA.

## 2. Materials and Methods

### 2.1. Materials and Buffers

If not stated otherwise, chemicals were purchased from Sigma Aldrich (Darmstadt, Germany), a subsidiary of Merck, or Carl Roth (Karlsruhe, Germany). Streptavidin was purchased from IBA Lifesciences (Göttingen, Germany) and horseradish-peroxidase-labelled streptavidin (HRP-streptavidin) from Biozol (Eching, Germany). CL reagents (luminol and hydrogen peroxide) were purchased as the Elistar Supernova reagent kit from Cyanagen (Bologna, Italy). *E. coli* serotype O/K polyclonal antibody and *Enterococcus* polyclonal antibody were provided by Thermo Fisher Scientific (Waltham, MA, USA). Polycarbonate foils (Makrolon® GP, 0.25 mm) were obtained from Modulor (Berlin, Germany). *E. coli* (DSM 1003) and *E. faecalis* (DSM 2570) were bought from the German Collection of Microorganisms and Cell Cultures (Braunschweig, Germany). Ultrapure water was used unless stated otherwise. Experiments with viable bacteria were performed in a laboratory with a biosafety level of 2.

Phosphate-buffered saline (PBS, pH 7.4) was prepared using 70 mM K<sub>2</sub>HPO<sub>4</sub>, 10 mM KH<sub>2</sub>PO<sub>4</sub> and 145 mM NaCl. As running buffer for the MCR-R, a 0.1% Tween® 20 solution in PBS (PBS-T) was used. Carbonate buffer with pH 9.6 was prepared from 15 mM Na<sub>2</sub>CO<sub>3</sub> and 35 mM NaHCO<sub>3</sub>; beef extract glycine buffer (BEG, pH 9.5) consisted of 505 mM glycine and 3% beef extract powder.

## 2.2. Bacterial Cultivation

*E. coli* (DSM 1003) and *E. faecalis* (DSM 2570) from cryo-cultures ( $-80\text{ }^{\circ}\text{C}$ ) were cultivated on tryptic soy agar plates overnight at  $37\text{ }^{\circ}\text{C}$ . For the preparation of stock suspensions, cells were harvested, washed two times by centrifuging (10 min, 4500 rpm,  $4\text{ }^{\circ}\text{C}$ ), and resuspending the sample in PBS (pH 8). Cell concentrations were determined via photometric measurements on a NanoPhotometer from Implen (Munich, Germany).

## 2.3. Biotinylation

The freshly prepared bacterial stock suspensions in PBS (pH 8) were diluted to a working concentration of  $10^9$  cells  $\text{mL}^{-1}$ , and biotin 3-sulfo-N-hydroxysuccinimide ester sodium salt (sNHS-biotin) was added to achieve an end concentration of  $2\text{ mg mL}^{-1}$ . The reaction mixture was incubated on ice at 100 rpm for 30 min. Afterwards, the cells were washed twice with 0.1 M glycine in PBS and once with PBS (10 min, 4500 rpm,  $4\text{ }^{\circ}\text{C}$ ). Finally, the cells were resuspended in PBS, and the cell concentration was determined using OD measurements and culture. The biotinylated bacteria were stored at  $4\text{ }^{\circ}\text{C}$ .

## 2.4. Production of Microarray Chips

Polycarbonate foils (0.25 mm) were used as a surface for the microarray chips and were prepared based on a protocol described elsewhere [36]. In short, foils were cut into a sheet of  $3 \times 3$  chips in the size of  $26 \times 76\text{ mm}$  using the CE 6000–40 cutting plotter from Graphtec Corporation (Yokohama, Japan), coated with succinylated Jeffamine<sup>®</sup> ED-2003 using a screen printer, and incubated at  $95\text{ }^{\circ}\text{C}$  for 2 h before washing and drying. Until further use, the sheets were stored at room temperature under reduced humidity. Affinity binders were immobilised in rows of five spots using the contact spotter BioOdyssey Calligrapher<sup>®</sup> MiniArrayer from Bio-Rad (Hercules, USA). The distance between the spots of one row was  $1100\text{ }\mu\text{m}$ , and the distance was  $1300\text{ }\mu\text{m}$  between the spots of different rows (diameter of spots  $150\text{ }\mu\text{m}$ ). Spotting solutions contained  $0.4\text{ mg mL}^{-1}$  1-ethyl-3-(3-(dimethylamino)propyl)carbodiimide (EDC),  $1.1\text{ mg mL}^{-1}$  N-hydroxysulfosuccinimide sodium salt (sulfo-NHS), and the reagents to be immobilised in PBS. End concentrations were  $1\text{ mg mL}^{-1}$  for lysozyme, ConA, PmB, and the antibacterial antibodies. Polyclonal antiperoxidase antibody from rabbit (1:40 dilution) and streptavidin ( $1\text{ mg mL}^{-1}$ ) were used as positive controls; the negative control was the spotting solution without any further reagent. In Figure 1 (right side), the spotting scheme is shown. Spotting took place at  $20\text{ }^{\circ}\text{C}$  and 55% relative humidity, and the sheets were incubated overnight under the same conditions. Afterwards, the sheets were divided into individual pieces, and microarray chips were assembled using a black polyoxymethylene (POM) carrier plate with in- and outlets and a double-sided adhesive (thickness  $140\text{ }\mu\text{m}$ ) with a cut-out flow channel ( $56\text{ }\mu\text{L}$ , Figure 1, left). Microarray chips were stored at  $4\text{ }^{\circ}\text{C}$  until further use.

## 2.5. Screening Assay

The whole assay—except for the desorption step—was automated on the Microarray Chip Reader—Research (MCR-R) built by GWK Präzisionstechnik (Munich, Germany). At the beginning of each measurement day, the device was set up by filling all tubes with running buffer and loading the used reagents (1% Casein in PBS for blocking, HRP-streptavidin diluted 1:2000 in running buffer, and the individual CL reagents (luminol and hydrogen peroxide)). The microarray chip holder on the MCR-R was heated to  $35\text{ }^{\circ}\text{C}$ . For every microarray chip, a darkframe picture was taken. For this, the microarray chip was inserted directly before measurement into the MCR-R, flushed with running buffer, and an image was recorded for 60 s without adding any reagent.

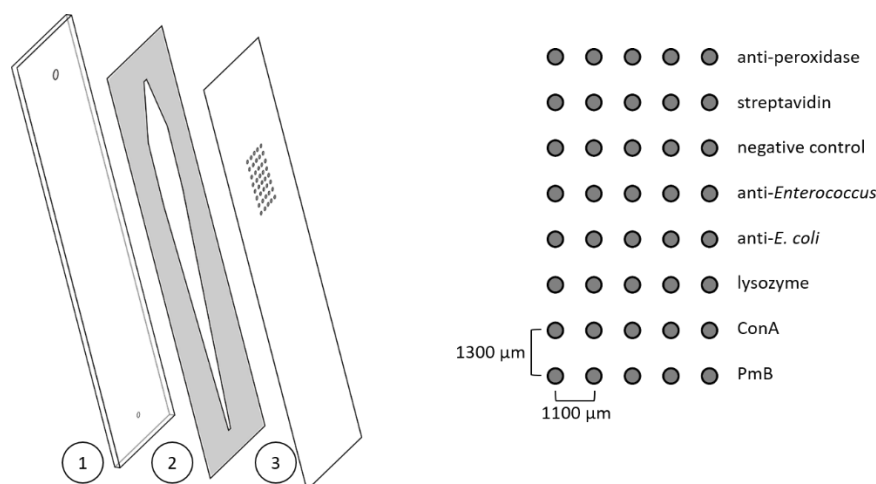


**Figure 1.** Left: scheme of a disassembled microarray chip consisting of a black polyoxymethylene carrier plate with in- and outlets (1); a double-sided adhesive with cut-out flow channel (2); and the polycarbonate sheet with immobilised reagents (3). On the right, the spotting scheme is shown.

The sample to be measured was injected into the sample port, and the measuring program was started. A total of 604  $\mu\text{L}$  of the sample was first transported to the chip ( $50 \mu\text{L s}^{-1}$ ) and then passed over the chip ( $1 \mu\text{L s}^{-1}$ ) using a stopped flow consisting out of ten increments with an incubation time of 30 s each. After a washing step with running buffer (2000  $\mu\text{L}$ ,  $150 \mu\text{L s}^{-1}$ ), the casein solution for blocking and the HRP-streptavidin solution were first transported to the chip ( $50 \mu\text{L s}^{-1}$ ) and then passed over the chip (both 600  $\mu\text{L}$ , 5 and  $2 \mu\text{L s}^{-1}$ ), followed each time by another washing step. Finally, the CL reagents (luminol and hydrogen peroxide) were mixed in a 1:1 ratio (both 200  $\mu\text{L}$ ) and injected into the chip ( $100 \mu\text{L s}^{-1}$ ), and an image was recorded immediately for 60 s. After an additional washing step (1000  $\mu\text{L}$ ,  $200 \mu\text{L s}^{-1}$ ), the microarray chip was removed directly from the device, and desorption was performed manually. Using a pipette, 100  $\mu\text{L}$  of desorption buffer was flushed through the chip. For experiments with an incubation step, the desorption buffer was incubated on the chip for 60 s and removed afterwards. The chip was then inserted back immediately into the device, and the previous steps were repeated, starting from the passing of the HRP-streptavidin. To avoid contamination between measurements, the tubes of the device were flushed during desorption (with a different chip) and after the second image acquisition (3 times 2500 mL,  $500 \mu\text{L s}^{-1}$ ). The detailed measuring program on the MCR-R containing volumes and flow rates for every step is shown in Table 1. A schematic fluidic plan as well as the pathways for reagents are shown in Supplementary Materials Figure S1 and Table S1.

**Table 1.** Measuring program on the MCR-R.

Step	Process	Volume/ $\mu\text{L}$	Flow Rate/ $\mu\text{L s}^{-1}$	Comments
1	Transport sample to chip	118	50	
2	Sample incubation	600	1	10 increments, pause 30 s
3	Wash chip	2000	150	
4	Block chip	90 600	50 5	Casein in PBS
5	Wash chip	2000	150	
6	Incubate HRP-streptavidin	118 600	50 2	
7	Wash chip	2000	150	

Table 1. Cont.

Step	Process	Volume/ $\mu\text{L}$	Flow Rate/ $\mu\text{L s}^{-1}$	Comments
8	Add CL reagents	400 (200 each)	100	Luminol and hydrogenperoxide
9	Take image			60 s exposure
10	Flush chip	1000	200	
11	Remove chip			Manual desorption
12	Flush device	2500	500	Sample loop
		2500	500	Sample way
		2500	500	Chip (extra washing chip)
13	Insert chip			
14	Incubate HRP-streptavidin	118	50	
		600	2	
15	Wash chip	2000	150	
16	Add CL reagents	400 (200 each)	100	Luminol and hydrogenperoxide
17	Take image			60 s exposure
18	Flush device	2500	500	Sample loop
		2500	500	Sample way
		2500	500	Chip

### 2.6. Data Evaluation

The software of the MCR-R device automatically subtracts the darkframe CL signals from the CL signals obtained during the measurements. The resultant files were evaluated using the software MCR spotreader (Stefan Weißenberger, Munich, Germany). A grid was placed over the image, with one box per spot. The software calculated the CL signal for each box as the mean of the 10 brightest pixels. The output for every immobilised reagent is given as the mean of the corresponding row (5 spots), and spots which deviated by more than 10% were excluded. The CL signal is then normalised for every measured microarray chip by dividing the CL signal of the spotted affinity binders by the CL signal of the spotted negative control.

$$\text{normalised CL signal (affinity binder)} = \frac{\text{mean CL signal (spotted affinity binder)}}{\text{mean CL signal (spotted negative control)}} \quad (1)$$

The mean-normalised CL signal is given as the mean of the microarray chips measured with the corresponding standard deviation between experiments, whereas  $n$  is the number of experiments.

Statistical analysis was performed in Excel using the Real Statistics Resource Pack software ((Release 7.6). Copyright (2013–2021) Charles Zaiontz. [www.real-statistics.com](http://www.real-statistics.com), accessed on 20 October 2022). A Shapiro–Wilk test ( $\alpha = 0.05$ ) was performed to check for normal distribution of data, whereas variance homogeneity was investigated with a Levene’s test (results not shown,  $\alpha = 0.05$ ). Depending on the outcome of these two tests, either a one-factor analysis of variance (ANOVA,  $\alpha = 0.05$ ) followed by a Tukey HSD test ( $\alpha = 0.05$ ) or a Kruskal–Wallis test ( $\alpha = 0.05$ ) followed by a Conover test ( $\alpha$  corrected with Bonferroni correction) was done. For effect sizes, Cohen’s  $d$  was calculated, classification was done according to Sawilowsky et al. [37].

## 3. Results and Discussion

### 3.1. Assay Concept

The flow-based CL microarray assay was established on the MCR-R. On this platform, reagent addition as well as imaging are executed automatically. Volumes and flow rates of

each reagent are controlled separately. Affinity binders are immobilised on the surface of the flow-through microarray chips. To start a measurement, the assembled microarray chip is inserted into the MCR-R. Samples containing biotinylated bacteria are incubated on the microarray chip in a stopped-flow manner in order to enhance the interaction time between the affinity binder and bacteria. For imaging, the HRP-streptavidin is flushed over the chip and binds to the biotin present at the bacteria's cell wall. CL reagents luminol and  $H_2O_2$  are mixed and flushed over the chip, after which the bound HRP-streptavidin catalyses the CL reaction and CL signals are recorded by a CCD camera installed in the MCR-R. For testing the desorption from the affinity binders, the microarray chip is removed and flushed by pipetting the desorption buffer into the chip and incubating depending on the desorption mode. The chip is inserted again for the second measurement starting from the HRP-streptavidin step (Figure 2).

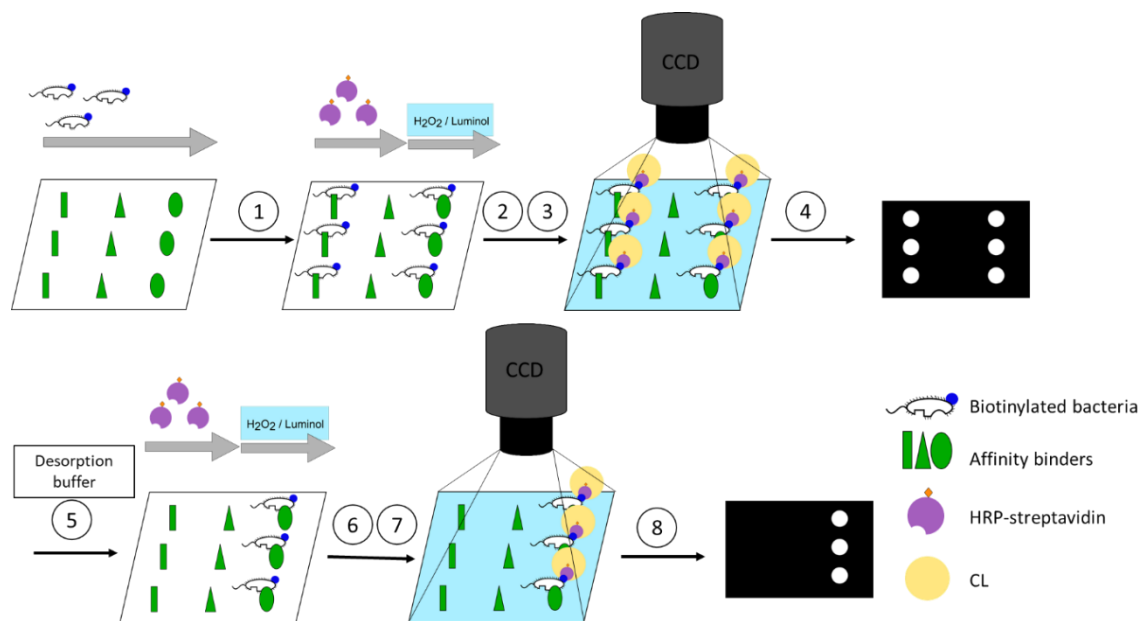


**Figure 2.** Concept of the screening assay. (1): Capture of the biotinylated bacteria through the affinity binders depending on the affinity. (2): Binding of the horseradish peroxidase (HRP)-labelled streptavidin. (3): Chemiluminescence (CL) reaction. (4): Image acquisition. (5): Desorption of bacteria by desorption buffer depending on reversing of affinity. (6): Binding of the HRP-streptavidin. (7): CL reaction. (8): Image acquisition.

### 3.2. Biotinylation of Bacteria

For detection of bound bacteria using CL via coupling with HRP-streptavidin, bacterial cells were biotinylated. As the biotinylation process consists of several washing steps, during which the cell suspension is centrifuged and the formed pellet is resuspended, cells could be lost or inactivated. The loss of total bacterial cells, or rather their recovery, was evaluated by photometric measurements, whereas their viability—or more specific, their culturability—was tested via culture.

For *E. coli*, for the total cells, a recovery of  $95 \pm 16\%$  ( $n = 10$ ;  $W(9) = 0.97$ ,  $p = 0.83$ ) was found, indicating little to no cell loss. For the culturability, a recovery of  $98 \pm 51\%$  ( $n = 7$ ;  $W(6) = 0.98$ ,  $p = 0.97$ ) was found. An ANOVA showed no significant difference between these data ( $F(1,15) = 0.08$ ,  $p = 0.77$ ).

At the same time, for *E. faecalis*, a recovery for total cells of only  $70 \pm 22\%$  ( $n = 9$ ;  $W(8) = 0.96$ ,  $p = 0.84$ ) and for culturable cells of  $75 \pm 29\%$  ( $n = 7$ ;  $W(6) = 0.95$ ,  $p = 0.74$ ) was found. Here again, no significant difference was found ( $F(1,15) = 0.16$ ,  $p = 0.70$ ). The recoveries for *E. coli* and *E. faecalis* total cells were significantly different ( $F(1,18) = 8.6$ ,

$p = 0.01$ ), which leads to the conclusion that the effect from the biotinylation process is diverse for different bacteria.

### 3.3. Assay Development

Before the assay can be used for the screening for binding and desorption of bacteria from affinity binders, the assay has to be established. For this, blank measurements (only PBS), control measurements with sNHS treated according to the biotinylation protocol, *E. coli* and *E. faecalis* without biotinylation, and measurements with the biotinylated bacteria were performed. For every affinity binder over the six different samples, a Kruskal–Wallis test was performed, and significant differences between the samples were found (PmB: *chi-square* (5) = 81.11,  $p = 4.90 \times 10^{-16}$ ; lysozyme: *chi-square* (5) = 58.94,  $p = 2.01 \times 10^{-11}$ ; anti-*E. coli*: *chi-square* (5) = 85.49,  $p = 5.95 \times 10^{-17}$ ; anti-*Enterococcus*: *chi-square* (5) = 82.32,  $p = 2.74 \times 10^{-16}$ ). Post-hoc Conover tests (corrected  $\alpha = 0.003$ ) were performed; the results therefore will be shown in the next relevant paragraphs.

First, we checked if the obtained CL signals stemmed from bound bacteria or from any unspecific bindings. Testing for (unspecific) bindings between HRP-streptavidin and affinity binders was conducted by performing the assay without adding bacteria and measuring only with PBS (Figure 3, lightest grey,  $n = 26–35$ ). For the affinity binders PmB ( $n = 35$ ,  $W(34) = 0.97$ ,  $p = 0.29$ ), for lysozyme ( $n = 26$ ,  $W(25) = 0.99$ ,  $p = 0.99$ ), and for both of the antibacterial antibodies (anti-*E. coli*:  $n = 35$ ,  $W(34) = 0.98$ ,  $p = 0.79$ ; anti-*Enterococcus*:  $n = 33$ ,  $W(32) = 0.98$ ,  $p = 0.91$ ), the mean-normalised CL signals were between 1.0 and 1.3, indicating little to no unspecific binding. For ConA, a specific interaction towards HRP was given [38], so a higher mean-normalised CL signal was expected. A mean-normalised CL signal of  $37.9 \pm 22.5$  ( $n = 35$ ,  $W(34) = 0.93$ ,  $p = 0.03$ ) confirmed these expectations, so we excluded ConA from further experiments.

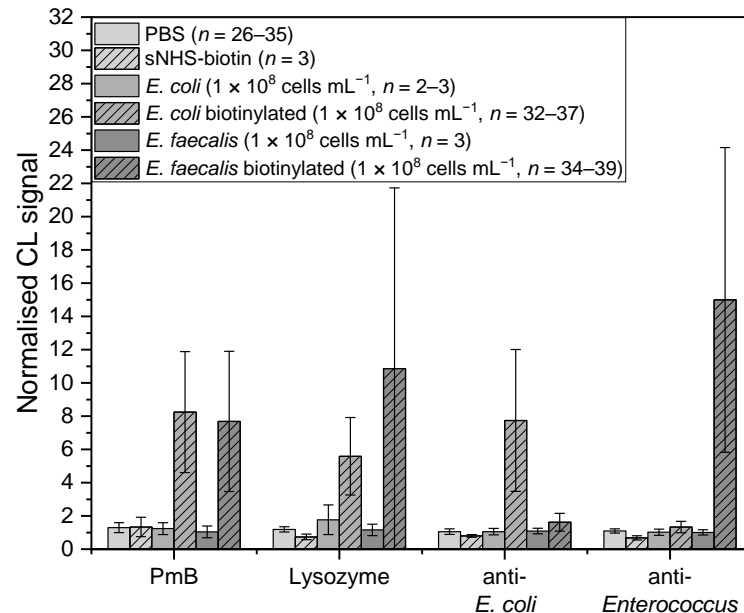


**Figure 3.** Normalised CL signals for the affinity binders Polymyxin B (PmB), lysozyme, *E. coli* serotype O/K polyclonal antibody (anti-*E. coli*) and *Enterococcus* polyclonal antibody (anti-*Enterococcus*). Control measurements for negative controls were conducted with PBS ( $n = 26–35$ , lightest grey), sNHS-biotin ( $n = 3$ , lightest grey shaded) and with bacteria without biotinylation ( $n = 2–3$ , medium and darkest grey). Positive control measurements were done with biotinylated bacteria ( $n = 32–39$ , medium and darkest grey shaded). Concentrations for measurements with bacteria were  $1 \times 10^8$  cells mL<sup>-1</sup>.

Another effect on the CL signal could derive from any remaining free sNHS-biotin from the biotinylation process that could attach to the affinity binder and cause a signal. Therefore, the sNHS-biotin solution was treated the same way as for the biotinylation of

bacteria. Normalised CL signals of immobilised streptavidin give information as to whether there is still sNHS-biotin left in the sample after washing or if it was completely removed. A Kruskal–Wallis test of the mean-normalised CL signal of the sNHS-biotin control with  $9.0 \pm 4.7$  ( $n = 3$ ) compared to  $1.4 \pm 0.4$  ( $n = 36$ ,  $W(35) = 0.95$ ,  $p = 0.10$ ) of the PBS blank shows that there is a significant difference between the data ( $\chi^2(1) = 8.1$ ,  $p = 0.004$ ), which was confirmed with a Conover test ( $t(37) = 3.17$ ,  $p = 0.003$ ,  $d = 6.60$ ). This indicates that some of the sNHS-biotin was indeed still left in the sample. Examining the mean-normalised CL signals (Figure 3, lightest grey, shaded,  $n = 3$ ) for PmB ( $t(111) = 0.12$ ,  $p = 0.91$ ), lysozyme ( $t(95) = 1.53$ ,  $p = 0.13$ ) and the antibodies (anti-*E. coli*:  $t(114) = 2.20$ ,  $p = 0.03$ ; anti-*Enterococcus*:  $t(108) = 2.83$ ,  $p = 0.006$ ) with values between 0.7 and 1.3. However, no significant differences between the blank measurements and the sNHS measurements were found. To verify that biotinylation on the bacteria is necessary and that no unspecific binding between them and the HRP-streptavidin occurs, the assay was performed with non-biotinylated *E. coli* and *E. faecalis* ( $1 \times 10^8$  cells  $\text{mL}^{-1}$ ) (Figure 3, middle and darkest grey,  $n = 2$ –3). Mean-normalised CL signals for PmB (*E. coli*:  $n = 2$ ,  $t(111) = 0.14$ ,  $p = 0.89$ , *E. faecalis*:  $n = 3$ ,  $t(111) = 0.90$ ,  $p = 0.37$ ), lysozyme ( $n = 3$ , *E. coli*:  $t(95) = 1.86$ ,  $p = 0.06$ , *E. faecalis*:  $t(95) = 0.31$ ,  $p = 0.76$ ), anti-*E. coli* ( $n = 3$ , *E. coli*:  $t(114) = 0.03$ ,  $p = 0.98$ , *E. faecalis*:  $t(114) = 0.18$ ,  $p = 0.86$ ), and anti-*Enterococcus* ( $n = 3$ , *E. coli*:  $t(108) = 0.79$ ,  $p = 0.43$ , *E. faecalis*:  $t(108) = 0.92$ ,  $p = 0.36$ ) were between 1.0 and 1.7. No significant difference from the blank measurements and therefore no unspecific binding was observed.

Last, the assay was verified using the biotinylated bacteria (Figure 3, middle and darkest grey, shaded,  $1 \times 10^8$  cells  $\text{mL}^{-1}$ ). For *E. coli*, the two affinity binders PmB and lysozyme gave mean-normalised CL signals of  $8.2 \pm 3.6$  ( $n = 36$ ,  $W(35) = 0.98$ ,  $p = 0.59$ ) and  $5.6 \pm 2.3$  ( $n = 32$ ,  $W(31) = 0.97$ ,  $p = 0.54$ ), respectively, which showed a significant difference from the measurements in PBS (PmB:  $t(111) = 13.26$ ,  $p = 1.21 \times 10^{-24}$ ,  $d = 2.18$ ; lysozyme:  $t(95) = 9.01$ ,  $p = 2.15 \times 10^{-14}$ ,  $d = 0.67$ ), indicating an interaction with the bacterial cells. For the anti-*E. coli* antibody, the mean-normalised CL signal was  $7.7 \pm 4.3$  ( $n = 37$ ,  $W(36) = 0.96$ ,  $p = 0.15$ ,  $t(114) = 15.62$ ,  $p = 4.18 \times 10^{-30}$ ,  $d = 3.68$ ), which also showed a significant difference from the blank measurements, whereas for the anti-*Enterococcus* antibody, it was  $1.3 \pm 0.3$  ( $n = 37$ ,  $W(36) = 0.98$ ,  $p = 0.64$ ,  $t(108) = 4.09$ ,  $p = 8.39 \times 10^{-5}$ ,  $d = 0.05$ ), which is a significant difference from the PBS but with a very small effect size. This outcome was expected, as the aforementioned antibodies should bind or should not bind with *E. coli*, respectively. Observing the overall effect size, the anti-*E. coli* antibody had the greatest effect and is therefore considered the best affinity binder, followed by PmB.

For *E. faecalis*, the two affinity binders PmB and lysozyme showed mean-normalised CL signals of  $7.7 \pm 4.2$  ( $n = 38$ ,  $W(37) = 0.91$ ,  $p = 0.005$ ,  $t(111) = 12.38$ ,  $p = 1.25 \times 10^{-22}$ ,  $d = 2.01$ ), and  $10.9 \pm 10.9$  ( $n = 34$ ,  $W(33) = 0.83$ ,  $p = 1.05 \times 10^{-4}$ ,  $t(95) = 9.16$ ,  $p = 1.03 \times 10^{-14}$ ,  $d = 1.48$ ), respectively, indicating significant differences to the blank measurement with PBS. The standard deviation for lysozyme was very high, suggesting a non-uniform interaction between the cells and the affinity binder. Additionally, the mean-normalised CL signals for the antibodies were as expected, with  $1.6 \pm 0.5$  ( $n = 39$ ,  $W(38) = 0.95$ ,  $p = 0.06$ ,  $t(114) = 6.30$ ,  $p = 5.87 \times 10^{-9}$ ,  $d = 1.47$ ) for the anti-*E. coli* and  $15.0 \pm 9.2$  ( $n = 36$ ,  $W(35) = 0.89$ ,  $p = 0.001$ ,  $t(108) = 14.80$ ,  $p = 9.86 \times 10^{-28}$ ,  $d = 2.66$ ) for the anti-*Enterococcus*, which are both significantly different from the blank measurements, but the anti-*Enterococcus* displayed the greatest effect size. Regarding the effect sizes, the anti-*Enterococcus* is found to be the best affinity binder.

Standard deviations for measurements with biotinylated bacteria revealed  $52 \pm 23\%$  ( $n = 8$ ,  $W(17) = 0.89$ ,  $p = 0.24$ ), which were significantly higher than without biotinylated bacteria, which showed values of  $23 \pm 11\%$  ( $n = 16$ ,  $W(15) = 0.88$ ,  $p = 0.04$ ;  $\chi^2(1) = 10.53$ ,  $p = 0.001$ ,  $t(22) = 4.31$ ,  $p = 2.82 \times 10^{-4}$ ,  $d = 1.81$ ). The measurements without biotinylated bacteria were used as blank measurements. Signals obtained are suspected to be unspecific bindings. On the other hand, the binding of living bacteria to the affinity binders seems to not be completely uniform, and a change in concentration, agglomeration

of bacteria cells, living-to-dead cell ratio, or the steric hindrance of affinity binders by biotin on the cell surface could impact the measured CL signals.

Overall, the standard deviation for biotinylated *E. coli* was  $42 \pm 12\%$  ( $n = 6$ ) lower than that of biotinylated *E. faecalis*,  $62 \pm 28$  ( $n = 6$ ). One reason could be that the interactions are more preferable for gram-negative than for gram-positive bacteria due to the differences in the cell walls. Additionally, the biotinylation process was found to have a greater effect on *E. faecalis* regarding cell numbers and culturability, indicating that the cells were more influenced by this reaction. Nonetheless, an ANOVA revealed no significant difference ( $F(1,6) = 1.8, p = 0.22$ ). For both bacteria, the respective antibodies worked best as affinity binders, which was expected, as commercial antibodies are designed to have a high affinity towards their antigen. PmB had a similar affinity for both bacteria, whereas lysozyme worked for *E. coli* as well but gave very unreproducible results for *E. faecalis*.

Next, we checked if the previous used bacterial concentration of  $1 \times 10^8$  cells  $\text{mL}^{-1}$  would be suitable for this assay. For this, different concentrations of the biotinylated bacteria ( $1 \times 10^7$ ,  $5 \times 10^7$  and  $1 \times 10^8$  cells  $\text{mL}^{-1}$ ) in PBS were measured. The measurements for 0 cells  $\text{mL}^{-1}$  (PBS) and  $1 \times 10^8$  cells  $\text{mL}^{-1}$  were the same as in the passage before, for which the results for the Shapiro–Wilk tests were also specified. For the following measurements, the significance level  $\alpha$  for the post-hoc Conover tests was corrected to 0.008 using Bonferroni correction.

For *E. coli*, the affinity binders PmB, lysozyme, and the anti-*E. coli* antibody were examined (Figure 4). For the anti-*E. coli* antibody ( $\text{chi-square}(3) = 59.41, p = 7.86 \times 10^{-13}$ ), the highest mean-normalised CL signal was obtained for the highest concentration with a value of  $7.7 \pm 4.3$  ( $n = 37$ ), which showed no significant difference compared to  $5 \times 10^7$  cells  $\text{mL}^{-1}$  with  $2.1 \pm 0.1$  ( $n = 3, t(74) = 2.49, p = 0.14$ ). However, compared to the  $1 \times 10^7$  cells  $\text{mL}^{-1}$  with  $1.5 \pm 0.4$  ( $n = 3, t(74) = 3.75, p = 3.48 \times 10^{-4}, d = 2.10$ ), a significant difference was found. Between the two lowest concentrations, on the other hand, no significant difference was found ( $t(74) = 0.92, p = 0.36$ ). The lowest concentration was the only one that showed no significant difference with the blank measurement ( $t(74) = 2.44, p = 0.02$ ).

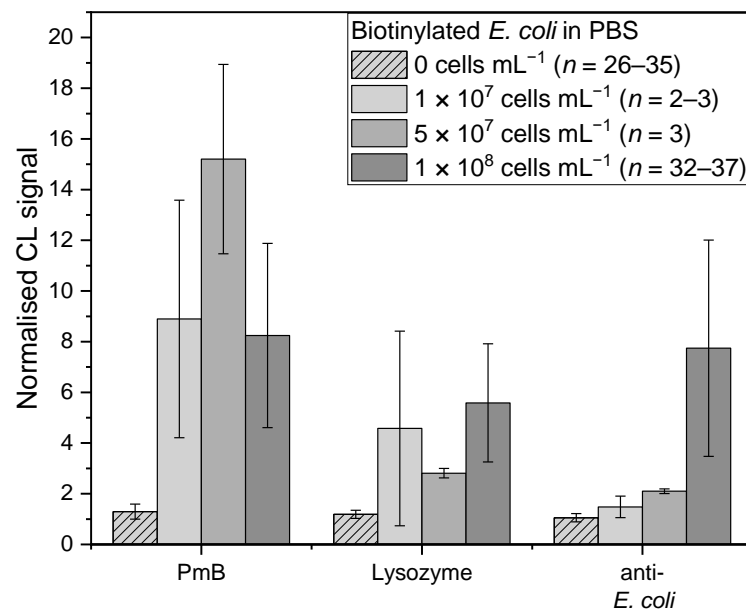


**Figure 4.** Measurements of biotinylated *E. coli* in PBS with different concentrations: 0 cells  $\text{mL}^{-1}$  (PBS,  $n = 26$ – $35$ , lightest grey shaded),  $1 \times 10^7$  cells  $\text{mL}^{-1}$  ( $n = 2$ – $3$ , lightest grey),  $5 \times 10^7$  cells  $\text{mL}^{-1}$  ( $n = 3$ , middle grey), and  $1 \times 10^8$  cells  $\text{mL}^{-1}$  ( $n = 32$ – $37$ , darkest grey) for affinity binders PmB, lysozyme, and anti-*E. coli*, respectively.

For PmB ( $\text{chi-square}(3) = 58.08, p = 1.51 \times 10^{-12}$ ), the highest mean-normalised CL signal was obtained for  $5 \times 10^7$  cells  $\text{mL}^{-1}$  ( $n = 3$ ) with  $15.2 \pm 3.7$ . No significant difference

was found compared to  $1 \times 10^7$  ( $8.9 \pm 4.7$ ,  $n = 3$ ,  $t(73) = 1.92$ ,  $p = 0.06$ ) and  $1 \times 10^8$  cells  $\text{mL}^{-1}$  ( $8.2 \pm 3.6$ ,  $n = 36$ ,  $t(73) = 2.62$ ,  $p = 0.01$ ). Additionally, these two concentrations were not significantly different ( $t(73) = 0.02$ ,  $p = 0.99$ ). For lysozyme ( $\chi^2(3) = 46.57$ ,  $p = 4.28 \times 10^{-10}$ ), the mean-normalised CL signals for  $1 \times 10^7$  and  $5 \times 10^7$  cells  $\text{mL}^{-1}$  as well as  $1 \times 10^8$  cells  $\text{mL}^{-1}$  were in the same range, with  $4.6 \pm 3.8$  ( $n = 2$ ),  $2.8 \pm 0.2$  ( $n = 3$ ) and  $5.6 \pm 2.3$  ( $n = 32$ ), respectively. All three showed no significant difference ( $1 \times 10^7$  and  $5 \times 10^7$ :  $t(59) = 1.11$ ,  $p = 0.27$ ;  $1 \times 10^7$  and  $1 \times 10^8$ :  $t(59) = 0.56$ ,  $p = 0.58$ ;  $5 \times 10^7$  and  $1 \times 10^8$ :  $t(59) = 2.35$ ,  $p = 0.02$ ).

For *E. faecalis*, the affinity binders PmB, lysozyme, and the anti-*Enterococcus* antibody were examined (Figure 5). PmB ( $\chi^2(3) = 59.15$ ,  $p = 8.92 \times 10^{-13}$ ) showed a similar trend to *E. coli*, in which  $5 \times 10^7$  cells  $\text{mL}^{-1}$  induced the highest mean-normalised CL signal of  $15.5 \pm 11.5$  ( $n = 3$ ), whereas  $1 \times 10^7$  and  $1 \times 10^8$  cells  $\text{mL}^{-1}$  generated significant similar values of  $4.3 \pm 1.0$  ( $n = 3$ ,  $t(75) = 1.72$ ,  $p = 0.09$ ) and  $7.7 \pm 4.2$  ( $n = 38$ ,  $t(75) = 1.67$ ,  $p = 0.10$ ), respectively. These two values are significantly similar, too ( $t(75) = 2.48$ ,  $p = 0.02$ ). For lysozyme ( $\chi^2(3) = 34.68$ ,  $p = 1.42 \times 10^{-7}$ ), mean-normalised CL signals for  $1 \times 10^7$  and  $5 \times 10^7$  cells  $\text{mL}^{-1}$  were  $1.1 \pm 0.1$  ( $n = 3$ ,  $t(61) = 0.87$ ,  $p = 0.39$ ) and  $1.1 \pm 0.8$  ( $n = 2$ ,  $t(61) = 0.02$ ,  $p = 0.98$ ), respectively, which are significant similar to the mean-normalised CL signals for blank measurements with PBS ( $n = 26$ ). As mentioned before, for  $1 \times 10^8$  cells  $\text{mL}^{-1}$  a mean-normalised CL signal of  $10.9 \pm 10.9$  ( $n = 34$ ) is significantly different to the blank measurements and holds a very high standard deviation. For anti-*Enterococcus* ( $\chi^2(3) = 54.70$ ,  $p = 7.97 \times 10^{-12}$ ), all three concentrations gave mean-normalised CL signals of the same range with  $15.5 \pm 4.6$  ( $1 \times 10^7$ ,  $n = 3$ ),  $18.0 \pm 11.5$  ( $5 \times 10^7$ ,  $n = 3$ ), and  $15.0 \pm 9.2$  ( $1 \times 10^8$ ,  $n = 36$ ) ( $1 \times 10^7$  and  $5 \times 10^7$ :  $t(70) = 0.63$ ,  $p = 0.53$ ;  $1 \times 10^7$  and  $1 \times 10^8$ :  $t(70) = 0.69$ ,  $p = 0.50$ ;  $5 \times 10^7$  and  $1 \times 10^8$ :  $t(70) = 1.36$ ,  $p = 0.19$ ). According to the results for the anti-*E. coli* antibody with *E. coli* and the results for lysozyme with *E. faecalis*, a bacterial concentration of  $1 \times 10^8$  cells  $\text{mL}^{-1}$  is suitable for this screening assay.

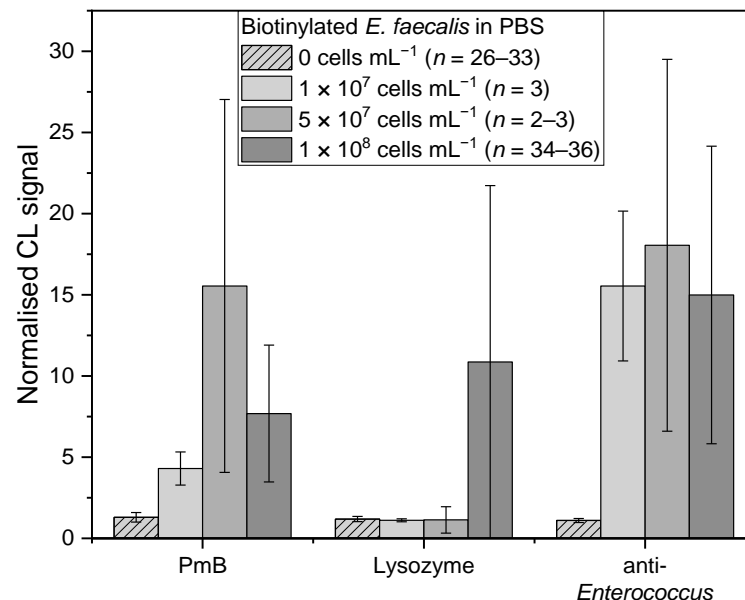


**Figure 5.** Measurements of biotinylated *E. faecalis* in PBS with different concentrations: 0 cells  $\text{mL}^{-1}$  (PBS,  $n = 26-33$ , lightest grey shaded),  $1 \times 10^7$  cells  $\text{mL}^{-1}$  ( $n = 3$ , lightest grey),  $5 \times 10^7$  cells  $\text{mL}^{-1}$  ( $n = 2-3$ , middle grey), and  $1 \times 10^8$  cells  $\text{mL}^{-1}$  ( $n = 34-36$ , darkest grey) for affinity binders PmB, lysozyme, and anti-*Enterococcus*, respectively.

### 3.4. Desorption Studies

For the investigation of the desorption properties of bacterial cells using the affinity binders, the microarray chips were eluted using six different desorption buffers in two different modes. The desorption buffer was either flushed over the chip or the chip was

filled with it, shortly incubated, and then emptied. As a control, blank measurements were performed by measuring PBS and eluting the chip. A change in the normalised CL signal after desorption was observed here as well. One explanation would be the inactivation of bound HRP-streptavidin through peroxide or the desorption buffers. Therefore, obtained data for samples were displayed as the normalised residual CL signal.

$$\text{residual CL signal} = \frac{\text{normalised CL signal (after elution)}}{\text{normalised CL signal (before elution)}} \quad (2)$$

$$\text{normalised residual CL signal} = \frac{\text{residual CL signal (sample)}}{\text{mean residual CL signal (blank measurement)}} \quad (3)$$

A value of 1 refers to a change of the normalised CL signal in the same range as for the blank measurements, any value below indicates a higher loss compared to the blank. The mean-normalised residual CL signal is given as the mean from the microarray chips measured with the corresponding standard deviation between experiments, whereas  $n$  is the number of experiments.

Based on the results from the concentration dependency, for the desorption studies, bacterial concentrations of  $1 \times 10^8$  cells  $\text{mL}^{-1}$  were used. For *E. coli*, the affinity binders PmB, lysozyme, and the anti-*E. coli* antibody were examined (all  $n = 3$ ). The no-desorption controls showed a CL signal reduction for all three affinity binders, giving normalised residual CL signals ranging from 0.61–0.77 (Figures 6a, 7 and 8a). An unwanted desorption of bacterial cells through the CL reagents luminol and hydrogen peroxide could be the reason. Another cause could be a weak affinity leading to the cells being washed away in the washing step after taking the first picture, as here, the flow rate is higher than in the other washing steps.

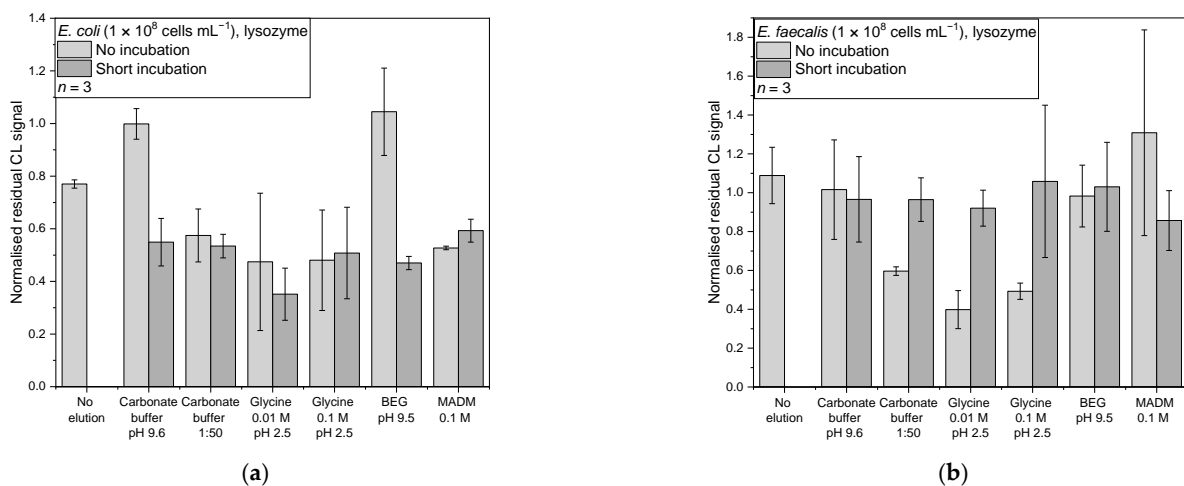


**Figure 6.** Normalised residual CL signals for desorption from the affinity binder lysozyme: (a) *E. coli* in PBS ( $n = 3$ ,  $1 \times 10^8$  cells  $\text{mL}^{-1}$ ) (b) *E. faecalis* in PBS ( $n = 3$ ,  $1 \times 10^8$  cells  $\text{mL}^{-1}$ ).

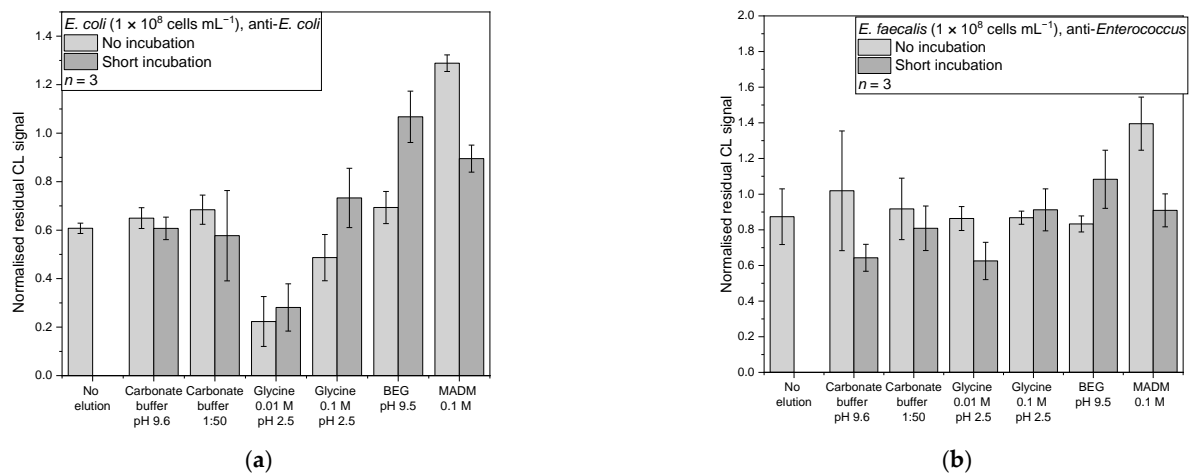


**Figure 7.** Normalised residual CL signals for desorption from the respective antibodies: (a) *E. coli* in PBS ( $n = 3$ ,  $1 \times 10^8$  cells mL<sup>-1</sup>) from anti-*E. coli* antibody; (b) *E. faecalis* in PBS ( $n = 3$ ,  $1 \times 10^8$  cells mL<sup>-1</sup>) from anti-*Enterococcus* antibody.

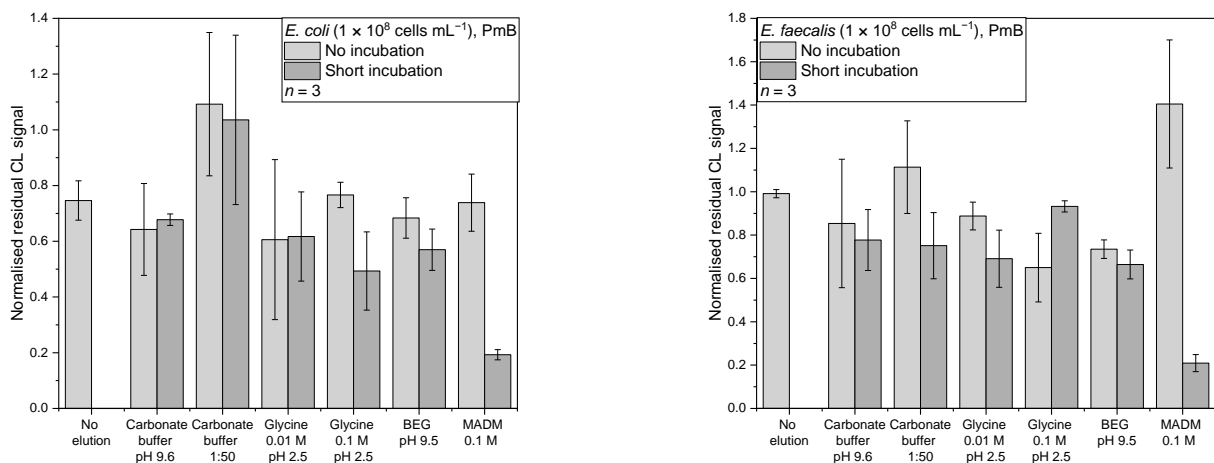


**Figure 8.** Normalised residual CL signals for desorption from the affinity binder PmB: (a) *E. coli* in PBS ( $n = 3$ ,  $1 \times 10^8$  cells mL<sup>-1</sup>); (b) *E. faecalis* in PBS ( $n = 3$ ,  $1 \times 10^8$  cells mL<sup>-1</sup>).

For *E. faecalis*, the affinity binders PmB, lysozyme, and the anti-*Enterococcus* antibody were further examined for their desorption properties (all  $n = 3$ ). The no-elution control for the first two showed mean-normalised CL signals of  $0.99 \pm 0.11$  and  $1.09 \pm 0.19$ , respectively, indicating a good affinity of the affinity binders for the bacteria (Figures 6b and 7b). Only for the antibody, a mean-normalised CL signal decrease of  $0.87 \pm 0.10$  was observed (Figure 8b).

### 3.4.1. Lysozyme

For *E. coli* and lysozyme, regarding the mean-normalised residual CL signal, the best desorption strategy was found to be 0.01 M glycine at pH 2.5 incubated for 1 min with a mean-normalised residual CL signal of  $0.35 \pm 0.18$  (Figure 6a). Other desorption strategies were in the range of 0.47–0.59, except for carbonate buffer (pH 9.6) and the BEG buffer (pH 9.5) applied without incubation, for which the mean-normalised residual CL signals were  $1.00 \pm 0.19$  and  $1.04 \pm 0.12$ , respectively.

The Kruskal–Wallis test showed that there is a significant difference between the data ( $\chi^2(12) = 26.38$ ,  $p = 0.01$ ). The following Conover test (corrected  $\alpha = 6.41 \times 10^{-4}$ ) revealed that the result from 0.01 M glycine with short incubation significantly differs from the no-elution control ( $t(26) = 4.45$ ,  $p = 1.45 \times 10^{-4}$ ,  $d = 3.39$ ), carbonate buffer without

incubation ( $t(26) = 5.20, p = 2.01 \times 10^{-5}, d = 5.23$ ), and BEG without incubation ( $t(26) = 5.14, p = 2.31 \times 10^{-5}, d = 5.61$ ). At the same time, it was the only one significantly different from the no-elution control. The Cohen's  $d$  values are all in the range for great effects. Concluding this, the 0.01 M glycine with incubation is the buffer of choice, although it is not significantly different from most other elution strategies.

For *E. faecalis* and lysozyme (Figure 6b), the best desorption buffer according to the mean-normalised residual CL signal was the 0.01 M glycine (pH 2.5) without incubation, with a normalised residual CL signal of  $0.40 \pm 0.10$ . The other buffers yielded normalised residual signals between 0.49 and 1.31. The Kruskal–Wallis test showed a significant difference in between the data ( $\chi^2(12) = 23.52, p = 0.02$ ). The following Conover test (corrected  $\alpha = 6.41 \times 10^{-4}$ ) revealed, that the result from 0.01 M glycine without incubation only significant differs from the no elution control ( $t(26) = 3.93, p = 5.54 \times 10^{-4}, d = 2.97$ ) and MADM without incubation ( $t(26) = 3.91, p = 5.54 \times 10^{-4}, d = 5.23$ ). Again, it was the only one significantly different from the no-elution control, and the Cohen's  $d$  values are in the range for great effects.

### 3.4.2. Antibodies

For the *E. coli* and the anti-*E. coli* antibody, (Figure 7a) 0.01 M glycine at pH 2.5 gave the lowest mean-normalised residual CL signals of  $0.22 \pm 0.10$  without incubation and  $0.28 \pm 0.10$  with short incubation. The other desorption methods showed mean-normalised residual CL signals from 0.49–1.29. An ANOVA showed that there are significant differences between the data ( $F(12,26) = 8.36, p = 3.5 \times 10^{-6}$ ). The post-hoc test showed that these methods are the only ones that differ from the no-elution control (no incubation:  $p = 0.001, d = 4.24$ ; incubation:  $p = 0.08, d = 3.60$ ). They both are significant similar ( $p = 1.00$ ), which indicates that a short incubation does not enhance the elution. The only other elution mode they do not differ from is the 0.1 M glycine without incubation (no incubation:  $p = 0.06$ ; incubation:  $p = 0.27$ ). The other elution modes are all significantly different from the two glycine elution modes ( $p$ -values all below 0.05). The effect sizes lie between 3.22 and 5.62, indicating great effects. Glycine buffers are widely used for the desorption of antibodies in affinity chromatography, so desorption was expected.

For the *E. faecalis* and the anti-*Enterococcus* antibodies, carbonate buffer and the 0.1 M glycine with short incubation had the best mean-normalised residual CL signals of  $0.64 \pm 0.08$  and  $0.63 \pm 0.11$ , respectively (Figure 7b). The other buffers had values between 0.81 and 1.40. A Kruskal–Wallis test showed that there is a significant difference in between the data ( $\chi^2(12) = 26.38, p = 0.04$ ). The following Conover test (corrected  $\alpha = 6.41 \times 10^{-4}$ ) revealed that the only significant difference was found between MADM without incubation ( $1.40 \pm 0.15$ ) with the carbonate buffer ( $t(26) = 4.48, p = 1.32 \times 10^{-4}, d = 5.14$ ) and the glycine ( $t(26) = 4.43, p = 1.48 \times 10^{-4}, d = 5.26$ ), both with a short incubation. However, there was no significant change from the no-elution control compared to all of the elution modes. This finding suggests that the affinity between *E. faecalis* and its corresponding antibody could not be broken by the used desorption strategies of different pH values and protein/salt contents.

### 3.4.3. PmB

For PmB and *E. coli* (Figure 8a), most of the desorption strategies showed similar mean-normalised residual CL signals between 0.49–0.77 except for the 1:50 dilution of carbonate buffer, which showed without and with incubation values of  $1.09 \pm 0.26$  and  $1.03 \pm 0.30$ , respectively. But the lowest mean-normalised residual CL signal of  $0.19 \pm 0.02$  was found for 0.1 M MADM in combination with the short incubation.

An ANOVA showed that there are significant differences between the data ( $F(12,26) = 5.75, p = 9.55 \times 10^{-5}$ ). The post-hoc test showed, that MADM with incubation is the only one significantly different from the no elution control ( $p = 0.01, d = 3.41$ ). It also is significantly different from carbonate buffer with incubation ( $p = 0.047, d = 2.98$ ), carbonate buffer 1:50 (no incubation:  $p = 2.18 \times 10^{-5}, d = 5.54$ ; incubation:  $p = 6.24 \times 10^{-5},$

$d = 5.19$ ), 0.1 M glycine without incubation ( $p = 0.01$ ,  $d = 3.53$ ), and BEG without incubation ( $p = 0.04$ ,  $d = 3.02$ ). Additionally, MADM without incubation was significantly different ( $p = 0.02$ ,  $d = 3.36$ ), indicating that a short incubation step is necessary for successful elution.

Initially, MADM should have been used for the desorption from ConA, but because of the multiplexing approach of this screening chip and the simultaneous test for other affinity binders, this unexpected result was obtained. A literature search revealed that bacterial cell wall lectins are known to have an affinity towards sugars [39]. Affinity between MADM and *E. coli* seems to be stronger than between *E. coli* and PmB.

For PmB and *E. faecalis* (Figure 8b), most of the desorption strategies gave a mean-normalised residual CL signal range of 0.65–1.11. Again, the 0.1 M MADM with short incubation showed the lowest mean-normalised residual CL signal of  $0.21 \pm 0.04$ . A Kruskal–Wallis test showed that there is a significant difference between the data ( $\chi^2(12) = 29.78$ ,  $p = 0.003$ ). The following Conover test (corrected  $\alpha = 6.41 \times 10^{-4}$ ) showed that not only was the MADM with incubation significantly different from the no elution control ( $t(26) = 5.73$ ,  $p = 4.94 \times 10^{-6}$ ,  $d = 4.99$ ) but that the 0.1 M glycine without incubation ( $t(26) = 4.01$ ,  $p = 4.53 \times 10^{-4}$ ,  $d = 2.18$ ) and BEG with incubation ( $t(26) = 4.13$ ,  $p = 3.25 \times 10^{-4}$ ,  $d = 2.09$ ) were as well. Focusing on MADM, an significant difference to the no incubation mode was observed ( $t(26) = 6.75$ ,  $p = 3.66 \times 10^{-7}$ ,  $d = 7.63$ ). Here, the effect an incubation step can have is very obvious. MADM with incubation is also significantly different from carbonate buffer 1:50 without incubation ( $t(26) = 5.73$ ,  $p = 4.94 \times 10^{-6}$ ,  $d = 5.77$ ), 0.01 M glycine without incubation ( $t(26) = 4.39$ ,  $p = 1.66 \times 10^{-4}$ ,  $d = 4.33$ ), and 0.1 M glycine with incubation ( $t(26) = 5.03$ ,  $p = 3.10 \times 10^{-5}$ ,  $d = 4.61$ ).

#### 4. Conclusions

In this work, a flow-based CL microarray was developed for the rapid screening of affinity binders for the capture of bacteria. Both gram-positive and gram-negative bacteria were successfully biotinylated for their detection via HRP-streptavidin and CL. The four affinity binders PmB, lysozyme, anti-*E. coli* antibody, and anti-*Enterococcus* antibody were immobilised on the microarray surface and screened using this assay. For *E. coli*, the respective antibody was found to be the best affinity binder, followed by PmB, and these were best eluted with 0.01 M glycine and MADM, respectively. For *E. faecalis*, the respective antibody was found to be the best affinity binder, although in this study, no suitable desorption method was found. For both bacteria, the elution from PmB with MADM could be enhanced by a short incubation step. The necessity of such a screening platform to simplify the search for new combinations of affinity binders and bacteria was shown, as desorption behaviours differed sometimes between *E. faecalis* and *E. coli*. One important advantage of the screening platform was found to be the ability of testing desorption buffers on the whole microarray chip at once, leading in our case to unexpected new desorption reagents.

With this study, the principle of a microarray-based affinity binder screening platform was established using CL as detection method, but the principle could also be applied to microarray assays using fluorescence-based or label-free detection. The microarray has space for up to  $18 \times 5$  different affinity binders, which enables a high throughput in screening. Desorption buffers used in this work were only a selection of buffers that could be screened for desorption. Additionally, the methods for desorption can be expanded as needed—for example, through longer incubation intervals. After successful screening of affinity binders and respective desorption methods, they can be applied for affinity enrichment of bacteria—for example, affinity-based filtration.

**Supplementary Materials:** The following supporting information can be downloaded at: <https://www.mdpi.com/article/10.3390/s22228606/s1>; Table S1: Pathway for reagents during the measuring program on the MCR-R., Figure S1: Schematic fluidic plan of the MCR-R.

**Author Contributions:** Conceptualization, J.N., M.E. and M.S.; writing—original draft preparation, J.N.; writing—review and editing, J.N., M.E. and M.S.; supervision, M.E. and M.S. All authors have read and agreed to the published version of the manuscript.

**Funding:** Supported by Deutsche Forschungsgemeinschaft (DFG) through TUM International Graduate School of Science and Engineering (IGSSE), GSC 81.

**Institutional Review Board Statement:** Not applicable.

**Informed Consent Statement:** Not applicable.

**Data Availability Statement:** Data will be made available upon reasonable request.

**Conflicts of Interest:** The authors declare no conflict of interest.

## References

1. Tsuru, A.; Setoguchi, T.; Kawabata, N.; Hirotsu, M.; Yamamoto, T.; Nagano, S.; Yokouchi, M.; Kakoi, H.; Kawamura, H.; Ishidou, Y.; et al. Enrichment of bacteria samples by centrifugation improves the diagnosis of orthopaedics-related infections via real-time PCR amplification of the bacterial methicillin-resistance gene. *BMC Res. Notes* **2015**, *8*, 288. [[CrossRef](#)] [[PubMed](#)]
2. Kim, J.-H.; Oh, S.-W. Optimization of bacterial concentration by filtration for rapid detection of foodborne *Escherichia coli* O157:H7 using real-time PCR without microbial culture enrichment. *J. Food Sci.* **2019**, *84*, 3241–3245. [[CrossRef](#)] [[PubMed](#)]
3. Peskoller, C.; Niessner, R.; Seidel, M. Development of an epoxy-based monolith used for the affinity capturing of *Escherichia coli* bacteria. *J. Chromatogr. A* **2009**, *1216*, 3794–3801. [[CrossRef](#)] [[PubMed](#)]
4. Sari, J.N.; Kandasamy, K.; Chen, Y.-C. Detection of *Escherichia coli* by combining an affinity-based method with contactless atmospheric pressure ionization mass spectrometry. *Separations* **2022**, *9*, 13. [[CrossRef](#)]
5. Lin, Y.-S.; Tsai, P.-J.; Weng, M.-F.; Chen, Y.-C. Affinity capture using vancomycin-bound magnetic nanoparticles for the MALDI-MS analysis of bacteria. *Anal. Chem.* **2005**, *77*, 1753–1760. [[CrossRef](#)]
6. Abdel-Hamid, I.; Ivnitski, D.; Atanasov, P.; Wilkins, E. Flow-through immunofiltration assay system for rapid detection of *E. coli* O157:H7. *Biosens. Bioelectron.* **1999**, *14*, 309–316. [[CrossRef](#)]
7. Liu, J.-C.; Chen, W.-J.; Li, C.-W.; Mong, K.-K.T.; Tsai, P.-J.; Tsai, T.-L.; Lee, Y.C.; Chen, Y.-C. Identification of *Pseudomonas aeruginosa* using functional magnetic nanoparticle-based affinity capture combined with MALDI MS analysis. *Analyst* **2009**, *134*, 2087–2094. [[CrossRef](#)]
8. Ott, S.; Niessner, R.; Seidel, M. Preparation of epoxy-based macroporous monolithic columns for the fast and efficient immunofiltration of *Staphylococcus aureus*. *J. Sep. Sci.* **2011**, *34*, 2181–2192. [[CrossRef](#)]
9. Yang, G.; Huang, M.; Wang, Y.; Chen, G.; Zhao, Y.; Xu, H. Streptavidin-exposed magnetic nanoparticles for lectin magnetic separation (LMS) of *Staphylococcus aureus* prior to three quantification strategies. *Microchim. Acta* **2019**, *186*, 813. [[CrossRef](#)]
10. Bicart-See, A.; Rottman, M.; Cartwright, M.; Seiler, B.; Gamini, N.; Rodas, M.; Penary, M.; Giordano, G.; Oswald, E.; Super, M.; et al. Rapid isolation of *Staphylococcus aureus* pathogens from infected clinical samples using magnetic beads coated with Fc-mannose binding lectin. *PLoS ONE* **2016**, *11*, e0156287. [[CrossRef](#)]
11. Dey, P.; Fabri-Faja, N.; Calvo-Lozano, O.; Terborg, R.A.; Belushkin, A.; Yesilkoy, F.; Fàbrega, A.; Ruiz-Rodríguez, J.C.; Ferrer, R.; González-López, J.J.; et al. Label-free bacteria quantification in blood plasma by a bioprinted microarray based interferometric point-of-care device. *ACS Sens.* **2019**, *4*, 52–60. [[CrossRef](#)] [[PubMed](#)]
12. Wunderlich, A.; Torggler, C.; Elsässer, D.; Lück, C.; Niessner, R.; Seidel, M. Rapid quantification method for *Legionella pneumophila* in surface water. *Anal. Bioanal. Chem.* **2016**, *408*, 2203–2213. [[CrossRef](#)] [[PubMed](#)]
13. Langer, V.; Hartmann, G.; Niessner, R.; Seidel, M. Rapid quantification of bioaerosols containing *L. pneumophila* by Coriolis®  $\mu$  air sampler and chemiluminescence antibody microarrays. *J. Aerosol Sci.* **2012**, *48*, 46–55. [[CrossRef](#)]
14. Langer, V.; Niessner, R.; Seidel, M. Stopped-flow microarray immunoassay for detection of viable *E. coli* by use of chemiluminescence flow-through microarrays. *Anal. Bioanal. Chem.* **2011**, *399*, 1041–1050. [[CrossRef](#)]
15. Hsu, K.-L.; Pilobello, K.T.; Mahal, L.K. Analyzing the dynamic bacterial glycome with a lectin microarray approach. *Nat. Chem. Biol.* **2006**, *2*, 153–157. [[CrossRef](#)]
16. Xi, F.; Gao, J.; Wang, J.; Wang, Z. Discrimination and detection of bacteria with a label-free impedimetric biosensor based on self-assembled lectin monolayer. *J. Electroanal. Chem.* **2011**, *656*, 252–257. [[CrossRef](#)]
17. Gehring, A.G.; Albin, D.M.; Reed, S.A.; Tu, S.-I.; Brewster, J.D. An antibody microarray, in multiwell plate format, for multiplex screening of foodborne pathogenic bacteria and biomolecules. *Anal. Bioanal. Chem.* **2008**, *391*, 497–506. [[CrossRef](#)]
18. Gehring, A.G.; Brewster, J.D.; He, Y.; Irwin, P.L.; Paoli, G.C.; Simons, T.; Tu, S.-I.; Uknalis, J. Antibody microarray for *E. coli* O157:H7 and Shiga Toxin in microtiter plates. *Sensors* **2015**, *15*, 30429–30442. [[CrossRef](#)]
19. Gantelius, J.; Bass, T.; Sjöberg, R.; Nilsson, P.; Andersson-Svahn, H. A lateral flow protein microarray for rapid and sensitive antibody assays. *Int. J. Mol. Sci.* **2011**, *12*, 7748–7759. [[CrossRef](#)]
20. Kim, H.; Chung, D.-R.; Kang, M. A new point-of-care test for the diagnosis of infectious diseases based on multiplex lateral flow immunoassays. *Analyst* **2019**, *144*, 2460–2466. [[CrossRef](#)]

21. Delehanty, J.B.; Ligler, F.S. A microarray immunoassay for simultaneous detection of proteins and bacteria. *Anal. Chem.* **2002**, *74*, 5681–5687. [[CrossRef](#)]
22. Knauer, M.; Ivleva, N.P.; Niessner, R.; Haisch, C. A flow-through microarray cell for the online SERS detection of antibody-captured *E. coli* bacteria. *Anal. Bioanal. Chem.* **2012**, *402*, 2663–2667. [[CrossRef](#)]
23. Barreiros dos Santos, M.; Aguil, J.P.; Prieto-Simón, B.; Sporer, C.; Teixeira, V.; Samitier, J. Highly sensitive detection of pathogen *Escherichia coli* O157:H7 by electrochemical impedance spectroscopy. *Biosens. Bioelectron.* **2013**, *45*, 174–180. [[CrossRef](#)]
24. Wojciechowski, J.; Danley, D.; Cooper, J.; Yazvenko, N.; Taitt, C.R. Multiplexed electrochemical detection of *Yersinia pestis* and staphylococcal enterotoxin B using an antibody microarray. *Sensors* **2010**, *10*, 3351–3362. [[CrossRef](#)]
25. Leva-Bueno, J.; Peyman, S.A.; Millner, P.A. A review on impedimetric immunosensors for pathogen and biomarker detection. *Med. Microbiol. Immunol.* **2020**, *209*, 343–362. [[CrossRef](#)]
26. Gehring, A.; Barnett, C.; Chu, T.; DebRoy, C.; D'Souza, D.; Eaker, S.; Fratamico, P.; Gillespie, B.; Hegde, N.; Jones, K.; et al. A high-throughput antibody-based microarray typing platform. *Sensors* **2013**, *13*, 5737–5748. [[CrossRef](#)] [[PubMed](#)]
27. Wolter, A.; Niessner, R.; Seidel, M. Detection of *Escherichia coli* O157:H7, *Salmonella typhimurium*, and *Legionella pneumophila* in water using a flow-through chemiluminescence microarray readout system. *Anal. Chem.* **2008**, *80*, 5854–5863. [[CrossRef](#)] [[PubMed](#)]
28. Seidel, M.; Niessner, R. Chemiluminescence microarrays in analytical chemistry: A critical review. *Anal. Bioanal. Chem.* **2014**, *406*, 5589–5612. [[CrossRef](#)] [[PubMed](#)]
29. Velkov, T.; Roberts, K.D.; Nation, R.L.; Thompson, P.E.; Li, J. Pharmacology of polymyxins: New insights into an 'old' class of antibiotics. *Future Microbiol.* **2013**, *8*, 711–724. [[CrossRef](#)] [[PubMed](#)]
30. Ayoub Moubareck, C. Polymyxins and Bacterial Membranes: A review of antibacterial activity and mechanisms of resistance. *Membranes* **2020**, *10*, 181. [[CrossRef](#)] [[PubMed](#)]
31. Anspach, F.B. Endotoxin removal by affinity sorbents. *J. Biochem. Biophys. Methods* **2001**, *49*, 665–681. [[CrossRef](#)]
32. Huopalahti, R. (Ed.) *Bioactive Egg Compounds*; Springer: Berlin/Heidelberg, Germany, 2007; ISBN 9783540378853.
33. Da Silva Junior, A.G.; Frias, I.A.M.; Lima-Neto, R.G.; Sá, S.R.; Oliveira, M.D.L.; Andrade, C.A.S. Concanavalin A differentiates gram-positive bacteria through hierarchized nanostructured transducer. *Microbiol. Res.* **2021**, *251*, 126834. [[CrossRef](#)] [[PubMed](#)]
34. Jantra, J.; Kanatharana, P.; Asawatreratanakul, P.; Hedström, M.; Mattiasson, B.; Thavarungkul, P. Real-time label-free affinity biosensors for enumeration of total bacteria based on immobilized concanavalin A. *J. Environ. Sci. Health A Tox. Hazard. Subst. Environ. Eng.* **2011**, *46*, 1450–1460. [[CrossRef](#)] [[PubMed](#)]
35. Dao, T.N.T.; Yoon, J.; Jin, C.E.; Koo, B.; Han, K.; Shin, Y.; Lee, T.Y. Rapid and sensitive detection of *Salmonella* based on microfluidic enrichment with a label-free nanobiosensing platform. *Sens. Actuators B Chem.* **2018**, *262*, 588–594. [[CrossRef](#)]
36. Bemetz, J.; Kober, C.; Meyer, V.K.; Niessner, R.; Seidel, M. Succinylated Jeffamine ED-2003 coated polycarbonate chips for low-cost analytical microarrays. *Anal. Bioanal. Chem.* **2019**, *411*, 1943–1955. [[CrossRef](#)]
37. Sawilowsky, S.S. New Effect Size Rules of Thumb. *J. Mod. App. Stat. Meth.* **2009**, *8*, 597–599. [[CrossRef](#)]
38. Brattain, M.G.; Marks, M.E.; Pretlow, T.G. The purification of horseradish peroxidase by affinity chromatography on Sepharose-bound concanavalin A. *Anal. Biochem.* **1976**, *72*, 346–352. [[CrossRef](#)]
39. Aronson, M.; Medalia, O.; Schori, L.; Mirelman, D.; Sharon, N.; Ofek, I. Prevention of colonization of the urinary tract of mice with *Escherichia coli* by blocking of bacterial adherence with methyl alpha-D-mannopyranoside. *J. Infect. Dis.* **1979**, *139*, 329–332. [[CrossRef](#)]

## **5.3 Publication 3: Flow-Based CL-SMIA for the Quantification of Protein Biomarkers from Nasal Secretions in Comparison with Sandwich ELISA**

### **5.3.1 Summary**

In this third publication, the MCR-R was used to establish a flow-based CL-SMIA for the quantification of IFN- $\beta$ , a biomarker for immune response, in nasal secretions. Commercially available anti-IFN- $\beta$  antibodies designed for ELISA were used to develop the microarray assay. As in the previous publication, polycarbonate foils were used as the microarray surface. Immobilization of four different capture antibody concentrations allowed for a fast assay optimization. Flow-based microarray assays often require a higher amount of antibodies than static incubated assays like ELISA, so a pre-incubation step of the IFN- $\beta$  and the detection antibody before injection into the microarray chip was introduced. Pre-incubation was found to reach its maximum effect after 45 min. An additional incubation step on the microarray chip further enhanced signal performance. The assay was furthermore optimized regarding the concentration of strep-HRP, detection antibody concentration, and sample delivery over the chip after on-chip incubation. The optimized CL-SMIA was compared to ELISA performed with the same set of antibodies regarding assay performance, cost, and time. Calibration curves of both assays revealed similar detection limits. Comparing the costs of both assays, the cost for one foil-based microarray chip was calculated and published for the first time. Because of the relatively high cost for the microarray chip carrier plates, this sums up to comparable high fabrication costs. Therefore, for singleplex measurements and high sample throughput, ELISA is superior in assay cost. However, for multiplexed assays, which are easy to achieve with microarray assays, the CL-SMIA becomes more affordable than ELISA. The same principle applies to comparisons of assay times. Measurements in real nasal secretions revealed unfortunately low recoveries for both assays. However, we successfully established a CL-SMIA for the quantification of IFN- $\beta$ , which is comparable to ELISA in terms of assay performance and – for multiplexed applications – superior to ELISA regarding cost and time.

### **5.3.2 Own Contribution**

- Conceptualization of experiments
- Supervision of experiments conducted by M. Kröger (Master student)
- Data analysis (together with M. Kröger)
- Writing of manuscript

The first authorship of this publication is shared between me and M. Kröger.

### 5.3.3 Reprint Permission

Neumair, J.; Kröger, M.; Stütz, E.; Jerin, C.; Chaker, A.M.; Schmidt-Weber, C.B.; Seidel, M. Flow-Based CL-SMIA for the Quantification of Protein Biomarkers from Nasal Secretions in Comparison with Sandwich ELISA. *Biosensors* **2023**, *13*, 670. <https://doi.org/10.3390/bios13070670>

#### Open Access

© 2023 by the authors. Licensee MDPI, Basel, Switzerland. This article is an open access article distributed under the terms and conditions of the Creative Commons Attribution (CC BY) license (<https://creativecommons.org/licenses/by/4.0/>).

#### Permissions

No special permission is required to reuse all or part of article published by MDPI, including figures and tables. For articles published under an open access Creative Common CC BY license, any part of the article may be reused without permission provided that the original article is clearly cited. Reuse of an article does not imply endorsement by the authors or MDPI.

## Article

# Flow-Based CL-SMIA for the Quantification of Protein Biomarkers from Nasal Secretions in Comparison with Sandwich ELISA

Julia Neumair <sup>1,†</sup>, Marie Kröger <sup>1,†</sup>, Evamaria Stütz <sup>2</sup>, Claudia Jerin <sup>2</sup>, Adam M. Chaker <sup>2,3</sup>,  
Carsten B. Schmidt-Weber <sup>2</sup>  and Michael Seidel <sup>1,\*</sup> 

<sup>1</sup> Chair of Analytical Chemistry and Water Chemistry, TUM School of Natural Sciences, Technical University of Munich, Lichtenbergstr. 4, 85748 Garching, Germany; julia.neumair@tum.de (J.N.); marie.kroeger@tum.de (M.K.)

<sup>2</sup> Center of Allergy and Environment (ZAUM), Technical University of Munich and Helmholtz Center Munich, Member of the German Center of Lung Research (DZL), 80802 Munich, Germany; evamaria.stuetz@tum.de (E.S.); claudia.jerin@tum.de (C.J.); adam.chaker@tum.de (A.M.C.); csweber@tum.de (C.B.S.-W.)

<sup>3</sup> TUM School of Medicine, Department of Otorhinolaryngology, Klinikum Rechts der Isar, Technical University of Munich, 81675 Munich, Germany

\* Correspondence: michael.seidel@tum.de; Tel.: +49-89-289-54506

† These authors contributed equally to this work.

**Abstract:** Protein biomarkers in nasal secretions can be used as a measure to differentiate between allergies, airway diseases and infections for non-invasive diagnostics. The point-of-care quantification of biomarker levels using flow-based microarray facilitates precise and rapid diagnosis and displays the potential for targeted and effective treatment. For the first time, we developed a flow-based chemiluminescence sandwich microarray immunoassay (CL-SMIA) for the quantification of nasal interferon-beta (IFN- $\beta$ ) on the Microarray Chip Reader-Research (MCR-R). Polycarbonate foils are used as a cost-effective surface for immobilizing capture antibodies. By using a commercially available set of anti-human IFN- $\beta$  antibodies, the CL-SMIA can be compared directly to an enzyme-linked immunosorbent assay (ELISA) performed in microtiter plates concerning the bioanalytical performance and economic issues. Pre-incubation of the sample with detection antibodies facilitates the lower consumption of detection antibodies, as this allows for a longer interaction time between the antibody and the biomarker. The direct injection of pre-incubated samples into the microarray chips eliminates the adsorption of proteins in the tubing as well as the contamination of the tubing and valves of the MCR-R with clinical samples. The small flow cell allows for a low sample volume of 50  $\mu$ L. The limit of detection of 4.53 pg mL<sup>-1</sup> was slightly increased compared to a sandwich ELISA performed on microtiter plates which were 1.60 pg mL<sup>-1</sup>. The possibility to perform the CL-SMIA in a multiplexed mode makes it a promising assay for the rapid and cost-effective non-invasive detection of biomarkers in nasal secretions.

**Keywords:** biomarker; microarray; interferon; ELISA; microfluidic; chemiluminescence; nasal secretion



**Citation:** Neumair, J.; Kröger, M.; Stütz, E.; Jerin, C.; Chaker, A.M.; Schmidt-Weber, C.B.; Seidel, M. Flow-Based CL-SMIA for the Quantification of Protein Biomarkers from Nasal Secretions in Comparison with Sandwich ELISA. *Biosensors* **2023**, *13*, 670. <https://doi.org/10.3390/bios13070670>

Received: 5 May 2023

Revised: 12 June 2023

Accepted: 20 June 2023

Published: 22 June 2023



**Copyright:** © 2023 by the authors. Licensee MDPI, Basel, Switzerland. This article is an open access article distributed under the terms and conditions of the Creative Commons Attribution (CC BY) license (<https://creativecommons.org/licenses/by/4.0/>).

## 1. Introduction

Biomarkers are determinable biological indicators for complex processes in the human body and can be used to monitor different diseases of the upper and lower airways. Furthermore, they can facilitate the measurements of physiologic parameters such as blood sugar but also proteins or enzymes [1,2]. Body fluids are a great source of protein biomarkers [3], whereby non-invasive sampling is preferred, for example for urine and nasal secretions. The in nasal secretions pattern of biomarkers may indicate whether a patient's symptoms in the lower airways are caused by allergies or infections, and treatment can be adjusted accordingly [4,5]. Interferons, a group of class II cytokines, hereby play a

great role in the immune response during viral infections. Specifically, IFN- $\beta$  production is enhanced upon infection [6], making it a suitable biomarker for viral infections.

The detection and quantification of cytokines mostly rely on immuno-based methods [7,8], but also methods such as aptamer-based assays [9] or mass spectrometry [10] are used. Among the immunoassays, methods such as ELISAs (enzyme-linked immunosorbent assay) [7,11] and flow cytometry [12,13], as well as biosensors, are common. The latter utilizes different detection methods such as label-free approaches, including SPR (surface plasmon resonance) [14], or labeling with fluorescent [15] or chemiluminescent [16] labels.

For microarray assays, multiple catchers are immobilized on the microarray surface, enabling simultaneous detection of multiple analytes in one single measurement [17,18]. Microarrays can be performed in a good format [8,19,20], but the use of a chip or chip-like design holds the opportunity of simplifying the assay by allowing for flow-based approaches [21,22].

In this work, we developed a flow-based, chemiluminescence sandwich microarray immunoassay (CL-SMIA) for the quantification of IFN- $\beta$  from nasal secretions on the Microarray Chip Reader-Research (MCR-R). The MCR-R is a flow-based biosensor platform for CL detection via antibody microarray chips, where the reagents are directed automatically over the flow cell of microarray chips. The volumes and flow rates of these reagents can be adjusted as needed, which makes them much more flexible for assay optimization compared to static incubated immunoassay formats [23]. Features of this newest version of MCRs are described in detail elsewhere, where it has also been shown that the MCR-R can be used for diagnostic testing [24]. Using polycarbonate (PC) as a surface enables more cost-effective and faster production of microarray chips compared to glass surfaces [24,25]. Additionally, PC is available as flexible foil, which requires not only fewer resources but also handling can be simplified. Processes such as roll-to-roll fabrication can furthermore enhance the fabrication of microarray platforms [26].

This proof-of-concept study showed the feasibility of using foil-based microarray chips together with antibodies from a commercially available ELISA antibody kit for the detection of IFN- $\beta$ . Before automated CL detection on the MCR-R, the sample is pre-incubated with the detection antibody and is then injected into the microarray chip. This allows for a low sample volume of 50  $\mu$ L, as well as the possibility to stagger the measurements in time and, therefore, increase the sample quantity. Calibration of the spiked IFN- $\beta$  in diluted nasal secretions revealed a slightly increased, but similar detection limit, compared to a sandwich ELISA performed with the same antibody kit. Therefore, we see the CL-SMIA, with its ability for multiplexing, as a promising method for rapid and cost-effective point-of-care determination of biomarker levels.

## 2. Materials and Methods

### 2.1. Material and Buffers

If not stated otherwise, the chemicals were purchased from Sigma Aldrich (Darmstadt, Germany), a subsidiary of Merck, or Carl Roth (Karlsruhe, Germany). The R&D Systems Human IFN- $\beta$  DuoSet ELISA containing capture (CAB) and detection antibodies (DAB) for IFN- $\beta$ , recombinant human IFN- $\beta$  standards, as well as horseradish-peroxidase-labeled streptavidin (strep-HRP) and the substrate reagent kit for ELISA detection, were purchased from Bio-Techne (Wiesbaden, Germany). The assay buffer (Ab-33k), used for sample collection and as a sample matrix, was purchased from Merck Millipore (Darmstadt, Germany). The CL-reagents (luminol and hydrogen peroxide) were used from the Elistar Supernova reagent kit from Cyanagen (Bologna, Italy). The Strep-HRP, for the CL-SMIA, was purchased from Biozol (Eching, Germany) and the polycarbonate foils (Makrolon<sup>®</sup> GP, 0.25 mm) from Modulor (Berlin, Germany). Ultrapure water was used unless stated otherwise.

Phosphate buffered saline (PBS, pH 7.4) consisted of 137 mM NaCl, 2.7 mM KCl, 8.1 mM Na<sub>2</sub>HPO<sub>4</sub> and 1.5 mM KH<sub>2</sub>PO<sub>4</sub>. The washing buffer, used for the ELISA experiments, was a 0.05% Tween<sup>®</sup> 20 solution in PBS and the running buffer, for the CL-

SMIA, was a 0.1% Tween<sup>®</sup> 20 solution in PBS. The spotting buffer, used for microcontact printing, was prepared using 100 mg mL<sup>-1</sup> trehalose dihydrate, 2 mg mL<sup>-1</sup> 1-ethyl-3-(3-(dimethylamino)propyl)carbodiimide (EDC), 2 mg mL<sup>-1</sup> N-hydroxysulfosuccinimide sodium salt (sNHS) and 0.02 mg mL<sup>-1</sup> Pluronic<sup>®</sup> F-127.

## 2.2. Collection of Real Nasal Mucosal Lining Fluid Samples

Nasal mucosal lining fluid samples were collected during an ongoing clinical validation study. The “Airway Disease Analysis and Prevention” (ADAPT) study is an EIT Health-funded prospective observational biomarker study (funding number 19065) involving four academic and two industrial study partners. The nasal mucosal lining fluid samples used for this study have been exclusively collected at the Klinikum rechts der Isar of the Technical University of Munich (IRB approval 159/19S).

Nasal mucosal lining fluid samples were collected using Nasosorption<sup>™</sup> FX-I sampling devices (Hunt Developments Ltd., Midhurst, UK), as previously described [27]. Briefly, sampling was performed by carefully inserting one Nasosorption device into both nostrils for 60 s, while gently pressing on the ala nasi (wing of the nose), to collect the nasal mucosal lining fluid from the mucosal surface of the lumen of each nostril. The nasal samples were then eluted in a 300 µL assay buffer (Ab-33k) and centrifuged at 16,000 × g at 4 °C for 20 min. The samples were stored at -70 °C until further use.

The initial IFN-β concentrations of different biomarkers were measured with the MSD Mesoscale platform Meso QuickPlex SQ120 MM (Meso Scale Discovery, Inc., Rockville, MD, USA) using U-PLEX Custom Biomarker (hu) Assays and SECTOR for IFN-β, according to the manufacturer’s protocol. Samples with the lowest IFN-β levels were chosen and the IFN-β standards were added to reach the desired IFN-β concentrations.

## 2.3. Sandwich ELISA

### Assay

For the ELISA experiments, the protocol given by the manufacturer for the DuoSet was followed with minor changes. Experiments were conducted in MICROLON<sup>®</sup> 600, high binding, polystyrene 96-well plates with a flat bottom from Greiner Bio-One (Frickenhausen, Germany). In the following, the volumes are always meant for one well. First, a 100 µL of a 2.0 µg mL<sup>-1</sup> solution of anti-human IFN-β CAB in PBS were incubated over night at room temperature (RT). Afterwards, the ELISA plate was washed three times with a 400 µL washing buffer, each with the ELx405 Select plate washer from BioTek, Winooski, VT, USA. Residual active sites were blocked with 300 µL of a 1% casein solution in PBS for 1 h. After washing, 100 µL of the sample was added, as well as 15 µL of a 7.7% bovine serum albumin (BSA) solution in PBS to reach a 1% BSA concentration, as suggested by the manufacturer’s protocol. Incubation took place for 2 h at RT at 100 rpm. A total of 100 µL of a 62.5 ng mL<sup>-1</sup> anti-human IFN-β DAB solution, in 1% BSA in PBS, were added after another washing and incubated for 2 h at 100 rpm. Again, the plate was washed and 100 µL of a 40-fold dilution of the strep-HRP, contained in the DuoSet, was incubated at RT for 20 min at 100 rpm. After the last washing step, 100 µL of substrate solution (mixed from the substrate reagent kit according to its instructions) was incubated at RT in the dark until a baby blue colour developed or for a maximum of 20 min. In total, 50 µL of a 1 M sulfuric acid solution was added to stop the colour reaction and the plate was measured at 450 and 540 nm using a Synergy HT plate reader. For wavelength correction, the absorbance values at 540 nm were subtracted from the ones at 450 nm.

## 2.4. Flow-Based CL-SMIA

### 2.4.1. Preparation of Microarray Chips

As the surface for the microarray chips, PC foils were used and prepared similarly as described elsewhere [25]. In short, a CE 6000-40 cutting plotter from Graphtec Corporation (Yokohama, Japan) was used to cut the PC foil (0.25 mm) into sheets of 3 × 3 chips, each having a size of 26 × 76 mm with one pass. The device was adjusted to a cut force of 18 au.,

with a speed of  $15 \text{ cm s}^{-1}$  and acceleration of  $1 \text{ au}$ . For functionalization, a succinylated Jeffamine<sup>®</sup> ED-2003 was applied using a screen printer and incubated for 2 h at  $95 \text{ }^\circ\text{C}$ . After washing and drying, the sheets were stored at RT under reduced humidity until further use. Anti-human IFN- $\beta$  CAB, from the ELISA DuoSet, was immobilized via contact spotting using a BioOdyssey Calligrapher<sup>®</sup> MiniArrayer from Bio-Rad (Hercules, CA, USA). Rows of five spots, with distances of  $1300 \text{ }\mu\text{m}$  between the rows and  $1100 \text{ }\mu\text{m}$  between the spots of one row (spot size  $150 \text{ }\mu\text{m}$ ), were generated. CAB solutions of different concentrations were mixed 1:1 with the spotting buffer, leading to end concentrations of  $0.125$ ,  $0.25$ ,  $0.5$  and  $1 \text{ mg mL}^{-1}$ . As a positive control, polyclonal anti-peroxidase antibodies from a rabbit (1:40 dilution final) and PBS as negative control were mixed 1:1 with the spotting buffer. In Figure 1, the spotting scheme for optimization and calibration experiments using all four CAB concentrations is shown. For recovery experiments, only  $0.125 \text{ mg mL}^{-1}$  was immobilized. A temperature of  $20 \text{ }^\circ\text{C}$  and 55% relative humidity were used for spotting and incubating for 1 h. Afterwards, the sheets were separated into individual chips, which were stored at  $4 \text{ }^\circ\text{C}$  until further use. A double-sided adhesive with a cut-out flow channel (thickness  $140 \text{ }\mu\text{m}$ , channel size  $56 \text{ }\mu\text{L}$ ) was used to combine the PC chips with black polyoxymethylene carriers with in-and outlets to the finished microarray chips (Figure 1).

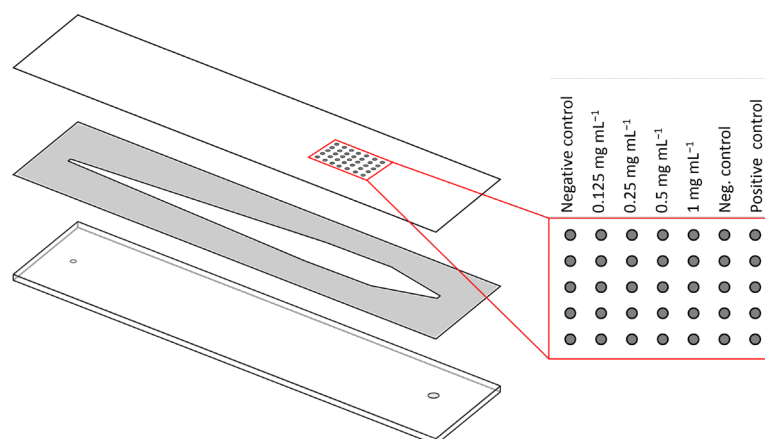


**Figure 1.** Schematic representation of the microarray chip setup. The polycarbonate chip with immobilized antibodies (**top**) is adhered with a double-sided adhesive with a cut-out flow channel (**middle**) to the polyoxymethylene carrier (**bottom**). On the right, the spotting scheme for optimization and calibration experiments is shown.

#### 2.4.2. Measurements with Flow-Based CL-SMIA

The CL-SMIA was conducted on the MCR-R built by GWK Präzisionstechnik (Munich, Germany). To prepare the device at the beginning of a measuring day, all tubes were filled with the running buffer. Additionally, all reagents used for the assay, namely a dilution of strep-HRP in the running buffer and the individual CL reagents, were loaded and the microarray chip holder was heated to  $37 \text{ }^\circ\text{C}$ .

For every microarray chip, first, a dark frame picture was taken by inserting it into the microarray chip holder, flushing it with a running buffer and recording an image for 60 s without any addition of CL reagents. Parameters that were optimized in this work are shown in Table 1. For measurements,  $50 \text{ }\mu\text{L}$  of the sample in the assay buffer was mixed with  $8.75 \text{ }\mu\text{L}$  of 6.9% BSA (final concentration 1%) and  $1.25 \text{ }\mu\text{L}$  biotinylated anti-human IFN- $\beta$  DAB from the ELISA DuoSet in a reaction tube and pre-incubated at  $37 \text{ }^\circ\text{C}$  and 100 rpm. Following this, the mixture was injected manually into the microarray chip using a pipette and incubated again. After reinserting the microarray chip into the MCR-R, the chip was flushed, first slowly ( $50 \text{ }\mu\text{L}$ ,  $0.5 \text{ }\mu\text{L s}^{-1}$ ), then faster ( $1500 \text{ }\mu\text{L}$ ,  $325 \text{ }\mu\text{L s}^{-1}$ ) with a running buffer. The Strep-HRP solution was passed over the chip ( $2.0 \text{ }\mu\text{L s}^{-1}$ ) and after another washing step ( $1500 \text{ }\mu\text{L}$ ,  $325 \text{ }\mu\text{L s}^{-1}$ ), the CL reagents were delivered over the chip in a 1:1 ratio ( $200 \text{ }\mu\text{L}$  each,  $100 \text{ }\mu\text{L s}^{-1}$ ). Immediately,

the CCD camera recorded an image for 60 s. After every measurement, the tubing was flushed with the running buffer. Table 2 shows the detailed measuring program on the MCR-R.

**Table 1.** Parameters for the chemiluminescence sandwich microarray immunoassay (CL-SMIA) for optimization experiments and final protocol.

Optimization of	Pre-Incubation/min	Incubation Chip/min	DAB /ng mL <sup>-1</sup>	Sample Delivery / $\mu\text{L s}^{-1}$	Dilution Strep-HRP
Strep-HRP	30	5	625.0	0.5	1:1500, 1:2000, 1:2500
Pre-incubation	15, 30, 45, 60	5	625.0	0.5	1:2500
Incubation chip	45	0, 1, 5, 10, 20	625.0	0.5	1:2500
Sample delivery	45	20	625.0	0.5, 1.0, 2.0, 4.0, 8.0	1:2500
DAB concentration	45	20	312.5, 625.0, 937.5, 1250, 1875	0.5	1:2500
Final	45	20	312.5	0.5	1:2500

**Table 2.** Measuring program for the flow-based CL-SMIA on the MCR-R (Microarray Chip Reader-Research).

Process	Volume/ $\mu\text{L}$	Time/min	Comments
Pre-incubation	Sample 50 DAB 1.25 BSA 6.9	45	
Injection into chip	60	20	With pipette
Insert chip into device			
	Volume/ $\mu\text{L}$	Flow rate/ $\mu\text{L s}^{-1}$	
Direct sample over chip	50	0.5	
Wash chip	1500	325	2 increments, pause 1 s
Incubate strep-HRP	160 600	50 2	
Wash chip	1500	325	2 increments, pause 1 s
Add CL reagents	400	100	Mixture 1:1
Take image			60 s exposure
Flush device	2500 2500 2500	500 500 500	Sample loop Sample way Chip (extra washing chip)

### 2.5. Data Evaluation

For every measurement, the software on the MCR-R automatically subtracted the CL signals of the dark frame from the CL signals of the actual measurement. The software MCR spotreader (Stefan Weißenberger, Munich, Germany) was used to evaluate the resulting CL signals by placing a grid over the image, resulting in one spot per box. Automatically, for every spot, a mean of the 10 brightest pixels was calculated. For every row of five spots corresponding to the antibody concentrations or controls, the mean was calculated omitting spots that deviated more than 10%.

## 3. Results and Discussion

### 3.1. ELISA

#### Calibration Curve

Before calibration of the anti-human IFN- $\beta$  ELISA was performed, the assay was optimized regarding blocking agent and antibody concentrations (Supplementary Materials Table S1).

For the calibration curve, the wavelength corrected absorbance at 450 nm was plotted semi-logarithmically ( $y$ -axis linear,  $x$ -axis logarithmic) versus the concentration of human IFN- $\beta$  standard and fitted with a four-parameter logistic fit (Equation (1)). The calibration curve is shown in Figure 2. A limit detection (LOD, Equation (2)) of  $1.60 \text{ pg mL}^{-1}$  and a median effective concentration (EC50) using Equation (1) of  $1082 \text{ pg mL}^{-1}$  were obtained.

$$y = A_{min} + \frac{(A_{max} - A_{min})}{\left(1 + \left(\frac{x_0}{x}\right)^h\right)} \quad (1)$$

$y$  represents the measured adsorption at IFN- $\beta$  standard concentration,  $x$ .  $A_{min}$  refers to the minimum asymptote, or the response of the sample, with no standard.  $A_{max}$  is the maximum asymptote, or the response of the samples, with a very high standard concentration approach.  $x_0$  is assigned the inflection point at which the curve changes direction and  $h$  is the slope of the curve. For curves without  $A_{max}$ , a reasonable upper limit was estimated by the software, still providing valuable measures.

$$\text{LOD} = \text{mean absorbance (blank)} + 3 \times \text{standard deviation (blank)} \quad (2)$$

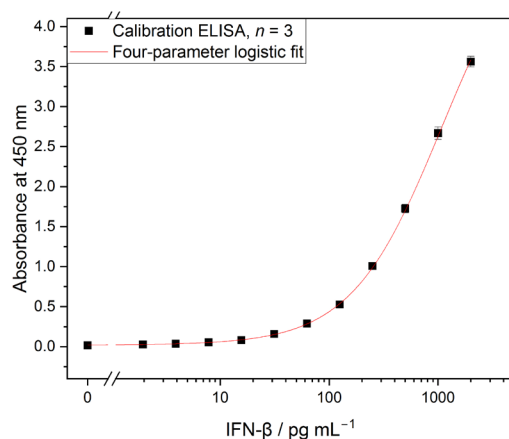


**Figure 2.** Calibration curve of ELISA for IFN- $\beta$  ( $n = 3$ ). Limit of detection (LOD)  $1.60 \text{ pg mL}^{-1}$ , median effective concentration (EC50)  $1082 \text{ pg mL}^{-1}$ .

### 3.2. Flow-Based CL-SMIA

Microarray chips for the CL-SMIA were produced using PC foils with a thickness of  $0.25 \text{ mm}$  [28,29]. In prior studies, PC plates with a thickness of  $1 \text{ mm}$  were used [24,25,30]. Thinner material has the advantage of easier and faster processing with the cutting plotter, as fewer passes of the blade make the process faster. Additionally, the separation of the individual chips, from the  $3 \times 3$  plate, is easier as breaking the thicker plates apart requires some strength and the foils can be cut using scissors. PC foils also hold the opportunity for roll-to-roll fabrication in the future.

CABs are immobilized via their free primary amines to the free carboxy groups on the chip surface by using EDC and sNHS. Adding the coupling reagents into the spotting solution only activates the surface where needed, which reduces unspecific binding and, therefore, makes blocking unnecessary. The small spot diameter of  $150 \mu\text{m}$  and the corresponding volume of  $0.9 \text{ nL}$  require only small amounts of CAB per row of spots on the microarray chip ( $0.6 \text{ ng}$ ), which reduces the costs for antibody microarrays compared to ELISA ( $200 \text{ ng}$ ).

For the flow-based CL-SMIA, the sample and DAB were first pre-incubated in a reaction tube to form an equilibrium of the IFN- $\beta$ -DAB complex before injecting the mixture directly into the flow cell of the microarray chip using a pipette. In this way, the DAB and sample do not have to pass the tubes and valves of the MCR-R, which reduces

the adsorption of both and allows for smaller volumes. Contamination of the tubes with the samples, and any possible carryover, was avoided as well. Additionally, this allowed the experiments to be staggered in time, which increases throughput.

After on-chip incubation, the microarray chip was inserted into the MCR-R, where the running buffer was delivered slowly ( $0.5 \mu\text{L s}^{-1}$ ) over the chip to slowly wash away the injected sample and to allow for further interactions. After further washing, detection took place in an automated way by flushing strep-HRP over the microarray chip, where it bound to the biotin tag of the DABs. Next, CL reagents luminol and hydrogen peroxide were flushed over the chip. The CL reaction was catalyzed in the places where the strep-HRP had bound. The assay principle is depicted in Figure 3.

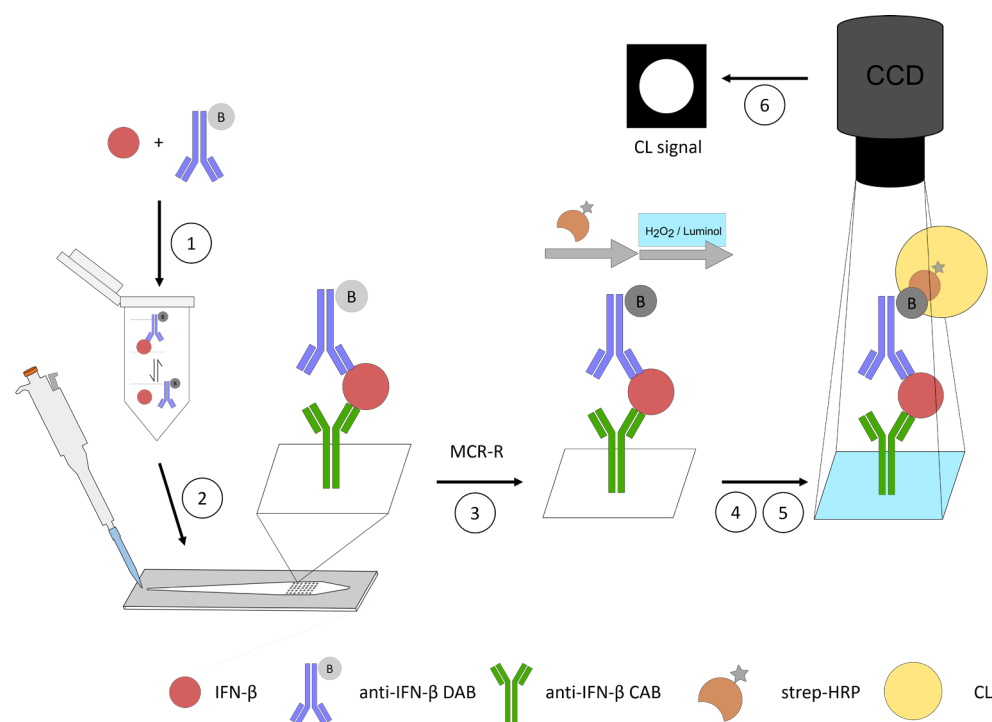


**Figure 3.** Schematic representation of the flow-based CL-SMIA. (1): pre-incubation of the sample and anti-human interferon beta (IFN- $\beta$ ) detection antibody (DAB). (2): Sample injection into the flow cell of the microarray chip and on-chip incubation and interaction of the IFN- $\beta$ -DAB complex with immobilized anti-human IFN- $\beta$  capture antibody (CAB). (3): Sample delivery in a flow cell of the microarray chip on MCR-R (Microarray Chip Reader-Research). (4): Streptavidin-horseradish peroxidase (strep-HRP). (5): CL reagents delivery over the chip. (6): Acquisition of image.

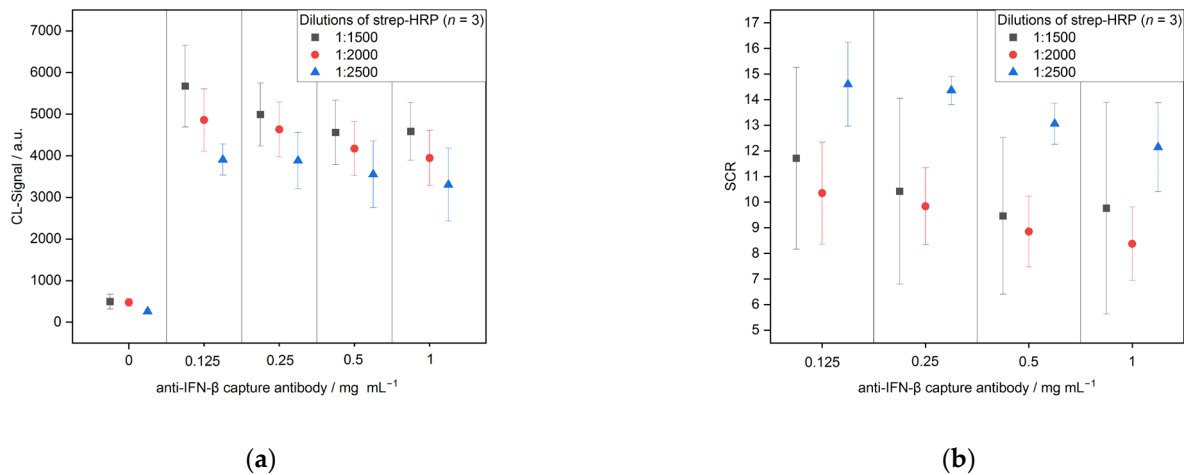
### 3.2.1. Optimization

First, the protocol for IFN- $\beta$  detection using the CL-SMIA was optimized with an IFN- $\beta$  concentration of  $125 \text{ pg mL}^{-1}$ . The dilution of strep-HRP, incubation time in the tube and flow cell of the microarray chip and the flow rate for sample delivery over the flow cell, as well as the concentration of DAB, were investigated. In Table 1, the parameters for the respective optimization steps are shown. Four different concentrations of immobilized CAB ( $0.125$ ,  $0.25$ ,  $0.5$  and  $1 \text{ mg mL}^{-1}$ ) were used.

The concentration of strep-HRP was optimized using three different dilutions in the running buffer ( $1:1500$ ,  $1:2000$  and  $1:2500$ , Figure 4). The highest CL signals were detected for the lowest dilution, thus, the highest concentration of strep-HRP ( $5672 \pm 985$  for  $0.125 \text{ mg mL}^{-1}$  CAB). This was expected, as a higher amount of strep-HRP enables more bound protein and, therefore, a higher signal. Moreover, the signals for negative control increased with a higher

strep-HRP concentration from  $259 \pm 44$  for 1:2500 to  $493 \pm 180$  (both for  $0.125 \text{ mg mL}^{-1}$  CAB). Therefore, the signal-to-control ratio (SCR) was calculated using Equation (3).

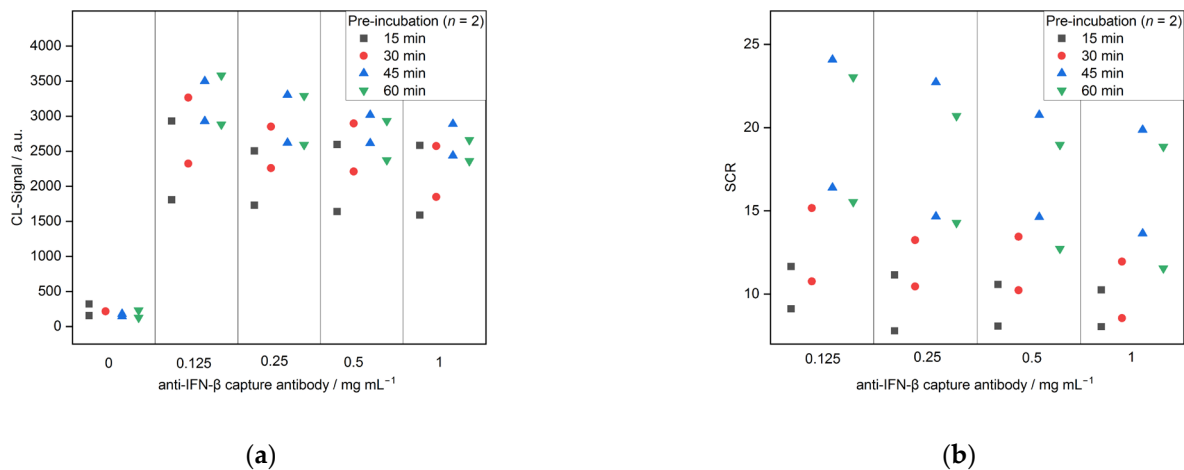
$$\text{SCR (CAB concentration)} = \frac{\text{mean CL signal (spotted CAB concentration)}}{\text{mean CL signal (spotted negative control)}} \quad (3)$$



**Figure 4.** Optimization of the strep-HRP dilutions for CL-SMIA ( $n = 3$ ): (a) chemiluminescence (CL)-signals and (b) signal-to-control ratios (SCRs).

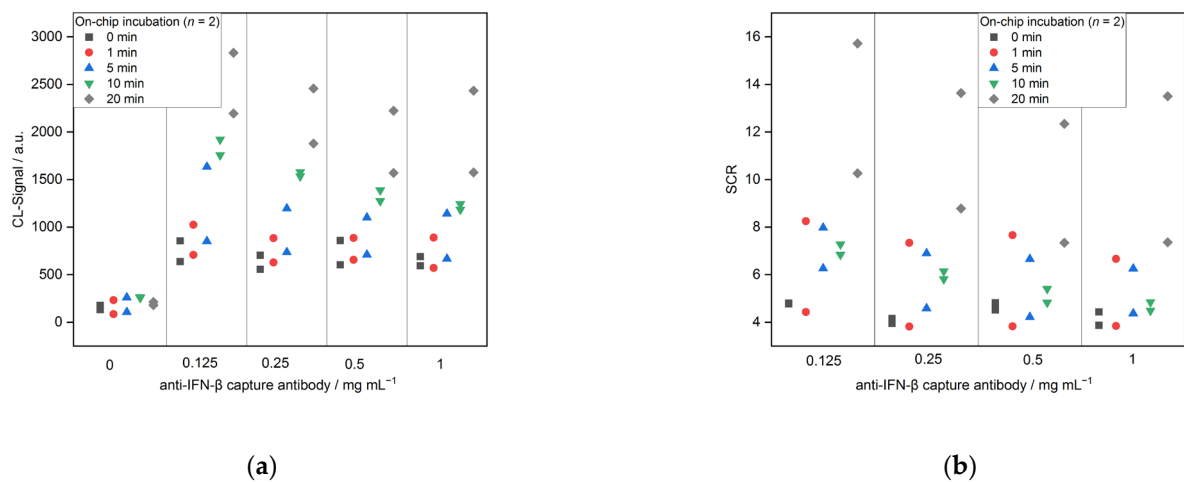
Hereby was found that the 1:2500 dilution yielded the best signal-to-control ratios ( $14.6 \pm 1.6$  for  $0.125 \text{ mg mL}^{-1}$  CAB). Moreover, this strep-HRP dilution showed the lowest standard deviations for SCR with  $8.9 \pm 4.7\%$  compared to  $16.8 \pm 1.8\%$  and  $34.9 \pm 5.3\%$  for the 1:2000 and 1:1500 ratios, respectively. In conclusion, a dilution of 1:2500 was chosen for further experiments. Over the CAB concentration range, the lower concentration led to lower signals and signal-to-control ratios. This indicates that an excessive amount of CAB on the microarray chip leads to a steric hindrance for the IFN- $\beta$ -DAB complex.

Secondly, the pre-incubation of the sample and DAB before injecting it into the flow cell of the microarray chip was optimized in terms of incubation time. Four different times (15, 30, 45 and 60 min) were tested, the results are depicted in Figure 5. Between 15 and 45 min, an increased incubation time led to an increase in the CL signal from 1808 and 2930 for 15 min to 2930 and 3500 for 45 min (both for  $0.125 \text{ mg mL}^{-1}$  CAB), as well as SCR from 11.7 and 9.1 to 16.4 and 24.1, respectively. Therefore, with longer incubation times, more IFN- $\beta$ -DAB complexes seem to be formed. For 60 min, the signals stayed in the same range, as for 45 min (2882 and 3580 for  $0.125 \text{ mg mL}^{-1}$  CAB), indicating that the equilibrium of complex formation was reached. Therefore, 45 min was chosen as the incubation time for the pre-incubation step.



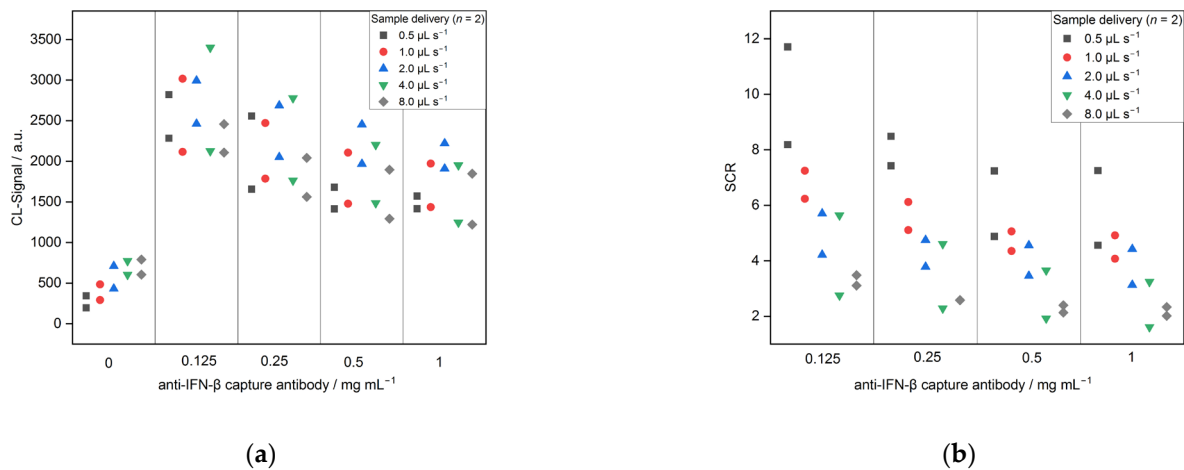
**Figure 5.** Optimization of pre-incubation step for CL-SMIA ( $n = 2$ ): (a) CL-signals and (b) SCRs.

The next step in the CL-SMIA was the incubation of the pre-incubated sample mixture on the microarray chip, so the IFN- $\beta$ -DAB complex can interact with the immobilized CABs. Five different incubation times (0, 1, 5, 10 and 20 min) were tested. Figure 6 shows a sharp increase in CL signals with increasing incubation times from 856 and 638 for 0 min to 2833 and 2195 for 20 min (both for 0.125 mg mL<sup>-1</sup> CAB). The negative control signals on the other hand all stayed at the same level, between 86 and 264. These results show that the SCRs showed the same trend increasing from 4.8 to 15.7 and 10.3, respectively. The longer the incubation time, the more time the complex has to interact with the immobilized CABs. As a result, 20 min were chosen for further measurements.



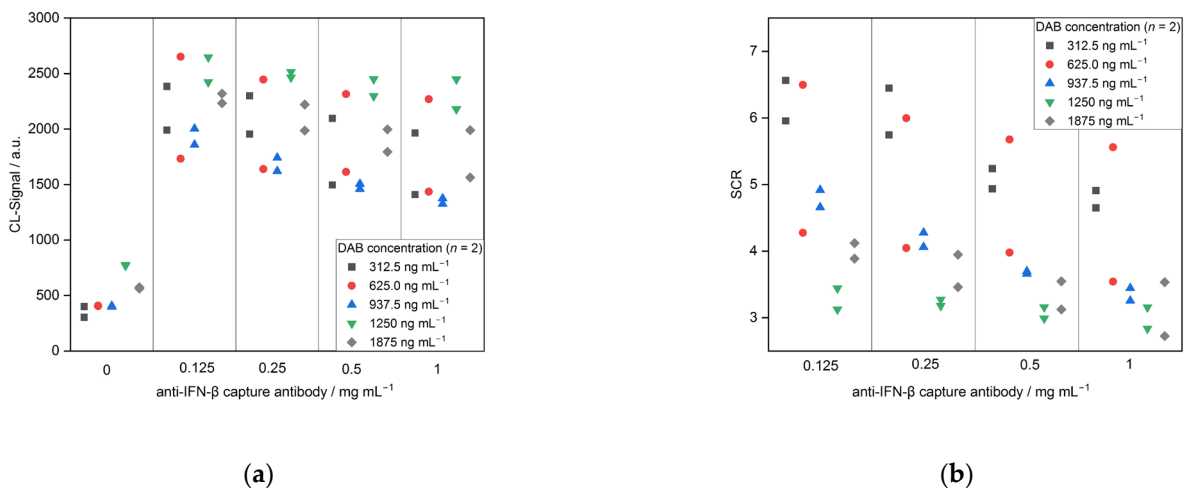
**Figure 6.** Optimization of incubation in microarray chip for CL-SMIA ( $n = 2$ ): (a) CL-signals and (b) SCRs.

Figure 7 shows the optimization of the flow rate used to deliver the sample over the flow cell of the chip inside the MCR-R. Five different flow rates were tested (0.5, 1.0, 2.0, 4.0 and 8.0  $\mu\text{L s}^{-1}$ ). The results show that the signal for the control increased from 345 and 195 for 0.5  $\mu\text{L s}^{-1}$  to 791 and 606 for 8.0  $\mu\text{L s}^{-1}$ . While for the higher flow rates, the antigen-antibody complex has less time to bind on the immobilized CAB. Likewise, the BSA present in the sample has less time to bind unspecifically on the microarray surface and, therefore, might have led to an increase in the CL signal for the negative control. Overall, the signal-to-control ratio decreased for higher flow rates from 8.2 and 11.7 for 0.5  $\mu\text{L s}^{-1}$  to 3 and 3.5 for 8.0  $\mu\text{L s}^{-1}$  (both for 0.125 mg mL<sup>-1</sup> CAB). Hence, the flow rate of 0.5  $\mu\text{L s}^{-1}$  was kept for all further experiments.



**Figure 7.** Optimization of sample delivery over the chip for CL-SMIA ( $n = 2$ ): (a) CL-signals and (b) SCRs.

As a last optimization step, the concentration of DAB in the sample-DAB-mix was examined with five concentrations (312.5, 625.0, 937.5, 1250 and 1875 ng mL $^{-1}$ ). The results are depicted in Figure 8. For the CL signals, no trend can be observed. Only for the negative controls, the CL signals for 1250 and 1875 ng mL $^{-1}$  (approx. 770 and 570) were higher than for the other three concentrations (all approx. 400). Looking at the SCRs, the highest ratios were obtained for 312.5 ng mL $^{-1}$  with 6.6 and 6.0 (0.125 mg mL $^{-1}$  CAB). An explanation for better results with a lower DAB concentration is the steric hindrance for the interaction with the immobilized CAB through an excess of the DABs binding to IFN- $\beta$ .



**Figure 8.** Optimization of DAB concentration for CL-SMIA ( $n = 2$ ): (a) CL-signals and (b) signal-to-control ratio.

### 3.2.2. Calibration

With this optimized assay protocol (312.5 ng mL $^{-1}$  DAB, 45 min pre-incubation, 20 min on-chip incubation, sample delivery over chip with 0.5  $\mu\text{L s}^{-1}$ , 1:2500 dilution of strep-HRP), calibration for IFN- $\beta$  was performed. Refined CL signals (according to Equation (4)) were plotted in Figure 9 semi-logarithmically ( $y$ -axis linear,  $x$ -axis logarithmic) versus the concentration of human IFN- $\beta$  standard and fitted with a four-parameter logistic fit (Equation (1)). As signals for 2000 and 4000 pg mL $^{-1}$  were in the saturation of the CCD camera, these values were excluded for fitting. The best calibration was obtained with 0.125 mg mL $^{-1}$  CAB, resulting in a LOD

of  $4.53 \text{ pg mL}^{-1}$  and an  $\text{EC}_{50}$  of  $3860 \text{ pg mL}^{-1}$ . Other fittings with corresponding LODs and  $\text{EC}_{50}$ s are shown in Supplementary Materials Figure S1b.

$$\text{refined CL signal} = \text{CL signal (CAB)} - \text{CL signal (negative control)} \quad (4)$$

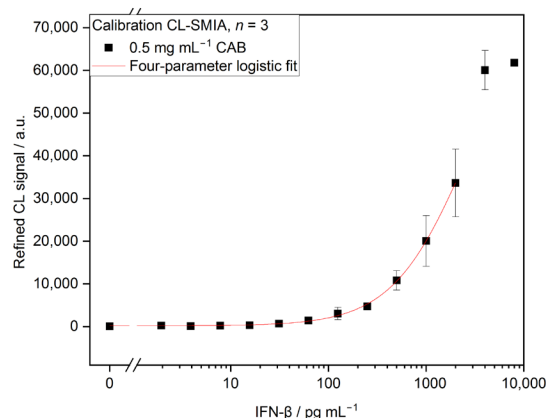


**Figure 9.** Calibration curve of CL-SMIA for IFN- $\beta$  with an immobilized CAB concentration of  $0.125 \text{ mg mL}^{-1}$  ( $n = 3$ ,  $\text{LOD } 4.53 \text{ pg mL}^{-1}$ ,  $\text{EC}_{50} 3860 \text{ pg mL}^{-1}$ ). IFN- $\beta$  concentrations of 2000 and  $4000 \text{ pg mL}^{-1}$  were excluded from fit due to CCD camera saturation.

### 3.3. Measurements in Nasal Samples

To test the assays in a real matrix, nasal samples were spiked with different concentrations ( $5.98$ ,  $12.04$ ,  $23.87$  and  $58.49 \text{ pg mL}^{-1}$ ) of IFN- $\beta$  and were measured in triplicates with both ELISA and CL-SMIA. For the  $5.98$  and  $12.04 \text{ pg mL}^{-1}$ , no recoveries could be calculated for CL-SMIA, while for ELISA, recoveries of  $71 \pm 6$  and  $87 \pm 2\%$  were found. For  $23.87$  and  $58.49 \text{ pg mL}^{-1}$ , ELISA showed recoveries of  $57 \pm 5\%$  and  $54 \pm 2\%$ , respectively. The CL-SMIA had lower recoveries with  $11 \pm 13\%$  ( $n = 2$ ) and  $14 \pm 6\%$ , respectively. The lower recoveries for CL-SMIA compared to ELISA can be reasoned by interactions between DAB and the matrix during pre-incubation, which is excluded for ELISA. Overall, the low recoveries for both assays show the matrix's influences.

### 3.4. Comparison of ELISA and CL-SMIA

For both ELISA and CL-SMIA, the same antibodies from a commercially available kit (R&D Systems Human IFN- $\beta$  DuoSet ELISA) were used. The LODs for ELISA and CL-SMIA are in the same range with  $1.60 \text{ pg mL}^{-1}$ , and  $4.53 \text{ pg mL}^{-1}$ , respectively. Both assays work in a sandwich format, meaning IFN- $\beta$  is captured by the immobilized anti-human IFN- $\beta$  CAB and detected by the biotinylated anti-human IFN- $\beta$  DAB. The main difference in the assay formats is the IFN- $\beta$ -DAB complex, which is formed during the pre-incubation step of CL-SMIA. This complex then binds to the CAB immobilized on the microarray chip, whereas the ELISA IFN- $\beta$  first interacts with CAB immobilized inside the microtiter well, before—and after blocking—the DAB binds. The difference in recoveries from the real samples might come from this difference in sample incubation.

We were able to produce foil-based microarray chips with a total cost of  $1.60 \text{ EUR}$  per microarray chip (Table 3). The biggest part, thereof, is represented by the assembly of the chip, more precisely the POM carrier plate and the double-sided adhesive. Since currently the POM carriers are bought from a small handcraft business, where they are cut into shape and outlets are drilled, the price of one carrier at the moment lies at  $1.15 \text{ EUR}$ . Further improvement of the manufacturing process by, for example, injection moulding will decrease the price of the carriers and, therefore, of the microarray chips. This is combined with the costs for measuring, adding up to  $2.37 \text{ EUR}$  for one CL-SMA measurement. For ELISA, measuring one 96-well microtiter plate costs  $86.19 \text{ EUR}$  and, therefore, one well is equal to  $0.90 \text{ EUR}$ . This means that, for a high number of samples and only for one biomarker, ELISA is more affordable than the CL-SMIA.

In this proof-of-concept study since only one antibody was immobilized on the microarray chip. However, up to 20 different antibodies could be immobilized, enabling the simultaneous detection of multiple biomarkers. Since, for ELISA, a separate measurement is required for each biomarker, CL-SMIA will be more affordable for the simultaneous detection of at least three different biomarkers.

**Table 3.** Costs for the production of one microarray chip, split into different steps of production.

	Cost	Comments
PC-chip surface	0.21 €	PC foil and coating
Spotting	0.002 €	Spotting buffer and CAB antibody
Assembly of microarray chip	1.38 €	POM carrier and adhesive
Total	1.60 €	

One aspect affecting the assay costs is the used amount of antibodies. While the CAB concentration for CL-SMIA is 63 times higher than for ELISA, its small spot volume of 0.9 nL, compared to 100 µL used in ELISA, requires a 362 times higher CAB amount for ELISA, compared to a spot row for the microarray chip (five spots). For DAB, on the other hand, the CL-SMIA requires a five times higher concentration and a three times higher amount per measurement than the ELISA. However, considering the total antibody amounts, one ELISA well costs only 0.65 EUR for the antibodies, while one microarray chip (one immobilized CAB row) costs only 0.07 EUR.

Additionally, the CL-SMIA only requires half of the sample volume as ELISA. The similar LODs of both assays prove that there is no disadvantage in using less sample volume. The smaller sample volume allows for the possibility of more measurements per sample. It also might allow for smaller volumes used for elution for nasal sample collection, which possible could lead to higher concentrations of eluted biomarkers. However, with the aim of further multiplexing the CL-SMIA, the proportion is shifted even more in favour of the CL-SMIA.

In terms of throughput, ELISA has a big advantage over CL-SMIA, as one microtiter plate contains 96 wells and several plates can be performed in one day. This allows for hundreds of sample measurements in one day, even if plate-wise calibration is performed. For the CL-SMIA, on the other hand, only 24 measurements are possible in one working day with an assay time of 1 h 15 min and staggering in time. This sums up to 25 h for 96 measurements if measured continuously or for four working days, while ELISA only needs 6 h (with pipetting steps), if the coating overnight is neglected (Table 4). Furthermore, one measurement needs this 6 h for ELISA, which makes the CL-SMIA more suitable for point-of-care applications. For simplifications, the plate-wise calibration for ELISA was neglected in these considerations.

**Table 4.** Comparison of CL-SMIA and ELISA regarding assay time. For sample and DAB incubation the assay steps for CL-SMIA change compared to ELISA since DAB and sample are first pre-incubated (1) and then incubated on the microarray chip (2). Time is for one ELISA 96-well microtiter plate or for one microarray chip for CL-SMIA. A total of 96 measurements correspond to one plate of ELISA and 96 continuous, stacked CL-SMIA measurements, respectively.

Assay Step	ELISA	CL-SMIA
Sample incubation	2 h	(2) 20 min on-chip
Blocking	1 h	-
DAB incubation	2 h	(1) 45 min pre-incubation
Detection	40 min	10 min
Total	1 measurement	1 h 15 min
	Duplicate	1 h 30 min
	96 measurements	25 h

#### 4. Conclusions

In this proof-of-concept study, a flow-based CL-SMIA for the quantification of IFN- $\beta$  in nasal secretions was developed using a commercially available ELISA antibody kit. For comparison, sandwich ELISA was performed with the same antibody set. The LODs for both assays are in the same size range, indicating similar assay efficiency. The short assay time of the CL-SMIA, below 2 h, and the possibility of staggering the time allows for the fast measuring of small sample sizes. Currently, the costs for CL-SMIA exceed the costs for ELISA, but with the further improvement of producing the microarray chips and the further multiplexing of the assay, a low cost can be achieved. In summation, we were able to show the concept of a flow-based CL-SMIA for the detection of biomarkers, which holds great potential for multiplexed screening of biomarkers in nasal secretions as a point-of-care application.

**Supplementary Materials:** The following supporting information can be downloaded at: <https://www.mdpi.com/article/10.3390/bios13070670/s1>, Table S1. ELISA optimization results. Figure S1. Results for calibration experiments of CL-SMIA for IFN- $\beta$ .

**Author Contributions:** Conceptualization, J.N., M.K., E.S., C.B.S.-W. and M.S.; validation, M.K.; formal analysis, J.N. and M.K.; investigation, M.K.; resources, E.S. and M.S.; data curation, J.N. and M.K.; writing—original draft preparation, J.N.; writing—review and editing, J.N., M.K., C.J., A.M.C., E.S., C.B.S.-W. and M.S.; visualization, J.N. and M.K.; supervision, J.N. and M.S.; project administration, E.S. and M.S.; funding acquisition, A.M.C. and C.B.S.-W.; C.J. and A.M.C. conducted the clinical study and A.M.C. was coordinating clinical investigator of the study. All authors have read and agreed to the published version of the manuscript.

**Funding:** This research was funded by EIT Health, a body of the European Union, grant number 19065.

**Institutional Review Board Statement:** The study was conducted in accordance with the Declaration of Helsinki and approved by the Ethics Committee of the Klinikum rechts der Isar of the Technical University of Munich. Ethics committee approvals were obtained in 2019, prior to initiation of the study: MUC TUM 159/19S (TUM). The study was registered in the German Clinical Trials Register and the WHO International Clinical Trials Registry Platform (registration number DRKS00023381).

**Informed Consent Statement:** Informed consent was obtained from all subjects involved in the study.

**Data Availability Statement:** Data will be made available upon reasonable request.

**Acknowledgments:** The authors wish to thank Martin Elsner for his scientific support.

**Conflicts of Interest:** The authors declare no conflict of interest.

#### References

1. Califf, R.M. Biomarker definitions and their applications. *Exp. Biol. Med.* **2018**, *243*, 213–221. [[CrossRef](#)] [[PubMed](#)]
2. Rifai, N.; Gillette, M.A.; Carr, S.A. Protein biomarker discovery and validation: The long and uncertain path to clinical utility. *Nat. Biotechnol.* **2006**, *24*, 971–983. [[CrossRef](#)] [[PubMed](#)]
3. Ahn, S.-M.; Simpson, R.J. Body fluid proteomics: Prospects for biomarker discovery. *Proteomics Clin. Appl.* **2007**, *1*, 1004–1015. [[CrossRef](#)] [[PubMed](#)]
4. Riechelmann, H.; Deutschle, T.; Rozsasi, A.; Keck, T.; Polzehl, D.; Bürner, H. Nasal biomarker profiles in acute and chronic rhinosinusitis. *Clin. Exp. Allergy* **2005**, *35*, 1186–1191. [[CrossRef](#)]
5. Zissler, U.M.; Ulrich, M.; Jakwerth, C.A.; Rothkirch, S.; Guerth, F.; Weckmann, M.; Schiemann, M.; Haller, B.; Schmidt-Weber, C.B.; Chaker, A.M. Biomatrix for upper and lower airway biomarkers in patients with allergic asthma. *J. Allergy Clin. Immunol.* **2018**, *142*, 1980–1983. [[CrossRef](#)]
6. Randall, R.E.; Goodbourn, S. Interferons and viruses: An interplay between induction, signalling, antiviral responses and virus countermeasures. *J. Gen. Virol.* **2008**, *89*, 1–47. [[CrossRef](#)]
7. Rebuli, M.E.; Speen, A.M.; Clapp, P.W.; Jaspers, I. Novel applications for a noninvasive sampling method of the nasal mucosa. *Am. J. Physiol. Lung Cell. Mol. Physiol.* **2017**, *312*, L288–L296. [[CrossRef](#)]

8. Hansel, T.T.; Tunstall, T.; Trujillo-Torralbo, M.-B.; Shamji, B.; Del-Rosario, A.; Dhariwal, J.; Kirk, P.D.W.; Stumpf, M.P.H.; Koopmann, J.; Telcian, A.; et al. A Comprehensive Evaluation of Nasal and Bronchial Cytokines and Chemokines Following Experimental Rhinovirus Infection in Allergic Asthma: Increased Interferons (IFN- $\gamma$  and IFN- $\lambda$ ) and Type 2 Inflammation (IL-5 and IL-13). *EBioMedicine* **2017**, *19*, 128–138. [[CrossRef](#)]
9. Guthrie, J.W.; Hamula, C.L.A.; Zhang, H.; Le, X.C. Assays for cytokines using aptamers. *Methods* **2006**, *38*, 324–330. [[CrossRef](#)]
10. Krueger, A.; Stoll, T.; Shah, A.K.; Sinha, R.; Frazer, I.H.; Hill, M.M. Antibody-Free Multiplex Measurement of 23 Human Cytokines in Primary Cell Culture Secretome Using Targeted Mass Spectrometry. *Anal. Chem.* **2020**, *92*, 3742–3750. [[CrossRef](#)]
11. Kim, S.T.; Muñoz-Grajales, C.; Dunn, S.E.; Schneider, R.; Johnson, S.R.; Touma, Z.; Ahmad, Z.; Bonilla, D.; Atenafu, E.G.; Hiraki, L.T.; et al. Interferon and interferon-induced cytokines as markers of impending clinical progression in ANA+ individuals without a systemic autoimmune rheumatic disease diagnosis. *Arthritis Res. Ther.* **2023**, *25*, 21. [[CrossRef](#)] [[PubMed](#)]
12. Scavuzzo, M.C.; Rocchi, V.; Fattori, B.; Ambrogio, F.; Carpi, A.; Ruffoli, R.; Manganelli, S.; Giannessi, F. Cytokine secretion in nasal mucus of normal subjects and patients with allergic rhinitis. *Biomed. Pharmacother.* **2003**, *57*, 366–371. [[CrossRef](#)] [[PubMed](#)]
13. Khalifian, S.; Raimondi, G.; Brandacher, G. The use of luminex assays to measure cytokines. *J. Investig. Dermatol.* **2015**, *135*, 1–5. [[CrossRef](#)] [[PubMed](#)]
14. Battaglia, T.M.; Masson, J.-F.; Sierks, M.R.; Beaudoin, S.P.; Rogers, J.; Foster, K.N.; Holloway, G.A.; Booksh, K.S. Quantification of cytokines involved in wound healing using surface plasmon resonance. *Anal. Chem.* **2005**, *77*, 7016–7023. [[CrossRef](#)]
15. Rahimian, A.; Siltanen, C.; Feyzizarnagh, H.; Escalante, P.; Revzin, A. Microencapsulated Immunoassays for Detection of Cytokines in Human Blood. *ACS Sens.* **2019**, *4*, 578–585. [[CrossRef](#)]
16. Joung, H.-A.; Hong, D.-G.; Kim, M.-G. A high sensitivity chemiluminescence-based CMOS image biosensor for the detection of human interleukin 5 (IL-5). In Proceedings of the 2012 IEEE Sensors, Taipei, Taiwan, 28–31 October; Staff, I., Ed.; IEEE: Piscataway, NJ, USA, 2012; pp. 1–3, ISBN 978-1-4577-1767-3.
17. Seidel, M.; Niessner, R. Automated analytical microarrays: A critical review. *Anal. Bioanal. Chem.* **2008**, *391*, 1521–1544. [[CrossRef](#)]
18. Boehm, N.; Riechardt, A.I.; Wiegand, M.; Pfeiffer, N.; Grus, F.H. Proinflammatory cytokine profiling of tears from dry eye patients by means of antibody microarrays. *Investig. Ophthalmol. Vis. Sci.* **2011**, *52*, 7725–7730. [[CrossRef](#)]
19. Thwaites, R.S.; Ito, K.; Chingono, J.M.S.; Coates, M.; Jarvis, H.C.; Tunstall, T.; Anderson-Dring, L.; Cass, L.; Rapeport, G.; Openshaw, P.J.; et al. Nasosorption as a Minimally Invasive Sampling Procedure: Mucosal Viral Load and Inflammation in Primary RSV Bronchiolitis. *J. Infect. Dis.* **2017**, *215*, 1240–1244. [[CrossRef](#)]
20. Knight, P.R.; Sreekumar, A.; Siddiqui, J.; Laxman, B.; Copeland, S.; Chinnaiyan, A.; Remick, D.G. Development of a sensitive microarray immunoassay and comparison with standard enzyme-linked immunoassay for cytokine analysis. *Shock* **2004**, *21*, 26–30. [[CrossRef](#)]
21. Chen, P.; Chung, M.T.; McHugh, W.; Nidetz, R.; Li, Y.; Fu, J.; Cornell, T.T.; Shanley, T.P.; Kurabayashi, K. Multiplex serum cytokine immunoassay using nanoplasmonic biosensor microarrays. *ACS Nano* **2015**, *9*, 4173–4181. [[CrossRef](#)]
22. Matson, R.S. Lateral Flow Microarray-Based ELISA for Cytokines. *Methods Mol. Biol.* **2023**, *2612*, 141–155. [[CrossRef](#)] [[PubMed](#)]
23. Seidel, M.; Niessner, R. Chemiluminescence microarrays in analytical chemistry: A critical review. *Anal. Bioanal. Chem.* **2014**, *406*, 5589–5612. [[CrossRef](#)] [[PubMed](#)]
24. Klüpfel, J.; Paßreiter, S.; Weidlein, N.; Knopp, M.; Ungerer, M.; Protzer, U.; Knolle, P.; Hayden, O.; Elsner, M.; Seidel, M. Fully Automated Chemiluminescence Microarray Analysis Platform for Rapid and Multiplexed SARS-CoV-2 Serodiagnostics. *Anal. Chem.* **2022**, *94*, 2855–2864. [[CrossRef](#)] [[PubMed](#)]
25. Bemetz, J.; Kober, C.; Meyer, V.K.; Niessner, R.; Seidel, M. Succinylated Jeffamine ED-2003 coated polycarbonate chips for low-cost analytical microarrays. *Anal. Bioanal. Chem.* **2019**, *411*, 1943–1955. [[CrossRef](#)]
26. Bose, I.; Ohlander, A.; Kutter, C.; Russom, A. An integrated all foil based micro device for point of care diagnostic applications. *Sens. Actuators B Chem.* **2018**, *259*, 917–925. [[CrossRef](#)]
27. Thwaites, R.S.; Jarvis, H.C.; Singh, N.; Jha, A.; Pritchard, A.; Fan, H.; Tunstall, T.; Nanan, J.; Nadel, S.; Kon, O.M.; et al. Absorption of Nasal and Bronchial Fluids: Precision Sampling of the Human Respiratory Mucosa and Laboratory Processing of Samples. *J. Vis. Exp.* **2018**, *131*, e56413. [[CrossRef](#)]
28. Klüpfel, J.; Paßreiter, S.; Rumpf, M.; Christa, C.; Holthoff, H.-P.; Ungerer, M.; Lohse, M.; Knolle, P.; Protzer, U.; Elsner, M.; et al. Automated detection of neutralizing SARS-CoV-2 antibodies in minutes using a competitive chemiluminescence immunoassay. *Anal. Bioanal. Chem.* **2023**, *415*, 391–404. [[CrossRef](#)]
29. Neumair, J.; Elsner, M.; Seidel, M. Flow-Based Chemiluminescence Microarrays as Screening Platform for Affinity Binders to Capture and Elute Bacteria. *Sensors* **2022**, *22*, 8606. [[CrossRef](#)]
30. Sollweck, K.; Streich, P.; Elsner, M.; Seidel, M. A Chip-Based Colony Fusion Recombinase Polymerase Amplification Assay for Monitoring of Antimicrobial Resistance Genes and Their Carrying Species in Surface Water. *ACS EST Water* **2021**, *1*, 584–594. [[CrossRef](#)]

**Disclaimer/Publisher’s Note:** The statements, opinions and data contained in all publications are solely those of the individual author(s) and contributor(s) and not of MDPI and/or the editor(s). MDPI and/or the editor(s) disclaim responsibility for any injury to people or property resulting from any ideas, methods, instructions or products referred to in the content.

## 6 Conclusion and Outlook

Rapid diagnosis of diseases is crucial for appropriate – and possibly life-saving - treatment. This thesis established three affinity-based isolation and detection methods, enhancing future diagnosis.

For the isolation of urinary EVs a monolithic immunoaffinity filtration was established, using anti-CD63 nanobodies as immunoaffinity binders. The macroporous structure of the monolith allows the filtration of larger volumes, while the easy-to-modify surface facilitates nanobody immobilization. Pioneering experiments showed that the elution of captured EVs was unsuccessful from directly immobilized nanobodies. Following that, a two-step approach was established, where GFP-labeled anti-CD63 nanobodies are attached to the monolithic surface via immunoaffinity towards immobilized anti-GFP nanobodies. The optimized protocol was used to isolate EVs from 30 mL of 1:4 diluted urine. Competitive and pH-dependent elution methods yielded smaller (ca. 36 nm) and larger (ca. 130 nm) vesicles, respectively. This means, this method not only allows for discrimination between surface-associated proteins and therefore the cells of origin, but also for size-discriminated isolation. Future investigation into different elution strategies might even improve the fractionation. For future routine use of this method, further development needs to be performed. Besides testing other nanobodies, an automated system will simplify the isolation process. Additionally, its application on larger sample volumes and even undiluted urine samples should be investigated.

The identification of new affinity binders for isolation methods requires a screening assay examining not only the binding of the affinity binder and its target, but also the elution. Therefore, as part of the REP-MAF project, a flow-based CL microarray screening assay based on polycarbonate foils was developed to find new affinity binders against pathogenic bacteria. *E. coli* and *E. faecalis* were biotinylated to detect them via strep-HRP, yielding  $98 \pm 51$  and  $75 \pm 29\%$  of culturable cells. The microarray panel allows for multiplexed screening for affinity binders and their elution buffers, leading to the unexpected finding of methyl alpha-D-mannopyranoside as a suitable elution buffer for Polymyxin B. Polymyxin B was also identified as a suitable affinity binder for both bacteria, but not as efficient as the respective antibodies. For future research, the microarray panel can be extended to up to 18 different affinity binders, varying for each target. Automated elution and testing of more elution methods are other ways to improve this method. Then it can be tested with real samples, and the identified affinity binders can be applied for affinity-based isolation methods, such as monolithic affinity filtration. This will allow the improvement of identification methods in diagnosis.

Biomarkers in nasal secretion can be used for the diagnosis of airway diseases. In the third project, a flow-based CL-SMIA was developed to quantify IFN- $\beta$  as a biomarker for viral infections. Antibodies were taken from a commercial ELISA kit, which was additionally compared to the CL-SMIA. After optimization of both assays, comparable detection limits of 4.53 pg mL<sup>-1</sup> for the CL-SMIA and 1.60 pg mL<sup>-1</sup> for the ELISA were found. A comparison of assay cost and time showed superiority of ELISA for large sample numbers but few different biomarkers, while the CL-SMIA was superior for few samples with various multiplexed biomarkers. Consequently, multiplexing would be the next step in optimizing this proof-of-concept. An adaption of the MCR-R for smaller volumes, both sample and reagents, might further advance the assay. This would allow for an automated sample injection into the microarray chip compared to the manual procedure. Cost-wise, the CL-SMIA might be improved by reducing the costs for the microarray chip carrier plate. In future, this system might be used for a rapid point-of-care analysis for upper airway infections.

Concluding, the versatility of affinity-based methods in biomarker isolation and detection from body fluids could be shown. Further development of the presented assays can help improve disease diagnosis and, consequently, their treatment.

## 7 References

1. Armstrong, L.E.; Johnson, E.C. Water Intake, Water Balance, and the Elusive Daily Water Requirement. *Nutrients* **2018**, *10*.
2. Biomarkers Definitions Working Group. Biomarkers and Surrogate Endpoints: Preferred Definitions and Conceptual Framework. *Clinical Pharmacology and Therapeutics* **2001**, *69*, 89–95.
3. Tothill, I.E. Biosensors for Cancer Markers Diagnosis. *Seminars in Cell & Developmental Biology* **2009**, *20*, 55–62.
4. Khan, I.H.; Ravindran, R.; Krishnan, V.V.; Awan, I.N.; Rizvi, S.K.; Saqib, M.A.; Shahzad, M.I.; Tahseen, S.; Ireton, G.; Goulding, C.W.; *et al.* Plasma Antibody Profiles as Diagnostic Biomarkers for Tuberculosis. *Clinical and Vaccine Immunology* **2011**, *18*, 2148–2153.
5. Guthrie, J.W. General Considerations when Dealing with Biological Fluid Samples. In *Comprehensive Sampling and Sample Preparation: Analytical Techniques for Scientists*; Pawliszyn, J., Ed.: Elsevier Science: Saint Louis, 2014, pp. 1–19.
6. Janssens, P.M.W. Recognizing and Differentiating Uncommon Body Fluids: Considerations and Tools for a Proper Practical Approach. *Clinica Chimica Acta* **2017**, *471*, 6–11.
7. Chiejina, M.; Kudaravalli, P.; Samant, H. Ascites. In *StatPearls [Internet]*; Chiejina, M., Kudaravalli, P., Samant, H., Eds.: StatPearls Publishing, 2023.
8. Sheer, T.A.; Runyon, B.A. Spontaneous Bacterial Peritonitis. *Digestive Diseases* **2005**, *23*, 39–46.
9. Wu, C.-H.; Silvers, C.R.; Messing, E.M.; Lee, Y.-F. Bladder Cancer Extracellular Vesicles Drive Tumorigenesis by Inducing the Unfolded Protein Response in Endoplasmic Reticulum of Nonmalignant Cells. *The Journal of Biological Chemistry* **2019**, *294*, 3207–3218.
10. Gámez-Valero, A.; Lozano-Ramos, S.I.; Bancu, I.; Lauzurica-Valdemoros, R.; Borràs, F.E. Urinary Extracellular Vesicles as Source of Biomarkers in Kidney Diseases. *Frontiers in Immunology* **2015**, *6*, 6.
11. Wang, S.; Kojima, K.; Mobley, J.A.; West, A.B. Proteomic Analysis of Urinary Extracellular Vesicles Reveal Biomarkers for Neurologic Disease. *EBioMedicine* **2019**, *45*, 351–361.
12. Ferreira, V.L.; Borba, H.H.; Bonetti, A.F. de; Leonart, L.P.; Pontarolo, R. Cytokines and Interferons: Types and Functions. In *Autoantibodies and Cytokines*; Khan, W.A., Ed.: IntechOpen, 2019.
13. Kastritis, P.L.; Bonvin, A.M.J.J. On the Binding Affinity of Macromolecular Interactions: Daring to Ask Why Proteins Interact. *Journal of the Royal Society, Interface* **2013**, *10*, 20120835.
14. Habtamu, H.B.; Sentic, M.; Silvestrini, M.; Leo, L. de; Not, T.; Arbault, S.; Manojlovic, D.; Sojic, N.; Ugo, P. A Sensitive Electrochemiluminescence Immunosensor for Celiac Disease Diagnosis Based on Nanoelectrode Ensembles. *Analytical Chemistry* **2015**, *87*, 12080–12087.
15. Langer, V.; Niessner, R.; Seidel, M. Stopped-Flow Microarray Immunoassay for Detection of Viable E. Coli by Use of Chemiluminescence Flow-Through Microarrays. *Analytical and Bioanalytical Chemistry* **2011**, *399*, 1041–1050.

16. Thermo Fisher Scientific. *Avidin-Biotin Interaction*. Available online: <https://www.thermofisher.com/de/de/home/life-science/protein-biology/protein-biology-learning-center/protein-biology-resource-library/pierce-protein-methods/avidin-biotin-interaction.html> (accessed on 12 October, 2023).
17. Karlsson, R.; Michaelsson, A.; Mattsson, L. Kinetic Analysis of Monoclonal Antibody-Antigen Interactions With a New Biosensor Based Analytical System. *Journal of Immunological Methods* **1991**, *145*, 229–240.
18. Bastos, M.; Abian, O.; Johnson, C.M.; Ferreira-da-Silva, F.; Vega, S.; Jimenez-Alesanco, A.; Ortega-Alarcon, D.; Velazquez-Campoy, A. Isothermal Titration Calorimetry. *Nature Reviews Methods Primers* **2023**, *3*, 1–23.
19. Friguet, B.; Chaffotte, A.F.; Djavadi-Ohanian, L.; Goldberg, M.E. Measurements of the True Affinity Constant in Solution of Antigen-Antibody Complexes by Enzyme-Linked Immunosorbent Assay. *Journal of Immunological Methods* **1985**, *77*, 305–319.
20. Liao, J.; Madahar, V.; Dang, R.; Jiang, L. Quantitative FRET (qFRET) Technology for the Determination of Protein-Protein Interaction Affinity in Solution. *Molecules* **2021**, *26*, 6339.
21. Deshpande, S.S. Antibodies: Biochemistry, Structure, and Function. In *Enzyme Immunoassays*, 1st ed; Deshpande, S.S., Ed.: Springer-Verlag New York Inc, 2012, pp. 24–51.
22. Ritter, M.A. Polyclonal and Monoclonal Antibodies. *Methods in Molecular Medicine* **2000**, *40*, 23–34.
23. Karn, A.E.; Bell, C.W.; Chin, T.F. Recombinant Antibody Technology. *ILAR Journal* **1995**, *37*, 132–141.
24. Janeway, C.A., JR; Travers, P.; Walport, M.; Shlomchik, M.J. The Structure of a Typical Antibody Molecule. In *Immunobiology: The Immune System in Health and Disease*. 5th edition; Charles A Janeway, JR, Travers, P., Walport, M., Shlomchik, M.J., Eds.: Garland Science, 2001.
25. Alberts, B.; Johnson, A.; Lewis, J.; Raff, M.; Roberts, K.; Walter, P., Eds. *Molecular Biology of the Cell*. 4th edition; Garland Science, 2002.
26. proteintech. *Polyclonal vs. Monoclonal Antibodies, Both Types Have Their Unique Advantages and Disadvantages and Can Be Used in a Wide Variety of Applications*; 2023. Available online: <https://www.ptglab.com/news/blog/polyclonal-vs-monoclonal-antibodies/> (accessed on 1 April, 2024).
27. evitria. *Recombinant Antibody Advantages and Disadvantages*; 2023. Available online: <https://www.evitria.com/journal/recombinant-antibodies/recombinant-antibody-advantages-disadvantages/> (accessed on 1 April, 2024).
28. de Marco, A. Recombinant Expression of Nanobodies and Nanobody-Derived Immunoreagents. *Protein Expression and Purification* **2020**, *172*, 105645.
29. Tang, H.; Gao, Y.; Han, J. Application Progress of the Single Domain Antibody in Medicine. *International Journal of Molecular Sciences* **2023**, *24*, 4176.
30. Salvador, J.-P.; Vilaplana, L.; Marco, M.-P. Nanobody: Outstanding Features for Diagnostic and Therapeutic Applications. *Analytical and Bioanalytical Chemistry* **2019**, *411*, 1703–1713.
31. Zhu, M.; Gong, X.; Hu, Y.; Ou, W.; Wan, Y. Streptavidin-Biotin-Based Directional Double Nanobody Sandwich ELISA for Clinical Rapid and Sensitive Detection of Influenza H5N1. *Journal of Translational Medicine* **2014**, *12*, 352.

32. Ma, L.; Sun, Y.; Kang, X.; Wan, Y. Development of Nanobody-Based Flow Injection Chemiluminescence Immunoassay for Sensitive Detection of Human Prealbumin. *Biosensors & Bioelectronics* **2014**, *61*, 165–171.
33. Ren, J.; Zhang, C.; Ji, F.; Jia, L. Characterization and Comparison of Two Peptide-Tag Specific Nanobodies for Immunoaffinity Chromatography. *Journal of Chromatography A* **2020**, *1624*, 461227.
34. Popovic, M.; Mazzega, E.; Toffoletto, B.; Marco, A. de. Isolation of Anti-Extra-Cellular Vesicle Single-Domain Antibodies by Direct Panning on Vesicle-Enriched Fractions. *Microbial Cell Factories* **2018**, *17*, 6.
35. Saw, P.E.; Xu, X.; Kim, S.; Jon, S. Biomedical Applications of a Novel Class of High-Affinity Peptides. *Accounts of Chemical Research* **2021**, *54*, 3576–3592.
36. Savini, F.; Loffredo, M.R.; Troiano, C.; Bobone, S.; Malanovic, N.; Eichmann, T.O.; Caprio, L.; Canale, V.C.; Park, Y.; Mangoni, M.L.; *et al.* Binding of an Antimicrobial Peptide to Bacterial Cells: Interaction With Different Species, Strains and Cellular Components. *Biochimica et Biophysica Acta. Biomembranes* **2020**, *1862*, 183291.
37. Moubareck, C.A. Polymyxins and Bacterial Membranes: A Review of Antibacterial Activity and Mechanisms of Resistance. *Membranes* **2020**, *10*.
38. Peskoller, C.; Niessner, R.; Seidel, M. Development of an Epoxy-Based Monolith Used for the Affinity Capturing of *Escherichia coli* Bacteria. *Journal of Chromatography A* **2009**, *1216*, 3794–3801.
39. Da Silva Junior, A.G.; Frias, I.A.M.; Lima-Neto, R.G.; Sá, S.R.; Oliveira, M.D.L.; Andrade, C.A.S. Concanavalin A Differentiates Gram-Positive Bacteria Through Hierarchized Nanostructured Transducer. *Microbiological Research* **2021**, *251*, 126834.
40. Su, D.; Kosciuk, T.; Yang, M.; Price, I.R.; Lin, H. Binding Affinity Determines Substrate Specificity and Enables Discovery of Substrates for N-Myristoyltransferases. *ACS Catalysis* **2021**, *11*, 14877–14883.
41. Lesnierowski, G.; Kijowski, J. Lysozyme. In *Bioactive Egg Compounds*; Huopalahti, R., López-Fandiño, R., Anton, M., Schade, R., Eds.: Scholars Portal: Berlin, Heidelberg, 2007, pp. 33–42.
42. Healthline. *Body Water Percentage: Average, Ideal, How to Maintain and Determine*; 2019. Available online: <https://www.healthline.com/health/body-water-percentage#body-water-charts> (accessed on 1 April, 2024).
43. Hu, S.; Loo, J.A.; Wong, D.T. Human Body Fluid Proteome Analysis. *Proteomics* **2006**, *6*, 6326–6353.
44. Lima-Oliveira, G.; Lippi, G.; Salvagno, G.L.; Picheth, G.; Guidi, G.C. Laboratory Diagnostics and Quality of Blood Collection. *Journal of Medical Biochemistry* **2015**, *34*, 288–294.
45. Bellagambi, F.G.; Lomonaco, T.; Salvo, P.; Vivaldi, F.; Hangouët, M.; Ghimenti, S.; Biagini, D.; Di Francesco, F.; Fuoco, R.; Errachid, A. Saliva Sampling: Methods and Devices. An Overview. *TrAC Trends in Analytical Chemistry* **2020**, *124*, 115781.
46. Foong, K.S.; Munigala, S.; Jackups, R.; Yarbrough, M.L.; Burnham, C.A.; Warren, D.K. Incidence and Diagnostic Yield of Repeat Urine Culture in Hospitalized Patients: an Opportunity for Diagnostic Stewardship. *Journal of Clinical Microbiology* **2019**, *57*.
47. Thomas, C.E.; Sexton, W.; Benson, K.; Sutphen, R.; Koomen, J. Urine Collection and Processing for Protein Biomarker Discovery and Quantification. *Cancer Epidemiology, Biomarkers & Prevention* **2010**, *19*, 953–959.
48. Do, T.Q.; Moshkani, S.; Castillo, P.; Anunta, S.; Pogosyan, A.; Cheung, A.; Marbois, B.; Faull, K.F.; Ernst, W.; Chiang, S.M.; *et al.* Lipids Including Cholesteryl Linoleate and

- Cholesteryl Arachidonate Contribute to the Inherent Antibacterial Activity of Human Nasal Fluid. *The Journal of Immunology* **2008**, *181*, 4177–4187.
49. Thwaites, R.S.; Jarvis, H.C.; Singh, N.; Jha, A.; Pritchard, A.; Fan, H.; Tunstall, T.; Nanan, J.; Nadel, S.; Kon, O.M.; *et al.* Absorption of Nasal and Bronchial Fluids: Precision Sampling of the Human Respiratory Mucosa and Laboratory Processing of Samples. *Journal of Visualized Experiments* **2018**.
  50. Seehusen, D.A.; Reeves, M.M.; Fomin, D.A. Cerebrospinal Fluid Analysis. *American Family Physician* **2003**, *68*, 1103–1109.
  51. Aponte, E.M.; Katta, S.; O'Rourke, M.C., Eds. *StatPearls [Internet]*; StatPearls Publishing, 2023.
  52. Eaton, D.C.; Pooler, J.; Vander, A.J. *Vander's Renal Physiology*, 7th ed; McGraw-Hill Medical: New York, 2009.
  53. Bouatra, S.; Aziat, F.; Mandal, R.; Guo, A.C.; Wilson, M.R.; Knox, C.; Bjorndahl, T.C.; Krishnamurthy, R.; Saleem, F.; Liu, P.; *et al.* The Human Urine Metabolome. *PLOS ONE* **2013**, *8*, e73076.
  54. Sarigul, N.; Korkmaz, F.; Kurultak, İ. A New Artificial Urine Protocol to Better Imitate Human Urine. *Scientific Reports* **2019**, *9*, 20159.
  55. Bartges, J. Discolored Urine. In *Nephrology and Urology of Small Animals*; Bartges, J., Polzin, D.J., Eds.: Wiley-Blackwell: Chichester, West Sussex, 2011, pp. 425–427.
  56. Adams, J.D.; Arnaoutis, G.; Johnson, E.C.; Jansen, L.T.; Bougatsas, D.; Capitan-Jimenez, C.; Mauromoustakos, A.; Panagiotakos, D.B.; Perrier, E.T.; Guelinckx, I.; *et al.* Combining Urine Color and Void Number to Assess Hydration in Adults and Children. *European Journal of Clinical Nutrition* **2021**, *75*, 1262–1266.
  57. How Does the Urinary System Work? In *InformedHealth.org [Internet]*: Institute for Quality and Efficiency in Health Care (IQWiG), 2006.
  58. Visible Body. *Urine Creation*. Available online: <https://www.visiblebody.com/learn/urinary/urine-creation> (accessed on 18 August, 2023).
  59. Uechi, K.; Asakura, K.; Ri, Y.; Masayasu, S.; Sasaki, S. Advantage of Multiple Spot Urine Collections for Estimating Daily Sodium Excretion: Comparison With Two 24-h Urine Collections as Reference. *Journal of Hypertension* **2016**, *34*, 204–214.
  60. Holm, A.; Aabenhus, R. Urine Sampling Techniques in Symptomatic Primary-Care Patients: A Diagnostic Accuracy Review. *BMC Family Practice* **2016**, *17*, 72.
  61. Witte, E.C.; Lambers Heerspink, H.J.; Zeeuw, D. de; Bakker, S.J.L.; Jong, P.E. de; Gansevoort, R. First Morning Voids Are More Reliable Than Spot Urine Samples to Assess Microalbuminuria. *Journal of the American Society of Nephrology* **2009**, *20*, 436–443.
  62. Liu, X.; Yin, P.; Shao, Y.; Wang, Z.; Wang, B.; Lehmann, R.; Xu, G. Which is the Urine Sample Material of Choice for Metabolomics-Driven Biomarker Studies? *Analytica Chimica Acta* **2020**, *1105*, 120–127.
  63. Chernesky, M.; Jang, D.; Chong, S.; Sellors, J.; Mahony, J. Impact of Urine Collection Order on the Ability of Assays to Identify *Chlamydia trachomatis* Infections in Men. *Sexually Transmitted Diseases* **2003**, *30*.
  64. Pernille, H.; Lars, B.; Marjukka, M.; Volkert, S.; Anne, H. Sampling of Urine for Diagnosing Urinary Tract Infection in General Practice - First-Void or Mid-Stream Urine? *Scandinavian Journal of Primary Health Care* **2019**, *37*, 113–119.
  65. van Keer, S.; Pattyn, J.; Tjalma, W.A.A.; van Ostade, X.; Ieven, M.; van Damme, P.; Vorsters, A. First-Void Urine: A Potential Biomarker Source for Triage of High-Risk Human Papillomavirus Infected Women. *European Journal of Obstetrics, Gynecology, and Reproductive Biology* **2017**, *216*, 1–11.

66. Amer, M.O.; Elsiey, H. Ascites: Causes, Diagnosis, and Treatment. In *Non-Alcoholic Steatohepatitis, Liver Cirrhosis and Hepatocellular Carcinoma: The Molecular Pathways*; Mezale, D., Ed.: IntechOpen, 2017.
67. diZerega, G.S.; Rodgers, K.E. Peritoneal Fluid. In *The Peritoneum*, 1st ed; diZerega, G.S., Rodgers, K.E., Eds.: Springer: New York, 2011, pp. 26–56.
68. Rudralingam, V.; Footitt, C.; Layton, B. Ascites Matters. *Ultrasound* **2017**, *25*, 69–79.
69. Grabau, C.M.; Crago, S.F.; Hoff, L.K.; Simon, J.A.; Melton, C.A.; Ott, B.J.; Kamath, P.S. Performance Standards for Therapeutic Abdominal Paracentesis. *Hepatology* **2004**, *40*, 484–488.
70. Hughes, J.A.; Bishop, T.H.; McIney, E.D.; Thomas, S.L.; Wessinger, J.M. Large Volume Paracentesis of 39.5 Liters Chylous Ascites in the Setting of High-Grade Follicular Lymphoma. *Radiology Case Reports* **2022**, *17*, 4276–4279.
71. Nguyen-Khac, E.; Thevenot, T.; Capron, D.; Dharancy, S.; Paupart, T.; Thabut, D.; Tiry, C. Are Ascitic Electrolytes Usable in Cirrhotic Patients? Correlation of Sodium, Potassium, Chloride, Urea, and Creatinine Concentrations in Ascitic Fluid and Blood. *European Journal of Internal Medicine* **2008**, *19*, 613–618.
72. Tarn, A.C.; Lapworth, R. Biochemical Analysis of Ascitic (Peritoneal) Fluid: What Should We Measure? *Annals of Clinical Biochemistry* **2010**, *47*, 397–407.
73. Garcia-Tsao, G. Ascites. In *Sherlock's Diseases of the Liver and Biliary System*, 12th ed; Dooley, J.S., Lok, A.S.F., Burroughs, A.K., Heathcote, E.J., Dooley, J., Sherlock, S., Eds.: Wiley-Blackwell: Chichester, West Sussex, UK, 2011, pp. 210–233.
74. Huang, L.-L.; Xia, H.H.-X.; Zhu, S.-L. Ascitic Fluid Analysis in the Differential Diagnosis of Ascites: Focus on Cirrhotic Ascites. *Journal of Clinical and Translational Hepatology* **2014**, *2*, 58–64.
75. Hernaez, R.; Hamilton, J.P. Unexplained Ascites. *Clinical Liver Disease* **2016**, *7*, 53–56.
76. Ginés, P.; Quintero, E.; Arroyo, V.; Terés, J.; Bruguera, M.; Rimola, A.; Caballería, J.; Rodés, J.; Rozman, C. Compensated Cirrhosis: Natural History and Prognostic Factors. *Hepatology* **1987**, *7*, 122–128.
77. Smith, E.M.; Jayson, G.C. The Current and Future Management of Malignant Ascites. *Clinical Oncology* **2003**, *15*, 59–72.
78. Moore, K.P.; Wong, F.; Gines, P.; Bernardi, M.; Ochs, A.; Salerno, F.; Angeli, P.; Porayko, M.; Moreau, R.; Garcia-Tsao, G.; *et al.* The Management of Ascites in Cirrhosis: Report on the Consensus Conference of the International Ascites Club. *Hepatology* **2003**, *38*, 258–266.
79. Arroyo, V. Pathophysiology, Diagnosis and Treatment of Ascites in Cirrhosis. *Annals of Hepatology* **2002**, *1*, 72–79.
80. Gallo, A.; Dedionigi, C.; Civitelli, C.; Panzeri, A.; Corradi, C.; Squizzato, A. Optimal Management of Cirrhotic Ascites: A Review for Internal Medicine Physicians. *Journal of Translational Internal Medicine* **2020**, *8*, 220–236.
81. Arroyo, V.; Ginès, P.; Gerbes, A.L.; Dudley, F.J.; Gentilini, P.; Laffi, G.; Reynolds, T.B.; Ring-Larsen, H.; Schölmerich, J. Definition and Diagnostic Criteria of Refractory Ascites and Hepatorenal Syndrome in Cirrhosis. International Ascites Club. *Hepatology* **1996**, *23*, 164–176.
82. Salerno, F.; Guevara, M.; Bernardi, M.; Moreau, R.; Wong, F.; Angeli, P.; Garcia-Tsao, G.; Lee, S.S. Refractory Ascites: Pathogenesis, Definition and Therapy of a Severe Complication in Patients With Cirrhosis. *Liver International* **2010**, *30*, 937–947.
83. Lv, Y.; Han, G.; Fan, D. Hepatic Hydrothorax. *Annals of Hepatology* **2018**, *17*, 33–46.

84. Kuiper, J.J.; van Buuren, H.R.; Man, R.A. de. Ascites in Cirrhosis: a Review of Management and Complications. *The Netherlands Journal of Medicine* **2007**, *65*, 283–288.
85. Lenz, K.; Buder, R.; Kapun, L.; Voglmayr, M. Treatment and Management of Ascites and Hepatorenal Aynndrome: An Update. *Therapeutic Advances in Gastroenterology* **2015**, *8*, 83–100.
86. Li, B.; Yang, C.; Qian, Z.; Huang, Y.; Wang, X.; Zhong, G.; Chen, J. Spontaneous Fungal Ascites Infection in Patients With Cirrhosis: An Analysis of 10 Cases. *Infectious Diseases and Therapy* **2021**, *10*, 1033–1043.
87. Gravito-Soares, M.; Gravito-Soares, E.; Lopes, S.; Ribeiro, G.; Figueiredo, P. Spontaneous Fungal Peritonitis: A Rare but Severe Complication of Liver Cirrhosis. *European Journal of Gastroenterology & Hepatology* **2017**, *29*, 1010–1016.
88. Jiang, Y.; Fan, C.; Dang, Y.; Zhao, W.; Lv, L.; Lou, J.; Li, L.; Ding, H. Clinical Characteristics and Early Diagnosis of Spontaneous Fungal Peritonitis/Fungiascites in Hospitalized Cirrhotic Patients With Ascites: A Case-Control Study. *Journal of Clinical Medicine* **2023**, *12*.
89. Rogers, D.F. Physiology of Airway Mucus Secretion and Pathophysiology of Hypersecretion. *Respiratory Care* **2007**, *52*, 1134-49.
90. Ringers, C.; Olstad, E.W.; Jurisch-Yaksi, N. The Role of Motile Cilia in the Development and Physiology of the Nervous System. *Philosophical Transactions of the Royal Society of London. Series B, Biological Siences* **2020**, *375*, 20190156.
91. Castelli, S.; Arasi, S.; Pawankar, R.; Matricardi, P.M. Collection of Nasal Secretions and Tears and Their Use in Allergology. *Current Opinion in Allergy and Clinical Immunology* **2018**, *18*, 1–9.
92. Ramvikas, M.; Arumugam, M.; Chakrabarti, S.R.; Jaganathan, K.S. Chapter Fifteen - Nasal Vaccine Delivery. In *Micro- and Nanotechnology in Vaccine Development*; Skwarczynski, M., Tóth, I., Eds.: William Andrew: Amsterdam, [Netherlands], 2017, pp. 279–301.
93. Fahy, J.V.; Dickey, B.F. Airway Mucus Function and Dysfunction. *The New England Journal of Medicine* **2010**, *363*, 2233–2247.
94. Shuter, J.; Hatcher, V.B.; Lowy, F.D. *Staphylococcus aureus* Binding to Human Nasal Mucin. *Infection and Immunity* **1996**, *64*, 310–318.
95. Atanasova, K.R.; Reznikov, L.R. Strategies for Measuring Airway Mucus and Mucins. *Respiratory Research* **2019**, *20*, 261.
96. Ferdman, R.M.; Linzer, J.F. The Runny Nose in the Emergency Department: Rhinitis and Sinusitis. *Clinical Pediatric Emergency Medicine* **2007**, *8*, 123–130.
97. Alobid, I.; Benítez, P.; Bernal-Sprekelsen, M.; Roca, J.; Alonso, J.; Picado, C.; Mullol, J. Nasal Polyposis and its Impact on Quality of Life: Comparison Between the Effects of Medical and Surgical Treatments. *Allergy* **2005**, *60*, 452–458.
98. Silvers, W.S. The Skier's Nose: A Model of Cold-Induced Rhinorrhea. *Annals of Allergy* **1991**, *67*, 32–36.
99. Hellings, P.W.; Klimek, L.; Cingi, C.; Agache, I.; Akdis, C.; Bachert, C.; Bousquet, J.; Demoly, P.; Gevaert, P.; Hox, V.; *et al.* Non-Allergic Rhinitis: Position Paper of the European Academy of Allergy and Clinical Immunology. *Allergy* **2017**, *72*, 1657–1665.
100. Varghese, M.; Glaum, M.C.; Lockey, R.F. Drug-Induced Rhinitis. *Clinical and Experimental Allergy* **2010**, *40*, 381–384.
101. Orban, N.; Maughan, E.; Bleach, N. Pregnancy-Induced Rhinitis. *Rhinology* **2013**, *51*, 111–119.

102. Georgalas, C.; Jovancevic, L. Gustatory Rhinitis. *Current Opinion in Otolaryngology & Head and Neck Surgery* **2012**, *20*, 9–14.
103. Ciftci, Z.; Catli, T.; Hanci, D.; Cingi, C.; Erdogan, G. Rhinorrhoea in the Elderly. *European Archives of Oto-Rhino-Laryngology* **2015**, *272*, 2587–2592.
104. van Rijswijk, J.B.; Blom, H.M.; Fokkens, W.J. Idiopathic Rhinitis, the Ongoing Quest. *Allergy* **2005**, *60*, 1471–1481.
105. Kotz, S.; Pechtold, L.; Jörres, R.A.; Nowak, D.; Chaker, A.M. Occupational Rhinitis. *Allergologie Select* **2021**, *5*, 51–56.
106. Munkholm, M.; Mortensen, J. Mucociliary Clearance: Pathophysiological Aspects. *Clinical Physiology and Functional Imaging* **2014**, *34*, 171–177.
107. Merkus, F.W.; Verhoef, J.C.; Schipper, N.G.; Marttin, E. Nasal Mucociliary Clearance as a Factor in Nasal Drug Delivery. *Advanced Drug Delivery Reviews* **1998**, *29*, 13–38.
108. Kaliner, M.A. Human Nasal Host Defense and Sinusitis. *Journal of Allergy and Clinical Immunology* **1992**, *90*, 424–430.
109. Ganz, T. Antimicrobial Polypeptides in Host Defense of the Respiratory Tract. *The Journal of Clinical Investigation* **2002**, *109*, 693–697.
110. Kaliner, M.A. Human Nasal Respiratory Secretions and Host Defense. *The American Review of Respiratory Disease* **1991**, *144*, S52-6.
111. Pelosi, P. Perireceptor Events in Olfaction. *Journal of Neurobiology* **1996**, *30*, 3–19.
112. Klimek, L.; Rasp, G. Norm Values for Eosinophil Cationic Protein in Nasal Secretions: Influence of Specimen Collection. *Clinical and Experimental Allergy* **1999**, *29*, 367–374.
113. Watelet, J.-B.; Gevaert, P.; Holtappels, G.; van Cauwenberge, P.; Bachert, C. Collection of Nasal Secretions for Immunological Analysis. *European Archives of Oto-Rhino-Laryngology* **2004**, *261*, 242–246.
114. Massey, C.J.; Del Diaz Valle, F.; Abuzeid, W.M.; Levy, J.M.; Mueller, S.; Levine, C.G.; Smith, S.S.; Bleier, B.S.; Ramakrishnan, V.R. Sample Collection for Laboratory-Based Study of the Nasal Airway and Sinuses: a Research Compendium. *International Forum of Allergy & Rhinology* **2020**, *10*, 303–313.
115. Riechelmann, H.; Deutschle, T.; Friemel, E.; Gross, H.J.; Bachem, M. Biological Markers in Nasal Secretions. *The European Respiratory Journal* **2003**, *21*, 600–605.
116. Lo Cicero, A.; Stahl, P.D.; Raposo, G. Extracellular Vesicles Shuffling Intercellular Messages: For Good or for Bad. *Current Opinion in Cell Biology* **2015**, *35*, 69–77.
117. Sheta, M.; Taha, E.A.; Lu, Y.; Eguchi, T. Extracellular Vesicles: New Classification and Tumor Immunosuppression. *Biology* **2023**, *12*.
118. Couch, Y.; Buzàs, E.I.; Di Vizio, D.; Gho, Y.S.; Harrison, P.; Hill, A.F.; Lötvall, J.; Raposo, G.; Stahl, P.D.; Théry, C.; *et al.* A Brief History of Nearly EV-Erything - The Rise and Rise of Extracellular Vesicles. *Journal of Extracellular Vesicles* **2021**, *10*, e12144.
119. van der Pol, E.; Böing, A.N.; Harrison, P.; Sturk, A.; Nieuwland, R. Classification, functions, and Clinical Relevance of Extracellular Vesicles. *Pharmacological Reviews* **2012**, *64*, 676–705.
120. Huotari, J.; Helenius, A. Endosome Maturation. *The EMBO Journal* **2011**, *30*, 3481–3500.
121. Gurung, S.; Perocheau, D.; Touramanidou, L.; Baruteau, J. The Exosome Journey: From Biogenesis to Uptake and Intracellular Signalling. *Cell Communication and Signaling* **2021**, *19*, 47.
122. Hessvik, N.P.; Llorente, A. Current Knowledge on Exosome Biogenesis and Release. *Cellular and Molecular Life Sciences* **2018**, *75*, 193–208.

123. Tricarico, C.; Clancy, J.; D'Souza-Schorey, C. Biology and Biogenesis of Shed Microvesicles. *Small GTPases* **2017**, *8*, 220–232.
124. Atkin-Smith, G.K.; Tixeira, R.; Paone, S.; Mathivanan, S.; Collins, C.; Liem, M.; Goodall, K.J.; Ravichandran, K.S.; Hulett, M.D.; Poon, I.K.H. A Novel Mechanism of Generating Extracellular Vesicles During Apoptosis via a Beads-On-A-String Membrane Structure. *Nature Communications* **2015**, *6*, 7439.
125. Caruso, S.; Atkin-Smith, G.K.; Baxter, A.A.; Tixeira, R.; Jiang, L.; Ozkocak, D.C.; Santavanond, J.P.; Hulett, M.D.; Lock, P.; Phan, T.K.; *et al.* Defining the Role of Cytoskeletal Components in the Formation of Apoptopodia and Apoptotic Bodies During Apoptosis. *Apoptosis* **2019**, *24*, 862–877.
126. Arraud, N.; Linares, R.; Tan, S.; Gounou, C.; Pasquet, J.-M.; Mornet, S.; Brisson, A.R. Extracellular Vesicles from Blood Plasma: Determination of Their Morphology, Size, Phenotype and Concentration. *Journal of Thrombosis and Haemostasis* **2014**, *12*, 614–627.
127. Sun, Y.; Xia, Z.; Shang, Z.; Sun, K.; Niu, X.; Qian, L.; Fan, L.-Y.; Cao, C.-X.; Xiao, H. Facile Preparation of Salivary Extracellular Vesicles for Cancer Proteomics. *Scientific Reports* **2016**, *6*, 24669.
128. Zonneveld, M.I.; Brisson, A.R.; van Herwijnen, M.J.C.; Tan, S.; van de Lest, C.H.A.; Redegeld, F.A.; Garsen, J.; Wauben, M.H.M.; Nolte-'t Hoen, E.N.M. Recovery of Extracellular Vesicles From Human Breast Milk Is Influenced by Sample Collection and Vesicle Isolation Procedures. *Journal of Extracellular Vesicles* **2014**, *3*.
129. Andre, F.; Scharz, N.E.C.; Movassagh, M.; Flament, C.; Pautier, P.; Morice, P.; Pomel, C.; Lhomme, C.; Escudier, B.; Le Chevalier, T.; *et al.* Malignant Effusions and Immunogenic Tumour-Derived Exosomes. *The Lancet* **2002**, *360*, 295–305.
130. Akers, J.C.; Ramakrishnan, V.; Nolan, J.P.; Duggan, E.; Fu, C.-C.; Hochberg, F.H.; Chen, C.C.; Carter, B.S. Comparative Analysis of Technologies for Quantifying Extracellular Vesicles (EVs) in Clinical Cerebrospinal Fluids (CSF). *PLOS ONE* **2016**, *11*, e0149866.
131. Zaborowski, M.P.; Balaj, L.; Breakefield, X.O.; Lai, C.P. Extracellular Vesicles: Composition, Biological Relevance, and Methods of Study. *Bioscience* **2015**, *65*, 783–797.
132. Johnstone, R.M.; Adam, M.; Hammond, J.R.; Orr, L.; Turbide, C. Vesicle Formation During Reticulocyte Maturation. Association of Plasma Membrane Activities With Released Vesicles (Exosomes). *Journal of Biological Chemistry* **1987**, *262*, 9412–9420.
133. Yu, Y.; Gool, E.; Berckmans, R.J.; Coumans, F.A.W.; Barendrecht, A.D.; Maas, C.; van der Wel, N.N.; Altevogt, P.; Sturk, A.; Nieuwland, R. Extracellular Vesicles From Human Saliva Promote Hemostasis by Delivering Coagulant Tissue Factor to Activated Platelets. *Journal of Thrombosis and Haemostasis* **2018**, *16*, 1153–1163.
134. Emerson, L.E.; Barker, H.; Tran, T.; Barker, S.; Enslow, S.; Ou, M.; Hoffman, C.; Jones, M.; Pascual, D.W.; Edelmann, M.J. Extracellular Vesicles Elicit Protective Immune Responses Against Salmonella Infection. *Journal of Extracellular Vesicles* **2022**, *11*, e12267.
135. Caobi, A.; Nair, M.; Raymond, A.D. Extracellular Vesicles in the Pathogenesis of Viral Infections in Humans. *Viruses* **2020**, *12*.
136. DeLeo, A.M.; Ikezu, T. Extracellular Vesicle Biology in Alzheimer's Disease and Related Tauopathy. *Journal of Neuroimmune Pharmacology* **2018**, *13*, 292–308.
137. Kamińska, A.; Platt, M.; Kasprzyk, J.; Kuśnierz-Cabala, B.; Gala-Błądzińska, A.; Woźnicka, O.; Jany, B.R.; Krok, F.; Piekoszewski, W.; Kuźniewski, M.; *et al.* Urinary

- Extracellular Vesicles: Potential Biomarkers of Renal Function in Diabetic Patients. *Journal of Diabetes Research* **2016**, 2016, 5741518.
138. Miranda, K.C.; Bond, D.T.; McKee, M.; Skog, J.; Păunescu, T.G.; Da Silva, N.; Brown, D.; Russo, L.M. Nucleic Acids Within Urinary Exosomes/Microvesicles are Potential Biomarkers for Renal Disease. *Kidney International* **2010**, 78, 191–199.
  139. Lee, H.; Kang, S.J.; Lee, J.; Park, K.H.; Rhee, W.J. Isolation and Characterization of Urinary Extracellular Vesicles From Healthy Donors and Patients With Castration-Resistant Prostate Cancer. *International Journal of Molecular Sciences* **2022**, 23.
  140. Lin, S.-Y.; Chang, C.-H.; Wu, H.-C.; Lin, C.-C.; Chang, K.-P.; Yang, C.-R.; Huang, C.-P.; Hsu, W.-H.; Chang, C.-T.; Chen, C.-J. Proteome Profiling of Urinary Exosomes Identifies Alpha 1-Antitrypsin and H2B1K as Diagnostic and Prognostic Biomarkers for Urothelial Carcinoma. *Scientific Reports* **2016**, 6, 34446.
  141. Fernández-Llama, P.; Khositseth, S.; Gonzales, P.A.; Star, R.A.; Pisitkun, T.; Knepper, M.A. Tamm-Horsfall Protein and Urinary Exosome Isolation. *Kidney International* **2010**, 77, 736–742.
  142. Bijnsdorp, I.V.; Maxouri, O.; Kardar, A.; Schelfhorst, T.; Piersma, S.R.; Pham, T.V.; Vis, A.; van Moorselaar, R.J.; Jimenez, C.R. Feasibility of Urinary Extracellular Vesicle Proteome Profiling Using a Robust and Simple, Clinically Applicable Isolation Method. *Journal of Extracellular Vesicles* **2017**, 6, 1313091.
  143. Salih, M.; Fenton, R.A.; Knipscheer, J.; Janssen, J.W.; Vredenburg-van den Berg, M.S.; Jenster, G.; Zietse, R.; Hoorn, E.J. An Immunoassay for Urinary Extracellular Vesicles. *American Journal of Physiology. Renal Physiology* **2016**, 310, F796-F801.
  144. Guan, S.; Yu, H.; Yan, G.; Gao, M.; Sun, W.; Zhang, X. Characterization of Urinary Exosomes Purified With Size Exclusion Chromatography and Ultracentrifugation. *Journal of Proteome Research* **2020**, 19, 2217–2225.
  145. Nordin, J.Z.; Lee, Y.; Vader, P.; Mäger, I.; Johansson, H.J.; Heusermann, W.; Wiklander, O.P.B.; Hällbrink, M.; Seow, Y.; Bultema, J.J.; *et al.* Ultrafiltration With Size-Exclusion Liquid Chromatography for High Yield Isolation of Extracellular Vesicles Preserving Intact Biophysical and Functional Properties. *Nanomedicine: Nanotechnology, Biology, and Medicine* **2015**, 11, 879–883.
  146. Musante, L.; Bontha, S.V.; La Salvia, S.; Fernandez-Piñeros, A.; Lannigan, J.; Le, T.H.; Mas, V.; Erdbrügger, U. Rigorous Characterization of Urinary Extracellular Vesicles (uEVs) in the Low Centrifugation Pellet - A Neglected Source for uEVs. *Scientific Reports* **2020**, 10, 3701.
  147. Cheng, L.; Sun, X.; Scicluna, B.J.; Coleman, B.M.; Hill, A.F. Characterization and Deep Sequencing Analysis of Exosomal and Non-Exosomal miRNA in Human Urine. *Kidney International* **2014**, 86, 433–444.
  148. Chen, Q.-G.; Chen, L.; Zhong, Q.-H.; Zhang, L.; Jiang, Y.-H.; Li, S.-Q.; Qin, T.-Y.; Sun, F.; You, X.-H.; Yang, W.-M.; *et al.* Optimization of Urinary Small Extracellular Vesicle Isolation Protocols: Implications in Early Diagnosis, Stratification, Treatment and Prognosis of Diseases in the Era of Personalized Medicine. *American Journal of Translational Research* **2020**, 12, 6302–6313.
  149. Rood, I.M.; Deegens, J.K.J.; Merchant, M.L.; Tamboer, W.P.M.; Wilkey, D.W.; Wetzels, J.F.M.; Klein, J.B. Comparison of Three Methods for Isolation of Urinary Microvesicles to Identify Biomarkers of Nephrotic Syndrome. *Kidney International* **2010**, 78, 810–816.
  150. Dhondt, B.; Geurickx, E.; Tulkens, J.; van Deun, J.; Vergauwen, G.; Lippens, L.; Miinalainen, I.; Rappu, P.; Heino, J.; Ost, P.; *et al.* Unravelling the Proteomic Landscape of

- Extracellular Vesicles in Prostate Cancer by Density-Based Fractionation of Urine. *Journal of Extracellular Vesicles* **2020**, *9*, 1736935.
151. Lane, R.E.; Korbie, D.; Trau, M.; Hill, M.M. Purification Protocols for Extracellular Vesicles. In *Extracellular Vesicles*: Humana Press, New York, NY, 2017, pp. 111–130.
  152. Gerlach, J.Q.; Krüger, A.; Gallogly, S.; Hanley, S.A.; Hogan, M.C.; Ward, C.J.; Joshi, L.; Griffin, M.D. Surface Glycosylation Profiles of Urine Extracellular Vesicles. *PLOS ONE* **2013**, *8*, e74801.
  153. Lozano-Ramos, I.; Bancu, I.; Oliveira-Tercero, A.; Armengol, M.P.; Menezes-Neto, A.; Del Portillo, H.A.; Lauzurica-Valdemoros, R.; Borràs, F.E. Size-Exclusion Chromatography-Based Enrichment of Extracellular Vesicles From Urine Samples. *Journal of Extracellular Vesicles* **2015**, *4*, 27369.
  154. Sidhom, K.; Obi, P.O.; Saleem, A. A Review of Exosomal Isolation Methods: Is Size Exclusion Chromatography the Best Option? *International Journal of Molecular Sciences* **2020**, *21*, 6466.
  155. Cytiva. *Fundamentals of Size Exclusion Chromatography, How size exclusion chromatography (SEC) works and how you use it to purify proteins*; 2022. Available online: <https://www.cytivalifesciences.com/en/us/solutions/protein-research/knowledge-center/protein-purification-methods/size-exclusion-chromatography> (accessed on 18 September, 2023).
  156. Guan, S.; Yu, H.; Yan, G.; Gao, M.; Sun, W.; Zhang, X. Size-Dependent Sub-Proteome Analysis of Urinary Exosomes. *Analytical and Bioanalytical Chemistry* **2019**, *411*, 4141–4149.
  157. Oeyen, E.; van Mol, K.; Baggerman, G.; Willems, H.; Boonen, K.; Rolfo, C.; Pauwels, P.; an Jacobs; Schildermans, K.; Cho, W.C.; *et al.* Ultrafiltration and Size Exclusion Chromatography Combined With Asymmetrical-Flow Field-Flow Fractionation for the Isolation and Characterisation of Extracellular Vesicles From Urine. *Journal of Extracellular Vesicles* **2018**, *7*, 1490143.
  158. Konoshenko, M.Y.; Lekchnov, E.A.; Vlassov, A.V.; Laktionov, P.P. Isolation of Extracellular Vesicles: General Methodologies and Latest Trends. *BioMed Research International* **2018**, *2018*, 8545347.
  159. Rider, M.A.; Hurwitz, S.N.; Meckes, D.G. ExtraPEG: A Polyethylene Glycol-Based Method for Enrichment of Extracellular Vesicles. *Scientific Reports* **2016**, *6*, 23978.
  160. Konoshenko, M.Y.; Lekchnov, E.A.; Bryzgunova, O.E.; Kiseleva, E.; Pyshnaya, I.A.; Laktionov, P.P. Isolation of Extracellular Vesicles From Biological Fluids via the Aggregation-Precipitation Approach for Downstream miRNAs Detection. *Diagnostics* **2021**, *11*.
  161. System Biosciences. *ExoQuick-TC*. Available online: <https://www.systembio.com/products/exosome-research/exosome-isolation/original-exoquick/tissue-culture-and-most-biofluids/exoquick-tc> (accessed on 20 September, 2023).
  162. Thermo Fisher Scientific. *Total Exosome Isolation Reagent (From Urine), Invitrogen™*. Available online: <https://www.thermofisher.com/order/catalog/product/4484452> (accessed on 20 September, 2023).
  163. Samsonov, R.; Shtam, T.; Burdakov, V.; Glotov, A.; Tsyrlina, E.; Berstein, L.; Nosov, A.; Evtushenko, V.; Filatov, M.; Malek, A. Lectin-Induced Agglutination Method of Urinary Exosomes Isolation Followed by mi-RNA Analysis: Application for Prostate Cancer Diagnostic. *The Prostate* **2016**, *76*, 68–79.

164. Ghosh, A.; Davey, M.; Chute, I.C.; Griffiths, S.G.; Lewis, S.; Chacko, S.; Barnett, D.; Crapoulet, N.; Fournier, S.; Joy, A.; *et al.* Rapid Isolation of Extracellular Vesicles From Cell Culture and Biological Fluids Using a Synthetic Peptide With Specific Affinity for Heat Shock Proteins. *PLOS ONE* **2014**, *9*, e110443.
165. Hildonen, S.; Skarpen, E.; Halvorsen, T.G.; Reubsaet, L. Isolation and Mass Spectrometry Analysis of Urinary Extraexosomal Proteins. *Scientific Reports* **2016**, *6*, 36331.
166. Yang, J.S.; Lee, J.C.; Byeon, S.K.; Rha, K.H.; Moon, M.H. Size Dependent Lipidomic Analysis of Urinary Exosomes From Patients With Prostate Cancer by Flow Field-Flow Fractionation and Nanoflow Liquid Chromatography-Tandem Mass Spectrometry. *Analytical Chemistry* **2017**, *89*, 2488–2496.
167. Woo, H.-K.; Sunkara, V.; Park, J.; Kim, T.-H.; Han, J.-R.; Kim, C.-J.; Choi, H.-I.; Kim, Y.-K.; Cho, Y.-K. Exodisc for Rapid, Size-Selective, and Efficient Isolation and Analysis of Nanoscale Extracellular Vesicles From Biological Samples. *ACS Nano* **2017**, *11*, 1360–1370.
168. Bajo-Santos, C.; Priedols, M.; Kaukis, P.; Paidere, G.; Gerulis-Bergmanis, R.; Mozolevskis, G.; Abols, A.; Rimsa, R. Extracellular Vesicles Isolation from Large Volume Samples Using a Polydimethylsiloxane-Free Microfluidic Device. *International Journal of Molecular Sciences* **2023**, *24*.
169. Ku, A.; Lim, H.C.; Evander, M.; Lilja, H.; Laurell, T.; Scheduling, S.; Ceder, Y. Acoustic Enrichment of Extracellular Vesicles From Biological Fluids. *Analytical Chemistry* **2018**, *90*, 8011–8019.
170. Wunsch, B.H.; Smith, J.T.; Gifford, S.M.; Wang, C.; Brink, M.; Bruce, R.L.; Austin, R.H.; Stolovitzky, G.; Astier, Y. Nanoscale Lateral Displacement Arrays for the Separation of Exosomes and Colloids Down to 20 nm. *Nature Nanotechnology* **2016**, *11*, 936–940.
171. Liang, L.-G.; Sheng, Y.-F.; Zhou, S.; Inci, F.; Li, L.; Demirci, U.; Wang, S. An Integrated Double-Filtration Microfluidic Device for Detection of Extracellular Vesicles From Urine for Bladder Cancer Diagnosis. *Methods in Molecular Biology* **2017**, *1660*, 355–364.
172. Barreiro, K.; Huber, T.B.; Holthofer, H. Isolating Urinary Extracellular Vesicles as Biomarkers for Diabetic Disease. *Methods in Molecular Biology* **2020**, *2067*, 175–188.
173. Shin, H.; Park, Y.H.; Kim, Y.-G.; Lee, J.Y.; Park, J. Aqueous Two-Phase System to Isolate Extracellular Vesicles From Urine for Prostate Cancer Diagnosis. *PLOS ONE* **2018**, *13*, e0194818.
174. Gustot, T.; Durand, F.; Lebrec, D.; Vincent, J.-L.; Moreau, R. Severe Sepsis in Cirrhosis. *Hepatology* **2009**, *50*, 2022–2033.
175. Canakis, A.; Canakis, J.; Lohani, M.; Ostrander, T. Spontaneous Bacterial Peritonitis in Cardiac Ascites: A Rare but Deadly Occurrence. *The American Journal of Case Reports* **2019**, *20*, 1446–1448.
176. Chuang, T.F.; Kao, S.C.; Tsai, C.J.; Lee, C.C.; Chen, K.S. Spontaneous Bacterial Peritonitis as the Presenting Feature in an Adult With Nephrotic Syndrome. *Nephrology, Dialysis, Transplantation* **1999**, *14*, 181–182.
177. Makharia, G.K.; Sharma, B.C.; Bhasin, D.K.; Singh, K. Spontaneous Bacterial Peritonitis in a Patient With Gastric Carcinoma. *Journal of Clinical Gastroenterology* **1998**, *27*, 269–270.
178. Sundaram, V.; Manne, V.; Al-Osaimi, A.M.S. Ascites and Spontaneous Bacterial Peritonitis: Recommendations From Two United States Centers. *Saudi Journal of Gastroenterology* **2014**, *20*, 279–287.

179. Schmid, S.A.; Wiest, R.; Salzberger, B.; Klebl, F. Spontan Bakterielle Peritonitis. *Medizinische Klinik - Intensivmedizin und Notfallmedizin* **2012**, *107*, 548–552.
180. Ding, X.; Yu, Y.; Chen, M.; Wang, C.; Kang, Y.; Lou, J. Causative Agents and Outcome of Spontaneous Bacterial Peritonitis in Cirrhotic Patients: Community-Acquired Versus Nosocomial Infections. *BMC Infectious Diseases* **2019**, *19*, 463.
181. Furey, C.; Zhou, S.; Park, J.H.; Foong, A.; Chowdhury, A.; Dawit, L.; Lee, V.; Vergara-Lluri, M.; She, R.; Kahn, J.; *et al.* Impact of Bacteria Types on the Clinical Outcomes of Spontaneous Bacterial Peritonitis. *Digestive Diseases and Sciences* **2023**, *68*, 2140–2148.
182. Lotte, R.; Courdurié, A.; Gaudart, A.; Emery, A.; Chevalier, A.; Tran, A.; Payen, M.; Ruimy, R. Spontaneous Bacterial Peritonitis: The Incremental Value of a Fast and Direct Bacterial Identification From Ascitic Fluids Inoculated in Blood Culture Bottles by MALDI-TOF MS for a Better Management of Patients. *Microorganisms* **2022**, *10*.
183. Runyon, B.A. Management of Adult Patients With Ascites due to Cirrhosis: An Update. *Hepatology* **2009**, *49*, 2087–2107.
184. Rogers, G.B.; Russell, L.E.; Preston, P.G.; Marsh, P.; Collins, J.E.; Saunders, J.; Sutton, J.; Fine, D.; Bruce, K.D.; Wright, M. Characterisation of Bacteria in Ascites - Reporting the Potential of Culture-Independent, Molecular Analysis. *European Journal of Clinical Microbiology & Infectious diseases* **2010**, *29*, 533–541.
185. Hardick, J.; Won, H.; Jeng, K.; Hsieh, Y.-H.; Gaydos, C.A.; Rothman, R.E.; Yang, S. Identification of Bacterial Pathogens in Ascitic Fluids From Patients With Suspected Spontaneous Bacterial Peritonitis by Use of Broad-Range PCR (16S PCR) Coupled With High-Resolution Melt Analysis. *Journal of Clinical Microbiology* **2012**, *50*, 2428–2432.
186. Enomoto, H.; Inoue, S.-I.; Matsuhisa, A.; Iwata, Y.; Aizawa, N.; Sakai, Y.; Takata, R.; Ikeda, N.; Hasegawa, K.; Nakano, C.; *et al.* Amplification of Bacterial Genomic DNA From all Ascitic Fluids With a Highly Sensitive Polymerase Chain Reaction. *Molecular Medicine Reports* **2018**, *18*, 2117–2123.
187. Krohn, S.; Böhm, S.; Engelmann, C.; Hartmann, J.; Brodzinski, A.; Chatzinotas, A.; Zeller, K.; Prywerek, D.; Fetzer, I.; Berg, T. Application of Qualitative and Quantitative Real-Time PCR, Direct Sequencing, and Terminal Restriction Fragment Length Polymorphism Analysis for Detection and Identification of Polymicrobial 16S rRNA Genes in Ascites. *Journal of Clinical Microbiology* **2014**, *52*, 1754–1757.
188. Goelz, H.; Wetzel, S.; Mehrbarzin, N.; Utzolino, S.; Häcker, G.; Badr, M.T. Next- and Third-Generation Sequencing Outperforms Culture-Based Methods in the Diagnosis of Ascitic Fluid Bacterial Infections of ICU Patients. *Cells* **2021**, *10*, 3226.
189. Kadri, K. Polymerase Chain Reaction (PCR): Principle and Applications. In *Synthetic Biology - New Interdisciplinary Science*; L. Nagpal, M., Boldura, O.-M., Baltă, C., Enany, S., Eds.: InTech, 2020.
190. Bio-Rad Laboratories. *What is Real-Time PCR (qPCR)?* Available online: <https://www.bio-rad.com/de-de/applications-technologies/what-real-time-pcr-qpcr?ID=LUSO4W8UU> (accessed on 10 October, 2023).
191. Cetecioglu, Z.; Ince, O.; Ince, B. Gel Electrophoresis Based Genetic Fingerprinting Techniques on Environmental Ecology. In *Gel Electrophoresis - Advanced Techniques*; Magdeldin, S., Ed.: InTech, 2012.
192. Shendure, J.; Balasubramanian, S.; Church, G.M.; Gilbert, W.; Rogers, J.; Schloss, J.A.; Waterston, R.H. DNA Sequencing at 40: Past, Present and Future. *Nature* **2017**, *550*, 345–353.
193. Feng, Y.; Chen, C.-L.; Chen, T.-H.; Liang, Y.-H.; Chen, H.-L.; Lin, C.-Y.; Chiu, C.-H. Application of Next-Generation Sequencing to Study Ascitic Microbiome in Cirrhotic

- Patients With or Without Spontaneous Bacterial Peritonitis. *Journal of Microbiology, Immunology, and Infection* **2015**, *48*, 504–509.
194. Fu, Y.; Chen, Q.; Xiong, M.; Zhao, J.; Shen, S.; Chen, L.; Pan, Y.; Li, Z.; Li, Y. Clinical Performance of Nanopore Targeted Sequencing for Diagnosing Infectious Diseases. *Microbiology Spectrum* **2022**, *10*, e0027022.
  195. Riechelmann, H.; Deutschle, T.; Rozsasi, A.; Keck, T.; Polzehl, D.; Bürner, H. Nasal Biomarker Profiles in Acute and Chronic Rhinosinusitis. *Clinical and Experimental Allergy* **2005**, *35*, 1186–1191.
  196. Meng, Y.; Lou, H.; Wang, Y.; Wang, C.; Zhang, L. The Use of Specific Immunoglobulin E in Nasal Secretions for the Diagnosis of Allergic Rhinitis. *The Laryngoscope* **2018**, *128*, E311-E315.
  197. Cameron, M.J.; Kelvin, D.J. Cytokines, Chemokines and Their Receptors. In *Madame Curie Bioscience Database [Internet]*: Landes Bioscience, 2013.
  198. König, K.; Klemens, C.; Haack, M.; Nicoló, M.S.; Becker, S.; Kramer, M.F.; Gröger, M. Cytokine Patterns in Nasal Secretion of Non-Atopic Patients Distinguish Between Chronic Rhinosinusitis With or Without Nasal Polyps. *Allergy, Asthma & Clinical Immunology* **2016**, *12*, 19.
  199. Comerlato Scotta, M.; Greff Machado, D.; Goecks Oliveira, S.; Moura, A. de; Rhoden Estorgato, G.; Souza, A.P.D. de; Nery Porto, B.; Araújo, P.D. de; Sarria, E.E.; Pitrez, P.M.; *et al.* Evaluation of Nasal Levels of Interferon and Clinical Severity of Influenza in Children. *Journal of Clinical Virology* **2019**, *114*, 37–42.
  200. Isaacs, A.; Lindenmann, J. Virus Interference. I. The Interferon. *Proceedings of the Royal Society of London. Series B, Biological sciences* **1957**, *147*, 258–267.
  201. Platanius, L.C. Mechanisms of Type-I- and Type-II-Interferon-Mediated Signalling. *Nature Reviews Immunology* **2005**, *5*, 375–386.
  202. Zimmermann, P.; Mänz, B.; Haller, O.; Schwemmler, M.; Kochs, G. The Viral Nucleoprotein Determines Mx Sensitivity of Influenza A Viruses. *Journal of Virology* **2011**, *85*, 8133–8140.
  203. Perng, Y.-C.; Lenschow, D.J. ISG15 in Antiviral Immunity and Beyond. *Nature Reviews Microbiology* **2018**, *16*, 423–439.
  204. Fan, J.-B.; Miyauchi, S.; Xu, H.-Z.; Liu, D.; Kim, L.J.Y.; Burkart, C.; Cheng, H.; Arimoto, K.; Yan, M.; Zhou, Y.; *et al.* Type I Interferon Regulates a Coordinated Gene Network to Enhance Cytotoxic T Cell-Mediated Tumor Killing. *Cancer Discovery* **2020**, *10*, 382–393.
  205. Dos Santos, J.M., B.; Soares, C.P.; Monteiro, F.R.; Mello, R.; do Amaral, J.B.; Aguiar, A.S.; Soledade, M.P.; Sucupira, C.; Paulis, M. de; Andrade, J.B.; *et al.* In Nasal Mucosal Secretions, Distinct IFN and IgA Responses Are Found in Severe and Mild SARS-CoV-2 Infection. *Frontiers in Immunology* **2021**, *12*, 595343.
  206. Creative Biolabs. *Sandwich ELISA with Streptavidin-biotin Detection*. Available online: <https://www.antibody-creativebiolabs.com/sandwich-elisa-with-streptavidin-biotin-detection.htm> (accessed on 4 October, 2023).
  207. Thermo Fisher Scientific. *Overview of ELISA*. Available online: <https://www.thermofisher.com/de/en/home/life-science/protein-biology/protein-biology-learning-center/protein-biology-resource-library/pierce-protein-methods/overview-elisa.html> (accessed on 4 October, 2023).
  208. Thermo Fisher Scientific. *Luminex Platform Technology*. Available online: <https://www.thermofisher.com/de/en/home/life-science/antibodies/immunoassays/procartaplex-assays-luminex/features.html> (accessed on 27 September, 2023).

209. Jochems, S.P.; Marcon, F.; Carniel, B.F.; Holloway, M.; Mitsi, E.; Smith, E.; Gritzfeld, J.F.; Solórzano, C.; Reiné, J.; Pojar, S.; *et al.* Inflammation Induced by Influenza Virus Impairs Human Innate Immune Control of Pneumococcus. *Nature Immunology* **2018**, *19*, 1299–1308.
210. Meso Scale Discovery. *Our Immunoassays*. Available online: [https://www.mesoscale.com/en/technical\\_resources/our\\_technology/our\\_immunoassays](https://www.mesoscale.com/en/technical_resources/our_technology/our_immunoassays) (accessed on 27 September, 2023).
211. Meso Scale Discovery. *Electrochemiluminescence*. Available online: [https://www.mesoscale.com/en/technical\\_resources/our\\_technology/ecl](https://www.mesoscale.com/en/technical_resources/our_technology/ecl) (accessed on 27 September, 2023).
212. Hansel, T.T.; Tunstall, T.; Trujillo-Torralbo, M.-B.; Shamji, B.; Del-Rosario, A.; Dhariwal, J.; Kirk, P.D.W.; Stumpf, M.P.H.; Koopmann, J.; Telcian, A.; *et al.* A Comprehensive Evaluation of Nasal and Bronchial Cytokines and Chemokines Following Experimental Rhinovirus Infection in Allergic Asthma: Increased Interferons (IFN- $\gamma$  and IFN- $\lambda$ ) and Type 2 Inflammation (IL-5 and IL-13). *EBioMedicine* **2017**, *19*, 128–138.
213. Jazaeri, S.; Goldsmith, A.M.; Jarman, C.R.; Lee, J.; Hershenson, M.B.; Lewis, T.C. Nasal Interferon Responses to Community Rhinovirus Infections are Similar in Controls and Children With Asthma. *Annals of Allergy, Asthma & Immunology* **2021**, *126*, 690-695.e1.
214. Martinson, N.; Gordhan, B.; Petkov, S.; Pillay, A.-D.; Seiphetlo, T.; Singh, N.; Otwombe, K.; Lebina, L.; Fredolini, C.; Chiodi, F.; *et al.* Proteomic Analysis of Mucosal and Systemic Responses to SARS-CoV-2 Antigen. *Vaccines* **2023**, *11*.
215. Olink. *Proximity Extension Assay (PEA) Technology*, 2022. Available online: <https://olink.com/our-platform/our-pea-technology/> (accessed on 28 September, 2023).
216. Wunderlich, A.; Torggler, C.; Elsässer, D.; Lück, C.; Niessner, R.; Seidel, M. Rapid Quantification Method for *Legionella pneumophila* in Surface Water. *Analytical and Bioanalytical Chemistry* **2016**, *408*, 2203–2213.
217. Göpfert, L.; Klüpfel, J.; Heinritz, C.; Elsner, M.; Seidel, M. Macroporous Epoxy-Based Monoliths for Rapid Quantification of *Pseudomonas Aeruginosa* by Adsorption Elution Method Optimized for qPCR. *Analytical and Bioanalytical Chemistry* **2020**, *412*, 8185–8195.
218. Bemetz, J.; Kober, C.; Meyer, V.K.; Niessner, R.; Seidel, M. Succinylated Jeffamine ED-2003 Coated Polycarbonate Chips for Low-Cost Analytical Microarrays. *Analytical and Bioanalytical Chemistry* **2019**, *411*, 1943–1955.
219. Neumair, J.; Elsner, M.; Seidel, M. Flow-Based Chemiluminescence Microarrays as Screening Platform for Affinity Binders to Capture and Elute Bacteria. *Sensors* **2022**, *22*.
220. Neumair, J.; Kröger, M.; Stütz, E.; Jerin, C.; Chaker, A.M.; Schmidt-Weber, C.B.; Seidel, M. Flow-Based CL-SMIA for the Quantification of Protein Biomarkers From Nasal Secretions in Comparison With Sandwich ELISA. *Biosensors* **2023**, *13*, 670.